UNIVERSITY OF SOUTHAMPTON

LASERS AND AMPLIFIERS IN BULK AND PLANAR WAVEGUIDE OXIDE CRYSTALS

Toby James Warburton

FACULTY OF SCIENCE
DEPARTMENT OF PHYSICS

Submitted for the degree of Doctor of Philosophy
April 1997

UNIVERSITY OF SOUTHAMPTON

ABSTRACT

FACULTY OF SCIENCE

PHYSICS

Doctor of Philosophy

LASERS AND AMPLIFIERS IN BULK AND PLANAR WAVEGUIDE OXIDE CRYSTALS

by Toby James Warburton

This thesis reports the results of investigations into efficient, miniature solid state lasers and optical amplifiers in rare earth doped oxide crystals.

Waveguides doped with the trivalent thulium ion were grown in YAG and YSO host crystals and lased, when optically pumped, at 2.012μm and 1.884μm, respectively. The Tm:YAG laser had absorbed power laser thresholds as low as 7mW and slope efficiencies as high as 68%. The planar devices were fabricated using the technique of liquid-phase epitaxy which produces waveguides of excellent optical quality and with very low propagation losses.

High gain optical amplifiers have been demonstrated in Nd:YAG planar waveguides pumped by a Ti:sapphire laser and a diode laser. A small-signal gain of 28.4dB was obtained in a waveguide fabricated by liquid-phase epitaxy; in the same waveguide 290mW of power was extracted for only ~550mW of absorbed pump power. A small-signal gain of 23.5dB was achieved in a Nd:YAG waveguide, fabricated by thermal bonding, for 250mW of absorbed pump power.

Pumping directly into the upper laser manifold of a bulk Nd:YAG rod, at 869nm, has produced a highly efficient laser on the quasi-three-level 946nm transition. The lower energy defect for a laser pumped in this manner relative to conventionally pumped Nd:YAG lasers should result in higher slope efficiencies and fewer thermal problems when pumped at high powers. Using such a pumping scheme a slope efficiency of 75% with respect to absorbed power was obtained.

Contents

Acknowledgements

My first thanks must go to my supervisor, Dr Anne Tropper for her support and guidance over the past years and for always knowing the answer to any question I might throw at her. I should also like to thank Professor Dave Hanna for keeping a watchful eye over me. Special thanks should also go to Dr Dave Shepherd, who has given me invaluable assistance during my time here - despite "wanting nothing to do with me". In addition I would like to thank the other members of the Crystal Waveguide Laser group with whom I have worked: Dr Alan Large, Tom Brown, Dr Stefan Guy and all the others too numerous to mention. Lots of thanks go to the co-workers from LETI who gave us lots of lovely waveguides to play with and without whom I may have been forced to go into the clean room. I should also like to thank the Engineering and Physical Sciences Research Council for their financial support.

At this point I should like to thank all my friends from home and the olden days in Southampton for staying my friends and for putting up with me no matter how rubbish I've been during the last few years.

Big thanks go to all the friends I have made while doing this degree, without whom another 3½ years in Southampton would have seemed a REALLY long time.

Finally I should like to offer my sincerest thanks to my parents who have made sure I've been fed, clothed and (relatively) sane during the seemingly interminable time I've spent in this city - thank you.

Chapter 1 - Introduction

1.1 Introduction

This thesis reports the results of a three year investigation into novel rare earth doped crystal lasers and optical amplifiers. The major part of the work completed in the course of producing this thesis has involved planar waveguide devices; the main aims of this work have been to build upon the work previously done on planar waveguide lasers, at the University of Southampton, and to extend this further to show the benefits that a planar geometry can offer, not only for low threshold lasers but also for efficient, high gain optical amplifiers.

Co-workers from the Laboratoire d'Electronique, de Technologie et d'Instrumentation (LETI) of Grenoble, France have developed a technique for fabricating low loss rare earth doped planar waveguides using liquid-phase epitaxy (LPE). The low loss nature of these waveguides is especially important for laser operation when the low additional propagation loss can enable the thresholds to be very low. These waveguides have been used extensively in my work including thulium doped yttrium aluminium garnet (Tm:YAG) planar waveguides, which have lased with slope efficiencies up to 68%, and thulium orthosilicate (Tm:YSO) waveguides both of which will be reported later in this thesis. Work done on the first high gain planar waveguide amplifiers in liquid-phase epitaxially grown and thermally bonded neodymium doped YAG (Nd:YAG) waveguides will also be presented.

Work has also been conducted on a bulk laser in Nd:YAG. Using an in-band pumping technique very high efficiency operation of the quasi-three-level 946nm transition has been possible with slope efficiencies as high as 75% with respect to absorbed power.

I will start by giving some background to the waveguide work done at Southampton University. In the remainder of this chapter I will discuss the motivation

for the work on crystal waveguides and outline some common methods of fabricating optical waveguides with particular emphasis on thermal bonding and liquid-phase epitaxy. The last section of this chapter will give an outline of the rest of the thesis.

1.2 Historical Overview

Much of the early work on laser pumped guided wave devices, in the 1970s, concentrated on the fibre geometry in both glasses and crystals [1,2,3]. These devices tended to be large and supported multiple waveguide modes; their cross section were typically up to 80μm in diameter. Lasing thresholds in an 80μm diameter Nd doped YAG fibre were, however, less than 1mW when pumped using an AlGaAs LED at 807nm [3].

Consideration was given at this time to a transverse pumping geometry[1] for solid state lasers which led to an interest in waveguides with a rectangular cross section [4]. In 1978, for example, a 60μm thick glass clad $LiNdP_4O_{12}$ (LNP) planar waveguide pumped by an argon ion laser lased with an incident power threshold of ~18mW [5] however maximum output power at 1.047μm was only ~5mW for 60mW of pump power. The waveguide was fabricated by sputtering SK12 glass onto the polished surfaces of the LNP crystal; propagation losses were relatively high for this system at ~ 3dB/cm for the TE_0 mode. In order to produce efficient, low threshold lasers a waveguide fabrication procedure needed to be developed which would result in lower loss waveguides, preferably in a wide variety of materials.

The work at Southampton University on crystal waveguide lasers began in 1988 in collaboration with the University of Sussex. The expertise of the team from Sussex University in the field of ion implantation led to the fabrication of optical waveguides using a Van der Graaf accelerator to implant He^+ ions into host materials. The first ion-implanted waveguide laser, reported in 1989, was a Nd:YAG planar device operating at

[1] This is equivalent to face pumping for planar waveguides - see Appendix C

1.064μm with a threshold of 8.5mW when pumped at 807nm [6]. Planar waveguide lasers were fabricated in a variety of Nd doped materials such as $YAlO_3$, $LiNbO_3$ and subsequently in $Gd_3Ga_5O_{12}$ [7,8,9]. In 1991 the first ion-implanted channel waveguide laser was fabricated, again in Nd:YAG, and lased with an absorbed power threshold of only 560μW when pumped at 807nm [10].

In 1992 a collaboration with LETI saw the fabrication of the first very low loss (~0.05dB / cm [11]) Nd:YAG planar waveguide using the liquid-phase epitaxial growth technique. Absorbed power lasing thresholds in this waveguide were as low as ~ 700μW when pumped with a Rhodamine 6G dye laser. A further advance at Southampton saw the operation of the first side-pumped waveguide laser in an LPE grown Nd:YAG waveguide.

Subsequent to this work and prior to my arrival 946nm Nd:YAG [12] and 1μm Yb:YAG lasers [13] were fabricated in LPE grown waveguides.

1.3 Planar Crystal Waveguides for Optical Devices

Planar waveguides have several advantages over traditional bulk crystal systems for rare earth doped solid state lasers and optical amplifiers and, indeed, can offer some advantages over the use of what is probably the most well known form of optical waveguide - the glass fibre - for such devices.

The main advantage that planar waveguide devices offer over bulk systems is due to the confinement of the pump and signal radiation, in one plane, resulting in much higher intensities over a given length than would be possible in a bulk crystal using the same pump or signal power. These high intensity-length products can result in lower pump power thresholds for lasers and higher gains per unit pump power in waveguide amplifiers than are achievable in bulk devices. It is important to remember, however, that waveguide fabrication can introduce an additional propagation loss into the material. In order to show a positive advantage over a bulk device in terms of laser threshold, for

example, it is necessary that the pump and signal confinement compensates for this additional loss. In the case of a planar waveguide with a depth of a few times the wavelength of the guided light and with relatively low propagation losses (~1dB / cm or below) then these conditions are usually satisfied and there will be an advantage in the use of a planar waveguide system.

The waveguide geometry is particularly suited to quasi-three-level laser transitions where the lower laser level is thermally populated. The resulting reabsorption loss at the laser wavelength may dominate any waveguide propagation loss rendering it less significant than is the case in four-level lasers. The advantage in terms of threshold which may be obtainable over bulk devices will, therefore, be even greater for quasi-three-level lasers than for four-level systems.

A number of properties of the planar geometry lend it particularly well to the development of high power waveguide devices. The planar geometry is uniquely compatible with the elliptical output beam shape from diode pump lasers which should enable simpler pump beam focusing techniques than have to be employed in bulk lasers. The ease of access to the pump and signal beams in the waveguide core and the slab geometry allow efficient heat removal for high power device operation. Operating a device in a thin slab can lower the likelihood of thermal fracture; the total pump power that can be used to operate at a constant fraction of the thermal fracture limit scales as wl/t, where w is the slab width, l is the length and t the thickness [14].

Crystalline laser host materials can offer a range of properties which make them more attractive for use in compact planar waveguide devices than glass hosts. Although propagation losses are typically greater than one would find in glass fibres for example[2], the spectral lines are sharper due to being predominantly homogeneously broadened; the sharp spectral lines result in larger peak cross sections than one would find in glass hosts

[2] LPE grown Nd:YAG losses can be 0.05dB/cm [11], glass fibre losses can be as low as 0.2dB/km [15]

enabling the production of much more compact devices. There are a vast range of possible transitions when one uses crystal hosts, at wavelengths ranging from the mid-infrared, for example at 3μm in erbium doped materials [16,17], through the common 1μm transitions of neodymium and ytterbium doped materials, to visible transitions via upconversion processes for example at 450nm in Tm:YLF [18]. 5d-4f inter-configurational transitions have even been operated in the near ultraviolet region of the spectrum in lasers such as that demonstrated in Ce^{3+} doped LaF_3 [19]. Transition metal doped crystals can also act as broadly tunable vibronic lasers, for example the Ti:sapphire laser or lasers with chromium doped into a variety of materials.

In addition to applications for lasers and amplifiers the high intensities possible in crystal waveguides have uses in the realms of non-linear optics. With larger nonlinearities in crystals than glasses, efficient second harmonic generation [20,21] and parametric oscillation [22] has been possible in crystal waveguides. Crystal host materials can also have much larger acousto-optic and electro-optic coefficients than glasses. Using the electro-optic effect in $LiNbO_3$, for example, has enabled the fabrication of mode-locked Nd^{3+} and Er^{3+} lasers [23,24].

In this thesis I will describe work performed on planar crystal waveguides fabricated using two techniques, liquid-phase epitaxy and thermal (or direct) bonding; there are, however a large number of fabrication techniques currently being investigated or being used to produce optical waveguides in crystals some of the more important of which I shall introduce in the next section.

1.4 Optical Waveguide Fabrication Techniques

Ion Implantation [25]

Ion implantation is an extremely versatile technique for fabricating optical waveguides. A collaboration between the University of Southampton and the University of Sussex has seen the fabrication of channel and planar ion-implanted waveguide lasers in a variety of host materials [26,27,28,29]. Typical propagation losses are around 1dB

/ cm in Nd:YAG, for example, although it is possible to produce low loss waveguides in some materials such as lead germanate glass where losses as low as 0.15dB / cm have been reported [26]. A disadvantage of ion implantation as a waveguide fabrication technique is the expense and complexity of the equipment required.

Proton Exchange

Proton exchange is a fabrication technique extensively used to produce waveguides in $LiNbO_3$ and $LiTaO_3$ and was first reported in 1982 [30]. Disadvantages of proton exchange include only extraordinary polarised light being guided and a reduction in the electro-optic coefficient of proton exchanged waveguides [31]. Losses can be as low as 0.1dB / cm using this technique [32].

Metal Indiffusion

Metal indiffusion is another technique widely used in the fabrication of optical waveguides in $LiNbO_3$ and $LiTaO_3$ although in this case both the ordinary and extraordinary polarisations are guided. Both planar and channel waveguides have been fabricated using this technique and propagation losses as low as 0.06dB / cm have been reported [33]. Rare earth ions can also be diffused into $LiNbO_3$ samples and this process has been used to produce a variety of waveguide lasers in this host material [34,35,36,37].

Crystal Fibre Growth

The most commonly used procedure for the growth of crystal fibres is the laser heated pedestal growth technique. Losses as low as 0.014dB / cm have been reported in Nd:YAG fibres grown using this method and lasers with submilliwatt thresholds have been produced [3,38]. The large cross-sectional area of the crystal fibre, however, results in very multimode waveguide devices.

Sol -Gel Processing

Sol-gel processing is a technique which has been extensively used for the

fabrication of glasses, ceramics and polymers [39]. Sol-gel processing has recently been extended to create films of certain non-linear crystalline materials such as KTP [40] and $BaTiO_3$ [41], although as yet no propagation losses have been reported.

Molecular Beam Epitaxy (MBE)

MBE is a growth technique which allows very accurate control of the layer composition and thickness, however, at a high capital cost. The technique has been used to produce waveguides in rare earth doped fluoride crystals with very high concentrations [42]; losses, however, have tended to be in the order of several dB / cm.

Pulsed Laser Deposition

Pulsed laser deposition (PLD) is a versatile technique which can be used in a variety of materials [43]. Recent work at the University of Southampton has led to the first report of lasing in a planar waveguide grown by PLD, in a Nd:GGG layer deposited onto a YAG substrate [44]. There are disadvantages with the PLD technique such as the difficulty in growing films with uniform thickness over a wide area of a substrate. Losses have often been reported of several dB / cm, however, recent reports of Nd:GGG waveguides have suggested losses as low as 0.6 dB / cm can be achieved [45]. The spectral characteristics of rare earth doped PLD grown films differ significantly from those of bulk crystals and there is a marked broadening of fluorescence lines which will result in decreases in peak cross sections relative to the bulk material and indeed to waveguides grown by some other techniques. PLD is, however, a promising technique due to its wide applicability and relative cheapness. Films can also be grown on substrates with lattice mismatches of up to 7%, compared to only 1-2% for liquid-phase epitaxy, for example [46,47].

1.5 Thermal Bonding

Thermal bonding is a technique which was first developed for bonding silicon wafers [48] and bonds the two materials via a complex phenomenon which includes Van der Waal's forces, static electrical charges and chemical bonding [49]. It is essential that

the two materials are extremely flat, smooth on a nanometer scale and clean. The bonding process takes place at high temperature and over a long period of time, approximately two weeks, since the longer the amount of time spent at high temperature the stronger the resulting bond [50]. The temperature should be just below that where interdiffusion between the adjacent faces occurs; interdiffusion might cause stresses in the bond.

Thermally bonded composite rods had previously been used in high power crystal laser systems. An undoped end-cap thermally bonded to the rod allows efficient thermal management of the laser system and can help to reduce reabsorption losses in quasi-three-level lasers [51,52]. What was, to our knowledge, the first rare earth doped optical waveguide fabricated using thermal bonding was investigated during research for this thesis[3], results for which are presented in Chapter 5 and Appendix B. Propagation losses in the Nd:YAG waveguide with pure YAG substrate and superstrate layers were found to be $\leq$2dB / cm, although it remains to be seen if such losses are the same for different bonded materials, or even for different waveguides in the same material.

One of the potential advantages for the use of thermal bonding technology for the fabrication of optical waveguides is due to the universality of the technique which should, in theory, allow the bonding of almost any two laser host materials allowing a vast range of waveguides in different rare earth doped materials. It should also be possible to bond materials with large differences in lattice constants allowing the possibility of fabricating waveguides with very large numerical apertures.

1.6 Liquid-Phase Epitaxy

Liquid-phase epitaxy (LPE) is an extremely promising technique for the fabrication of low loss rare earth doped optical waveguides. Nd:YAG waveguides have been grown with losses as low as 0.05dB / cm [11] which is approaching the scattering

[3] Fabricated by Onyx Optics, California

losses of bulk crystals. The technique involves the isothermal dipping of a substrate in a supercooled melt of constituent oxides. The horizontal dipping technique used was originally developed for the growth of iron garnet bubble films [53] but was extended to the growth of rare earth doped YAG on pure YAG substrates in 1972 when Ho^{3+} doped Er^{3+}, Tm^{3+}, Yb^{3+} codoped YAG thin films grown by LPE were observed to lase at 2.1μm when flashlamp pumped [54]. In 1973 LPE grown Nd:YAG thin film lasers were produced, again using flashlamp pumping [55]. In 1976 Grabmaier et al [56] refined the epitaxial growth technique to produce Nd:YAG layers at growth rates about 50 times that possible in the earlier experiments. Since this time significant work has been undertaken allowing the production of excellent optical quality rare earth doped YAG films [57].

In order to grow YAG films a Al_2O_3 rich mixture of Y_2O_3 and Al_2O_3 are dissolved in a PbO / B_2O_3 flux. The mixture of oxides and the flux are placed in a platinum crucible and melted in a vertical furnace which consists of two temperature controllable zones, as shown in figure 1.1, overleaf Homogeneity of the melt can be achieved by stirring it at a temperature of 1100°C for several hours. By reducing the temperature below the saturation temperature (supercooling) supersaturation of solution can be achieved. If the level of supercooling is low enough the solution will remain stable until a substrate is added to it. The substrate is rotated at 100 rpm, with the direction of rotation changing every 2 seconds, and is lowered into the melt. The garnet layer is able to crystallise onto the substrate surface with typical growth rates of around 2μm / minute. After the desired thickness of layer has been grown the substrate is removed from the melt and spun at 800rpm to remove any residual flux.

Rare earth dopants can be incorporated into the YAG layer by the addition of R_2O_3 oxides into the melt (where R is the rare earth ion required). Other substitutions can be performed by the addition of Ga_2O_3 and Lu_2O_3 to incorporate gallium and lutetium, respectively, into the layer. The addition of gallium into the waveguide increases the refractive index difference between the active layer and substrate by 1.1 ×

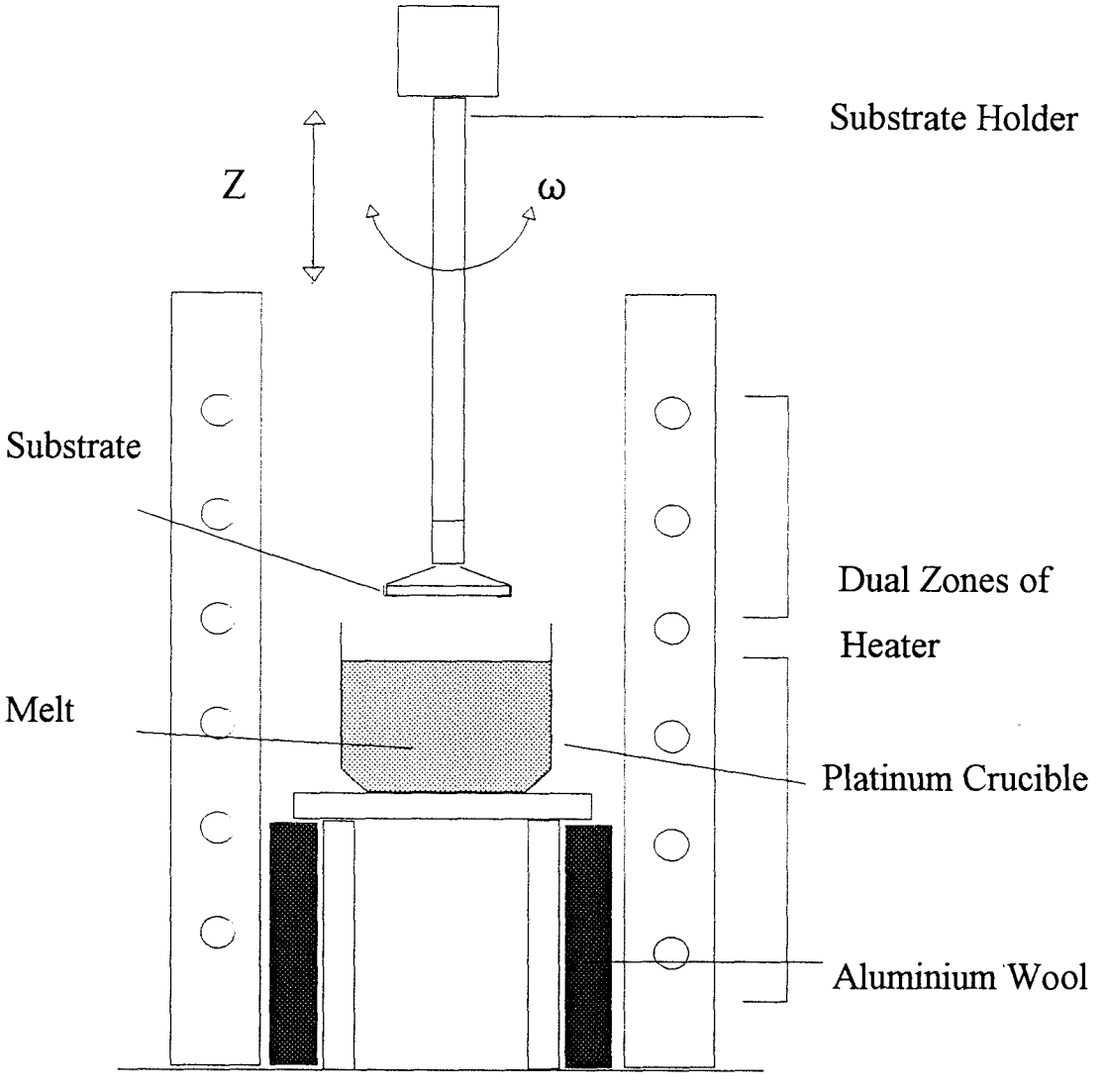

Figure 1.1 Apparatus for the liquid-phase epitaxial growth of thin films.
The substrates vertical position, z, and rotation rate, ω, can be accurately controlled

10^{-3} / at.% [58], compared to a value of 0.42 × 10^{-3} / at.% for Nd doping alone, for example. In LPE grown pure YAG films a positive lattice mismatch, between the layer and substrate lattice parameters, of 0.002Å is obtained; Ga and Nd substitutions change the lattice mismatch by -2.3Å / at.% and -2.1Å / at.% respectively [58]. Lutetium is, therefore, added to the film to compensate for this lattice mismatch which is a result of the large rare earth ion substituting for yttrium and the gallium ion substituting for aluminium in the crystal lattice. Lutetium changes the lattice mismatch by +0.78 Å / at.% [58].

A pure YAG cladding layer is grown over the waveguide film to reduce scattering losses and to protect the waveguide surface.

A collaboration between the Laboratoire d'Electronique, de Technologie et d'Instrumentation (LETI) of Grenoble, France and the University of Southampton has previously led to the production of low threshold waveguide lasers in liquid-phase epitaxially grown Nd:YAG and Yb:YAG waveguides [11,12,13].

One of the disadvantages of liquid-phase epitaxy is that waveguides had previously only been fabricated in the YAG crystal; LPE has, however, recently been used to grow, for the first time, waveguides in rare earth doped YSO which will be reported in Chapter 4 of this thesis. To grow the Tm:YSO films a solute of Y_2O_3, Tm_2O_3 and an excess of SiO_2 was dissolved in the PbO / B_2O_3 flux [59] The extension of the liquid-phase epitaxial technique to the growth of other materials, together with the fabrication of channel waveguides are two important future directions which need to be investigated further.

1.7 The YAG and YSO Laser Host Crystals

Yttrium aluminium garnet (YAG, $Y_3Al_5O_{12}$) is a cubic, isotropic crystal with space group symmetry O_h^{10} and has eight formula units in the unit cell. The lattice site symmetries of the ions are Y^{3+} (D_2), Al^{3+} (C_{3i} and S_4) and O^{2-} (C_1). Rare earth ions

doped into the YAG crystal substitute for the Y^{3+} ions in the crystal lattice on the D_2 point group symmetry sites [60]. As a result of the cubic symmetry of the YAG host rare earth ion dopants have unpolarised absorption and emission spectra. The high thermal conductivity and hardness of the YAG crystal make it a an ideal choice as a laser host material due to its resistance to thermal or physical fracture or strain.

Yttrium orthosilicate (YSO, Y_2SiO_5) is a monoclinic, biaxial crystal with space group symmetry C_{2h}^6. The three principal directions of the optical indicatrix can be identified, their orientation is a result of the biaxial nature of the crystal. The ⟨ 010⟩ axis which is the two fold symmetry axis of the crystal; the D_1 and D_2 directions are perpendicular to each other and to the ⟨010⟩ axis. The orientations of the crystal and the directions of the optical indicator are seen in figure 1.2, below.

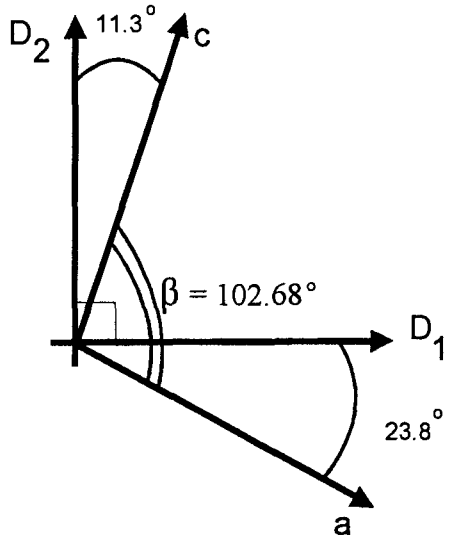

Figure 1.2 Orientation of the optical indicator and lattice vectors for YSO

The lattice parameters are :

$$a = 12.50\text{Å}; b = 6.72\text{Å}; c = 10.42\text{Å}.$$

The biaxial angle, β, is 102.68° [61]. Rare earth ions doped into the YSO host crystal occupy two yttrium sites which have C_1 symmetry [62].

1.8 Layout of Thesis

In Chapter 2 the theory of optical waveguides will be presented as will laser and amplifier theory. Chapter 3 gives details of the experimental procedures required to characterise the waveguides and of the laser and amplifier experiments performed. The studies carried out on liquid-phase epitaxially grown Tm:YAG and Tm:YSO waveguide lasers will be reported in Chapter 4. Results of the high gain amplifier experiments in epitaxially grown and thermally bonded Nd:YAG planar waveguides will be presented in Chapter 5. The final chapter of experimental results, Chapter 6, deals with modelling and operation of the bulk crystal in-band pumped 946nm Nd:YAG laser. Finally in Chapter 7 I will summarise the important results in this thesis and offer some conclusions and directions for future work. There are 4 Appendices at the end of the thesis, the first of which contains formulae which describe the overlap integrals between beams in planar waveguides, with particular emphasis on pump and signal beam overlap in waveguide amplifiers. Appendix B describes lasing experiments on the thermally bonded Nd:YAG waveguide which was used for some of the amplifier experiments described in Chapter 5. Appendix C describes a face-pumped Nd:YAG waveguide laser. Appendix D lists the publications which have arisen from the work done during the course of producing this thesis.

References

1. J.Stone and C.A.Burrus, Applied Optics **13**, 6, 1256-1258, 1974

2. H.P.Weber, P.F.Liao, B.C.Tofield and P.M.Bridenbaugh, Applied Physics Letters **26**, 12, 692-694, 1975

3. J.Stone, C.A.Burrus, A.G.Dentai and B.I.Miller, Applied Physics Letters **29**, 1, 37-39, 1976

4. K.Kubodera and K.Otsuka, Applied Optics **16**, 10, 2747-2752, 1977

5. K.Kubodera, J.Nakano, K.Otsuka and S.Miyazawa, Journal of Applied Physics **49**, 1, 65-69, 1978

6. P.J.Chandler, S.J.Field, D.C.Hanna, D.P.Shepherd, P.D.Townsend, A.C.Tropper and L.Zhang, Electronics Letters **25**, 15, 985-986, 1989

7. S.J.Field, D.C.Hanna, D.P.Shepherd, A.C.Tropper, P.J.Chandler, P.D.Townsend and L.Zhang, Electronics Letters **26**, 21, 1826-1827, 1990

8. S.J.Field, D.C.Hanna, D.P.Shepherd, A.C.Tropper, P.J.Chandler, P.D.Townsend and L.Zhang, Optics Letters **16**, 7, 481-483, 1991

9. S.J.Field, D.C.Hanna, A.C.Large, D.P.Shepherd, A.C.Tropper, P.J.Chandler, P.D.Townsend and L.Zhang, Optics Communications **86**, 2, 161-166, 1991

10. S.J.Field, D.C.Hanna, A.C.Large, D.P.Shepherd, A.C.Tropper, P.J.Chandler, P.D.Townsend and L.Zhang, Electronics Letters **27**, 25, 2375-2376, 1991

11. I.Chartier, B.Ferrand, D.Pelenc, S.J.Field, D.C.Hanna, A.C.Large, D.P.Shepherd and A.C.Tropper, Optics Letters **17**, 11, 810-812, 1992

12. D.C.Hanna, A.C.Large, D.P.Shepherd, A.C.Tropper, I.Chartier, B.Ferrand and D.Pelenc, Applied Physics Letters **63**, 1, 7-9, 1993

13. D.Pelenc, B.Chambaz, I.Chartier, C.Wyon, D.P.Shepherd, D.C.Hanna, A.C.Large and A.C.Tropper, Optics Communications **115**, 5, 491-497, 1995

14. A.Faulstich, H.J.Baker and D.R.Hall, Optics Letters **21**, 8, 594-596, 1996

15. G.Keiser, Optical Fiber Communications, Second Edition, McGraw-Hill, 1991

16. R.C.Stoneman, J.G.Lynn and L.Esterowitz, IEEE Journal of Quantum Electronics **28**, 4, 1041-1045, 1992

17. R.C.Stoneman and L.Esterowitz, Optics Letters **17**, 11, 816-818, 1992

18. T.Hebert, R.Wannemacher, R.M.Macfarlane and W.Lenth, Applied Physics Letters **60**, 21, 2592-2594, 1992

19. D.J.Ehrlich, P.F.Moulton and R.M.Osgood Jr, Optics Letters **5**, 8, 339-341, 1980

20. D.Delacourt, F.Armani and M.Papuchon, IEEE Journal of Quantum Electronics **30**, 1090-1099, 1994

21. M.L.Bortz, S.J.Field, M.M.Feyer, D.W.Nam, R.G.Waarts and D.F.Welch, IEEE Journal of Quantum Electronics **30**, 2953-2960, 1994

22. M.L.Bortz, M.A.Arbore and M.M.Feyer, Optics Letters **20**, 1, 49-51, 1995

23. E.Lallier, J.P.Pocholle, M.Papuchon, Q.He, M.De Micheli, D.B.Ostrowsky, C.Grezes-Besset and E.Pelletier, Electronics Letters **27**, 11, 936-937, 1991

24. H.Suche, L.Baumann, D.Hiller and W.Sohler, Electronics Letters **29**, 12, 1111-1112, 1993

25. P.D.Townsend, Reports on Progress in Physics **50**, 501-558, 1987

26. D.P.Shepherd, D.J.B.Brinck, J.Wang, A.C.Tropper, D.C.Hanna, G.Kakarantzas and P.D.Townsend, Optics Letters **19**, 13, 954-956, 1994

27. S.J.Field, Ion Implanted Crystal Waveguide Lasers, Ph.D. thesis, Department of Physics, University of Southampton, 1992

28. A.C.Large, Ion Implanted and Epitaxially Grown Crystal Waveguide Lasers, Ph.D. thesis, Department of Physics, University of Southampton, 1994

29. S.J.Field, D.C.Hanna, A.C.Large, D.P.Shepherd, A.C.Tropper, P.J.Chandler, P.D.Townsend and L.Zhang, OSA Proceedings on Advanced Solid State Lasers, Optical Society of America, Washington, DC, 1991, Vol.10, G.Dubé and L.Chase eds, p.353-357

30. J.L.Jackel, C.E.Rice and J.J.Veselka, Applied Physics Letters **41**, 607-608, 1982

31. F.Laurel, M.G.Roelefs and H.Hsiung, Applied Physics Letters **60**, 301, 1992

32. E.Lallier, J.P.Pochelle, M.Papuchon, Q.He, M.de Micheli and D.B.Ostrovsky, Electronics Letters **28**, 1428, 1992

33. P.Becker, R.Brinkmann, M.Dinand, W.Sohler and H.Suche, Applied Physics Letters **61**, 1257, 1992

34. J.K.Jones, J.P.de Sandro, M.Hempstead, D.P.Shepherd, A.C.Large, A.C.Tropper and J.S.Wilkinson, Optics Letters **20**, 1477-1479, 1995

35. R.Brinkmann, W.Sohler and H.Suche, Electronics Letters **27**, 5, 415-417, 1991

36. J.P.de Sandro, J.K.Jones, D.P.Shepherd, M.Hempstead, J.Wang and A.C.Tropper, IEEE Photonics Technology Letters **8**, 2, 1-3, 1996

37. M.Hempstead, J.S.Wilkinson and L.Reekie, IEEE Photonics Technology Letters **4**, 852-855, 1992

38. M.F.Digonnet, C.J.Gaeta, D.O'Meara and H.J.Shaw, Journal of Lightwave Technology **5**, 642, 1987

39. L.L.Hench and J.K.West, Chemical Reviews **90**, 1, 33-72, 1990

40. M.N.Kamalasanan, S.Chandra, P.C.Joshi and A.Mansingh, Applied Physics Letters **59**, 27, 3547, 1991

41. A.Munoz-Yague, C.Fontaine and E.Daran in Proceedings of Rare Earth Doped Optical Waveguides, B.Jaquier ed., L'Ecole de Physique des Houches, Les Houches, France, 1994, p.173

42. M.Shimbo, K.Furukawa, K.Fukuda and K.Tanzawa, Jounal of Applied Physics **60**, 2987-2989, 1986

43. K.L.Saenger, Pulsed Laser Deposition of Thin Films, ed. by D.B.Chrissey and

G.K.Hubler, Wiley.Interscience, 1994

44. D.S.Gill, A.A.Anderson, R.W.Eason, T.J.Warburton and D.P.Shepherd, Applied Physics Letters **69**, 1, 10-12, 1996

45. A.A.Anderson, C.Bonner, R.W.Eason, D.P.Shepherd, C.Grivas, D.S.Gill and N.Vainos, submitted to Applied Physics Letters

46. D.L.Lee, Electromagnetic Principles of Integrated Optics, Wiley International, p.187, 1986

47. J.W.Matthews and A.E.Blakeslee, Journal of Crystal Growth **27**, 118, 1974

48. M.Shimbo, K.Furukawa, K.Fukuda and K.Tanzawa, Journal of Applied Physics **60**, 2987-2989, 1986

49. J.Haisma, A.C.Bert, M.Spierings, U.K.P.Biermann and A.A.van Gorkum, Applied Optics **33**, 7, 1154-1169, 1994

50. T.V.Higgins, Laser Focus World, August 1991, p.45

51. H.Bruesselbach and D.S.Sumida, Optics Letters **21**, 7, 480-482, 1996

52. M.G.Jani, F.L.Naranjo, N.P.Barnes, K.E.Murray and G.E.Lockard, Optics Letters **20**, 8, 872-874, 1995

53. H.J.Levinstein, S.Licht, R.W.Landorf and S.Blank, Applied Physics Letters **19**, 486, 1971

54. J.P.Van der Ziel, W.A.Bonner, L.Kopf and L.G.Van Uitert, Physics Letters A

42, 1, 105-106, 1972

55. J.P.Van der Ziel, W.A.Bonner, L.Kopf and L.G.Van Uitert, Applied Physics Letters **22**, 12, 656-657, 1973

56. J.G.Grabmaier, R.D.Plättner, P.Möckel and W.W.Krühler, Journal of Crystal Growth **34**, 280-284, 1976

57. B.Ferrand, D.Pelenc, I.Chartier and Ch.Wyon, Journal of Crystal Growth **128**, 966-969, 1993

58. D.Pelenc, Doctorate Thesis, Université Joseph Fourier, Grenoble, France, 1993

59. A.Rameix, C.Borel, B.Ferrand, Ch.Wyon, D.P.Shepherd, T.J.Warburton, A.C.Tropper and D.C.Hanna, in Conference on Lasers and Electro-Optics Europe, Optical Society of America, Washington, DC, 1996, paper CFD1

60 J.B.Gruber, M.E.Hills, R.M.Macfarlane, C.A.Morrison, G.A.Turner, G.J.Quarles, G.J.Klintz and L.Esterowitz, Physical Review B **40**, 14, 9464-9478

61. C.Li, C.Wyon and R.Moncorgé, IEEE Journal of Quantum Electronics **28**, 4, 1209-1221, 1992

62. C.Li, R.Moncorgé, J.C.Souriau and Ch.Wyon, Optics Communications **101**, 356-360, 1993

Chapter 2 - Waveguide Laser and Amplifier Theory

2.1 Introduction

In this chapter some ideas concerning optical waveguides and waveguide lasers and amplifiers will be introduced. Many real waveguide systems can be described using the model of the simple asymmetric slab waveguide, which will be discussed. The theory of optical waveguides can be found in many textbooks [1,2,3], therefore this chapter will only serve as an introduction to the topic. Modelling of the threshold and slope efficiency of longitudinally pumped lasers will be presented, with particular emphasis on quasi-three-level lasers, this will then be adapted to take account of the waveguide geometry. Optical amplifier theory will be presented, which will also be adapted to a waveguide geometry.

2.2 The Asymmetric Slab Waveguide

The asymmetric slab waveguide consists of three elements; a substrate, which for the purpose of this analysis will be considered infinitely thick, a thin guiding layer of higher refractive index, and a superstrate layer, which often is air. Figure 2.1 shows such a system, with a substrate of refractive index n_3, a guiding layer with refractive index n_2,

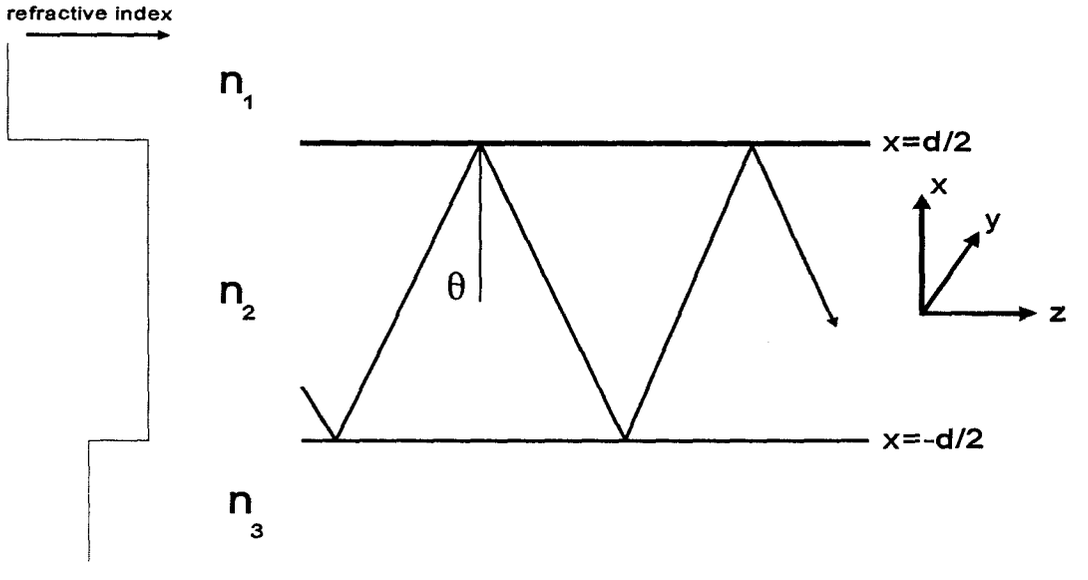

Figure 2.1 Schematic diagram of an optical wave in a planar waveguide

and a superstrate of n_1.

To analyse the propagation of an electromagnetic wave in such a medium we must first consider Maxwell's equations which may be written as

$$\underline{\nabla}\times\underline{E} = -\frac{\partial}{\partial t}\underline{B}(\underline{r},t) \tag{2.1}$$

$$\underline{\nabla}\times\underline{H}(\underline{r},t) = \frac{\partial}{\partial t}\underline{D}(\underline{r},t)+\underline{J}(\underline{r},t) \tag{2.2}$$

$$\underline{\nabla}\cdot\underline{D}(\underline{r},t) = \rho(\underline{r},t) \tag{2.3}$$

$$\underline{\nabla}\cdot\underline{B}(\underline{r},t) = 0 \tag{2.4}$$

where $\underline{E}$ and $\underline{H}$ are the electric and magnetic fields respectively, $\underline{D}$ and $\underline{B}$ represent the electric and magnetic displacements, $\underline{J}$ and ρ represent the current and charge sources. t is time and $\underline{r}$ corresponds to position in space. In an isotropic medium we can write the constitutive relations

$$\underline{B} = \mu\underline{H} \tag{2.5}$$

$$\underline{D} = \epsilon\underline{E} \tag{2.6}$$

where μ and ϵ are the magnetic permeability and electric permittivity of the material. If we assume there is no current flow, i.e. $\underline{J}$=0, and substitute the above into equations (2.1) and (2.2) we find

$$\nabla \times \underline{E}(\underline{r},t) = -\mu \frac{\partial}{\partial t} \underline{H}(\underline{r},t) \tag{2.7}$$

$$\nabla \times \underline{H}(\underline{r},t) = \epsilon \frac{\partial}{\partial t} \underline{E}(\underline{r},t) \tag{2.8}$$

In a waveguide we anticipate that the fields have a standing wave nature as a result of the superposition of upward and downward totally internally reflected waves, so we can suggest a sinusoidal profile in the guided region. Due to the evanescent nature of the waves outside the guided region the fields can be described by an exponential decay in the substrate and superstrate. We therefore need to find solutions to equations (2.7) and (2.8) which satisfy these conditions. If we assume propagation is along the z direction, as shown in figure 2.2, then a transverse electric, or TE, wave (as shown in figure 2.2) will have a field which can be written as

$$\underline{E}(\underline{r},t) = \hat{y}\, E_y(x,z) e^{i\omega t} \tag{2.9}$$

$E_y(x,z)$ can be characterised in three regions such that

$$E_y(x,y) = \begin{bmatrix} A_1 e^{-\alpha_{1x} x} & x > d/2 \\ A_2 \cos(k_{2x} x + \psi) & |x| \le d/2 \\ A_3 e^{+\alpha_{3x} x} & x < -d/2 \end{bmatrix} e^{ik_z z} \tag{2.10}$$

where A_1, A_2 and A_3 are amplitude coefficients and ψ is a phase term; α_{1x}, k_{2x}, and α_{3x} are the transverse wavenumbers in regions 1, 2 and 3 respectively, and can be found by the substitution of equation (2.10) into the Helmholtz equation, (2.11), which governs the behaviour of electromagnetic waves of frequency ω

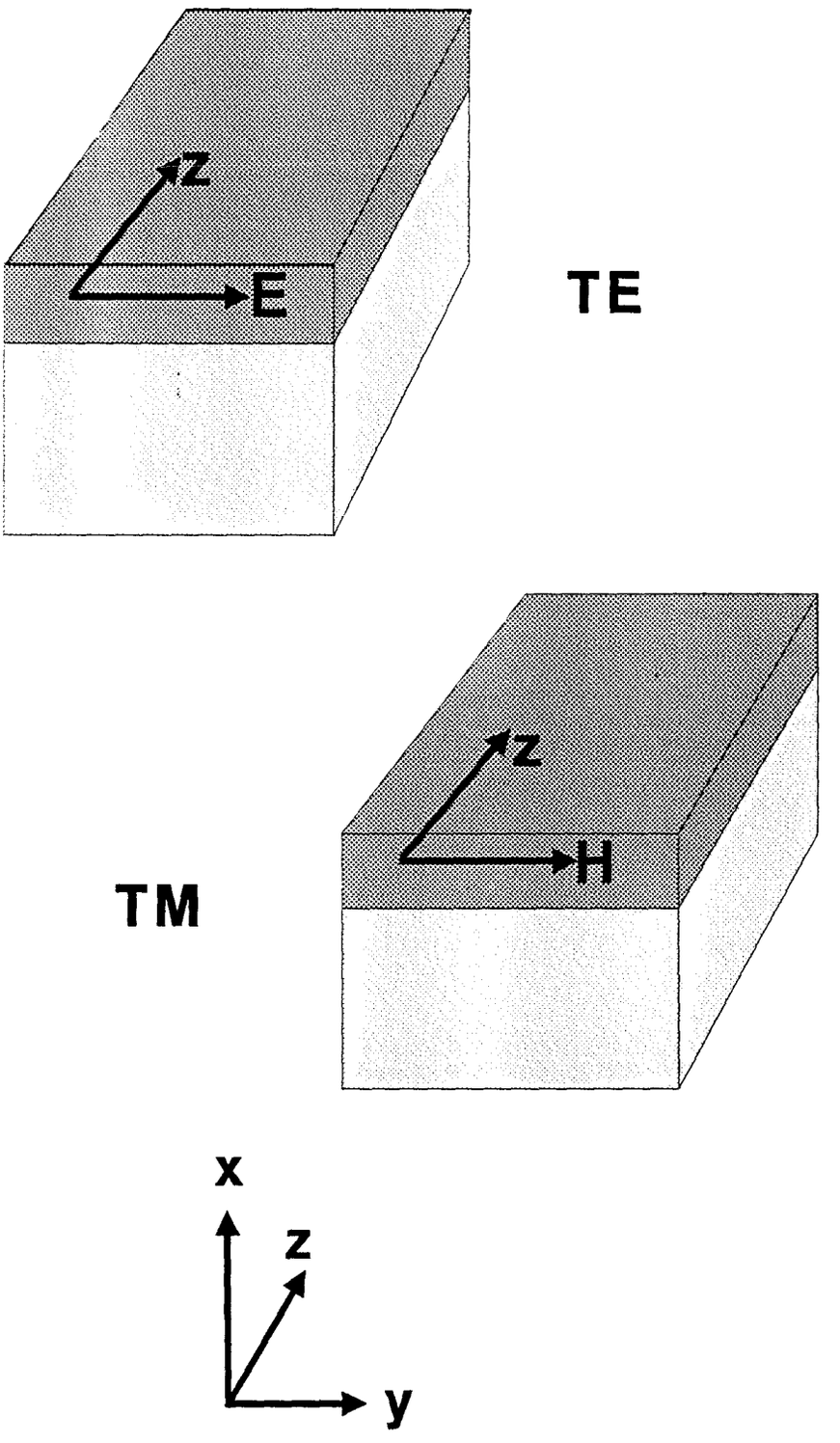

Figure 2.2 The orientation of the electric and magnetic field vectors in TE and TM modes

$$(\nabla^2 + \underline{k_0}^2)\underline{E}(\underline{r}) = 0 \tag{2.11}$$

where $c^2\underline{k_0}^2 = n^2\omega^2$ in a non-absorbing dielectric, $\underline{k_0}$ is the wavevector in free space of light with velocity c. Substitution of equation (2.10) into the Helmholtz equation yields the dispersion relations for each region

$$\alpha_{1x} = \sqrt{k_z^2 - \omega^2\mu_1\epsilon_1}$$

$$k_{2x} = \sqrt{\omega^2\mu_2\epsilon_2 - k_z^2} \tag{2.12}$$

$$\alpha_{3x} = \sqrt{k_z^2 - \omega^2\mu_3\epsilon_3}$$

The solutions to these equations can be found by noting the requirement of continuity of tangential $\underline{E}$ and $\underline{H}$ at the boundaries of region 2. Using equation (2.7) we can find the z component of the magnetic field

$$H_z(x,z) = \frac{i}{\omega\mu}\frac{\partial}{\partial x}E_y(x,z) \tag{2.13}$$

Substituting (2.10) into (2.13) gives

$$H_z(x,z) = \begin{bmatrix} \frac{-i\alpha_{1x}}{\mu\omega}A_1 e^{-\alpha_{1x}x} & x>d/2 \\ \frac{-ik_{2x}}{\omega\mu_2}A_2\sin(k_{2x}x+\psi) & |x|\le d/2 \\ \frac{i\alpha_{3x}}{\omega\mu_3}A_3 e^{\alpha_{3x}x} & x<-d/2 \end{bmatrix} e^{ik_z z} \tag{2.14}$$

Applying the boundary conditions at x=d/2 and eliminating A_1, A_2 results in

$$\tan(k_{2x}d/2+\psi) = \frac{\mu_2\alpha_{1x}}{\mu_1 k_{2x}} \tag{2.15}$$

A similar analysis can be used at x=-d/2. If the relation tan(x)=tan(x±mπ) is used these equations then become

$$k_{2x}d/2+\psi = \tan^{-1}\left(\frac{\mu_2\alpha_{1x}}{\mu_1 k_{2x}}\right) \pm m\pi \tag{2.16}$$

$$k_{2x}d/2-\psi = \tan^{-1}\left(\frac{\mu_2\alpha_{3x}}{\mu_3 k_{2x}}\right) \pm n\pi \tag{2.17}$$

Equations (2.16) and (2.17) can be added in order to eliminate ψ, which results in the equation

$$k_{2x}d-\tan^{-1}\left(\frac{\mu_2\alpha_{1x}}{\mu_1 k_{2x}}\right)-\tan^{-1}\left(\frac{\mu_2\alpha_{3x}}{\mu_3 k_{2x}}\right) = p\pi \tag{2.18}$$

An analogous treatment of the problem can be used to solve for the TM modes, which gives the equation

$$k_{2x}d-\tan^{-1}\left(\frac{\epsilon_2\alpha_{1x}}{\epsilon_1 k_{2x}}\right)-\tan^{-1}\left(\frac{\epsilon_2\alpha_{3x}}{\epsilon_3 k_{2x}}\right) = p\pi \tag{2.19}$$

These equations can be solved, either graphically or numerically using equation (2.12) to find k_{2x}. To simplify the solution of the two equations it is necessary to define several normalised variables in terms of the waveguide parameters [4]. The normalised frequency, υ, is given by

$$\upsilon = k_0 d\sqrt{n_2^2-n_3^2} \tag{2.20}$$

The waveguide parameter b is defined as

$$b = \frac{n_{eff}^2 - n_3^2}{n_2^2 - n_3^2} \tag{2.21}$$

In equation (2.21) n_{eff} is known as the effective index, and is given by $n_{eff} = k_z / k_o$. A further parameter, a, is defined which accounts for any asymmetry between the substrate and superstrate refractive indices, which is given below for both TE and TM modes

$$a^{TE} = \frac{n_3^2 - n_1^2}{n_2^2 - n_3^2} \tag{2.22}$$

$$a^{TM} = \frac{n_2^2}{n_1^2}(a^{TE}) \tag{2.23}$$

Using the above equations the guidance condition becomes

$$\upsilon\sqrt{1-b} = \tan^{-1}\left(M_1\sqrt{\frac{b}{1-b}}\right) + \tan^{-1}\left(M_2\sqrt{\frac{b+a}{1-b}}\right) + p\pi \tag{2.24}$$

M_1 and M_2 are scaling factors for TM modes, resulting from the differing asymmetry parameters, given by

$$M_1 = \frac{n_2^2}{n_3^2} \tag{2.25}$$

$$M_2 = \frac{n_2^2}{n_1^2} \tag{2.26}$$

The numerically evaluated solution of the guidance condition can be expressed in a graph of b against v for various values of p and a, as shown in figure 2.3.

The guidance condition may also be understood by considering the physical interpretation of the effective refractive index. If we assume that $n_1 < n_3 < n_2$, then the effective index can vary between values of n_2 and n_3. The value of n_{eff} is associated with the angle of light in the guide, θ, as shown in figure 2.1, in such a way that, as n_{eff} varies between n_3 and n_2, θ varies between $\pi/2$ and $\sin^{-1}(n_3 / n_2)$. If n_{eff} has a value close to that of n_2 the mode is well confined in the guide with very little of the field in the substrate or superstrate. However, if n_{eff} approaches the value of n_3, then the mode is near cut off, and much of the mode propagates in the substrate region.

For many laser and amplifier applications it is desirable to have a waveguide which supports a single mode, thus allowing diffraction limited performance of the output beam. Equation (2.24) enables a calculation of the size of waveguide which would result in the propagation of only one mode, in which case we can say that p=1. At the point where the second mode is just cut off, $n_{eff} = n_3$, from equation (2.21) we can say b = 0 therefore equation (2.24) becomes

$$\upsilon_1 = \tan^{-1}(M_2\sqrt{a})+\pi \qquad (2.27)$$

As only one mode is allowed to be confined a guide depth must be chosen such that

$$k_o d\sqrt{n_2^2-n_3^2} \leq \upsilon_1 \qquad (2.28)$$

so we can write

$$d_{sm} = \frac{\tan^{-1}(M_2\sqrt{a})+\pi}{k_0\sqrt{n_2^2-n_3^2}} \qquad (2.29)$$

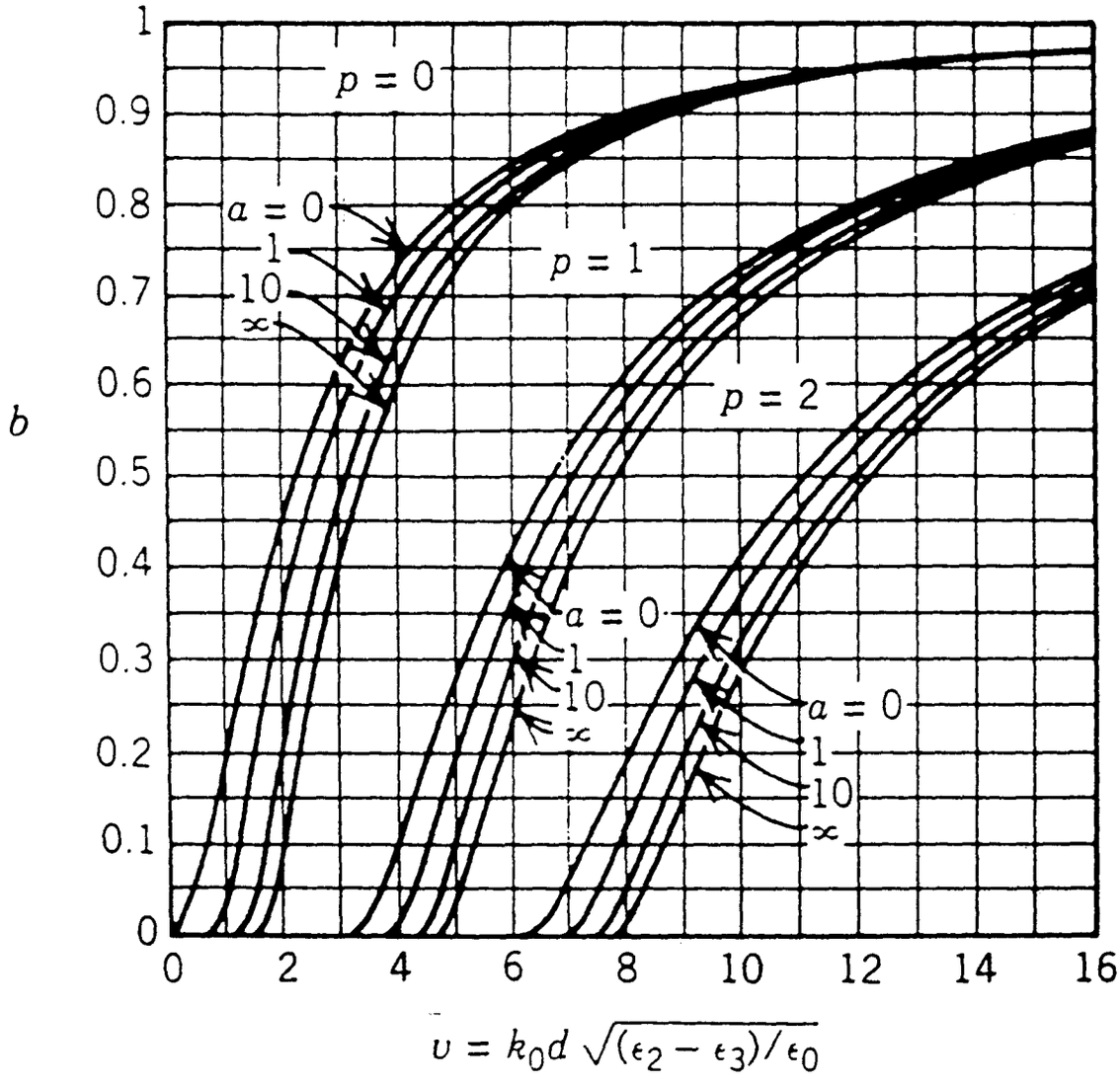

Figure 2.3 Normalised b-v diagram, taken from [1]

d_{sm} is the maximum depth of guide which will allow single mode operation.

The preferred choice of waveguide depth below d_{sm} will depend on a number of factors which should be considered and which depend upon, to a certain extent, the actual form of the guide itself. At waveguide depths just below d_{sm} most of the modal power is contained in the guided region, as the depth of the guide is reduced there is an increase in the modal power travelling in the substrate regions. Another factor to be considered is the peak intensity in the guide which increases with decreasing depth, until the point where the modal power in the guide drops off to such a level that the peak intensity tends to zero as the depth tends to zero. The optimum depth of guide will thus be as a result of a trade off between the modal power in the guided region and peak intensity, the exact nature of the compensation point will depend in part on waveguide losses, for high loss guides it may be preferable to have a large portion of the modal power travelling in the substrate, this would especially be true if the substrate itself were made of the same doped material as the guide and hence all the mode would experience gain.

2.3 Optically Pumped Waveguide Laser Theory

One reason for fabricating optical waveguides in rare earth doped laser host materials is to produce low threshold, efficient, waveguide lasers. The added confinement, and improved overlap, of the pump and signal beams can lead to significant advantages over bulk lasers.

In the following analysis I will assume that the waveguide mode has a Gaussian form in both the guided and unguided directions. This assumption will hold true in the plane of the guide as the pump and signal radiation see no confinement and have, therefore, a Gaussian profile. In the confined direction there will be a slight inaccuracy due to the difference in the overlap integrals between two Gaussian profiles and two waveguide mode profiles, as shown in Appendix A. This correction is very small for well confined modes in practical waveguide systems and so will be ignored in the rest of

this chapter.

I will start with a general case of a bulk longitudinally pumped four level laser, with a cavity of the form shown in figure 2.4.

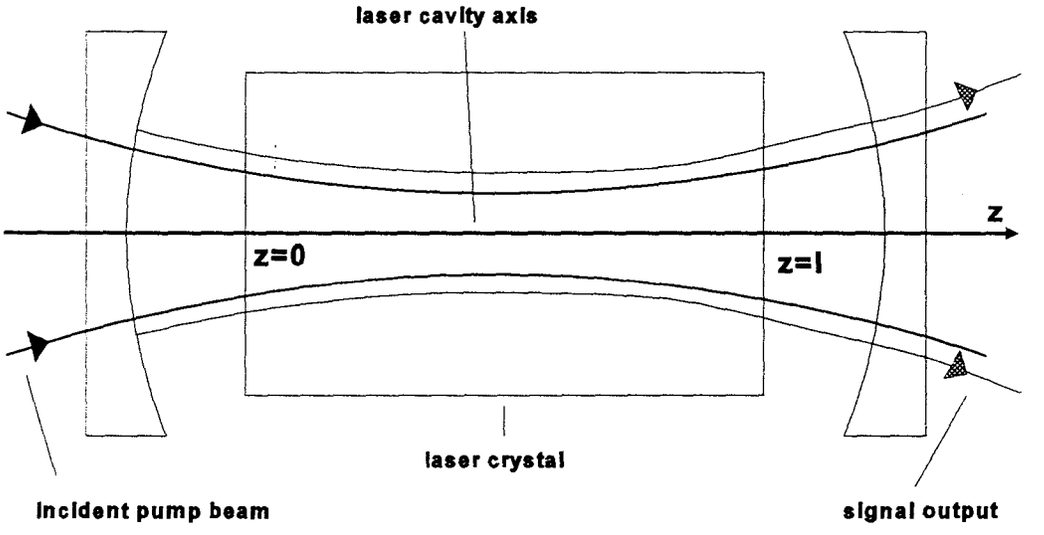

Figure 2.4 Schematic diagram of the pump and signal beam paths inside a bulk laser

The threshold for such a laser can be written as [5]

$$P_{th} = \frac{\pi h \nu_p}{4\sigma_e \tau_f}(\overline{w_p^2}+\overline{w_s^2})\cdot L \qquad (2.30)$$

where ν_p is the pump frequency, σ_e is the emission cross section at the laser wavelength, τ_f is the fluorescence lifetime, $\overline{w}_p$ and $\overline{w}_s$ are the average pump and signal spot sizes, and L is the round trip loss in the system. This equation assumes the pump and signal to be fundamental Gaussian modes.

To produce the optimum spot sizes for a bulk system the pump beam should be focused through the gain medium so as to minimise w_p and to maximise the gain the resulting pump spot size should be [5]

$$w_{p,\,opt} = \sqrt{\frac{\lambda l}{\sqrt{3}\pi n}} \tag{2.31}$$

where λ is the wavelength, l is the length of the gain medium, and n is its refractive index. Substituting equation (2.31) into (2.30) gives us the threshold obtainable in a bulk laser with optimum pump spot sizes,

$$P_{th} = \frac{h\nu_{pl}}{4\sqrt{3}\sigma_e\tau_f}(\lambda_p+\lambda_s)\cdot L \tag{2.32}$$

In a planar waveguide the pump and signal spot sizes are different in the guided and unguided planes, and so (2.30) becomes

$$P_{th} = \frac{\pi h\nu_p}{4\sigma_e\tau_f}[(\overline{w_{px}^2}+\overline{w_{sx}^2})^{1/2}(\overline{w_{py}^2}+\overline{w_{sy}^2})^{1/2}]\cdot L \tag{2.33}$$

where the subscripts x,y denote the spot sizes in the guided and unguided planes respectively. The division of equation (2.33) by equation (2.32) will give the relative thresholds of waveguide (P_{th}^{wg}) and bulk (P_{th}^{b}) systems

$$\frac{P_{th}^{wg}}{P_{th}^{b}} = \frac{\sqrt{3}\pi n(\overline{w_{px}^2}+\overline{w_{sx}^2})^{1/2}(\overline{w_{py}^2}+\overline{w_{sy}^2})^{1/2}}{l(\lambda_p+\lambda_s)}\cdot\frac{L_{wg}}{L_b} \tag{2.34}$$

where L_{wg} and L_b are the overall round trip losses for the waveguide and bulk systems respectively. It can be seen that the planar waveguide will have the largest advantage over the bulk system when the spot sizes in the waveguide are small and when there is a long length of the gain medium. One disadvantage with a waveguide system is that the

overall loss in the system is often larger than in the bulk, due to an additional propagation loss which is a consequence of the waveguide fabrication procedure. The ability to confine the mode to average spot sizes much smaller than is possible in a bulk system, can overcome this additional loss.

The slope efficiency, η, of such a laser system is given by [6]

$$\eta = \frac{T\nu_s}{L\nu_p}(1-e^{\alpha_p l})\eta_q\eta_{ps} \tag{2.35}$$

where T is the transmission of output coupler, η_q is the pumping quantum efficiency, η_{ps} is a factor representing the overlap between the pump and signal modes and is given by

$$\eta_{ps} = \frac{\overline{w_{sx}}\ \overline{w_{sy}}(2\overline{w_{px}^2}+\overline{w_{sx}^2})^{1/2}(2\overline{w_{py}^2}+\overline{w_{sy}^2})^{1/2}}{(\overline{w_{px}^2}+\overline{w_{sx}^2})(\overline{w_{py}^2}+\overline{w_{sy}^2})} \tag{2.36}$$

In terms of slope efficiency the main difference between bulk and waveguide cases is due to the larger propagation loss in the waveguide, which reduces the efficiency. To compensate for this a higher transmission output coupler must be used in a waveguide to get the same slope efficiency as the bulk system. The increase in output coupling results in higher overall loss in the system and hence has a detrimental effect on the threshold. For well confined modes however, in low loss waveguides, the threshold may still be lower while having the same slope efficiency as the bulk system.

Quasi-Three-Level Lasers

One area where waveguides have a particular advantage is for quasi-three-level transitions. In such a case there is a significant thermally induced population in the lower laser level, which results in a reabsorption loss at the laser wavelength. The additional reabsorption loss may be large relative to the waveguide propagation loss, which thus renders it less significant than in the four level case, and increases the advantage obtainable over a bulk system. Figure 2.5, overleaf, shows an energy level diagram for

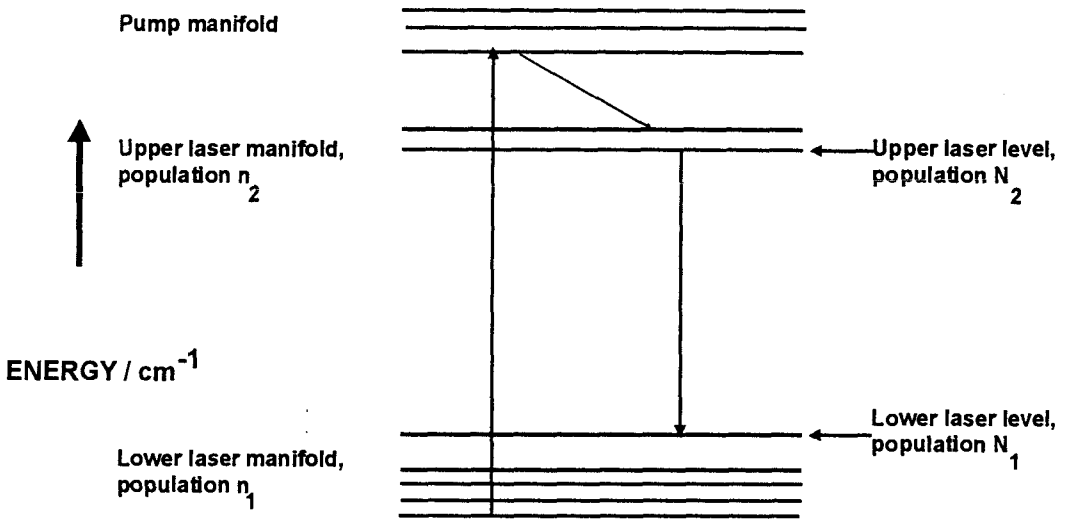

Figure 2.5 Typical energy level diagram for a quasi-three-level transition

a typical quasi-three-level transition. Optical pumping followed by a rapid nonradiative decay results in population in the upper laser level. The laser transition terminates on a Stark split level of the ground state manifold.

The populations of the Stark split upper and lower laser levels are related to the total population of their respective manifolds by the expression $N_{1,2} = f_{1,2} \cdot n_{1,2}$ where f_1 and f_2 are the fraction of the total population of the lower and upper manifolds which is in the laser level. Analysis of such a laser system starts with the steady state rate equations given in [7,8] from which we can write

$$\frac{d\Delta N(x,y,z)}{dt} = 0 \tag{2.37}$$

$$= (f_1 + f_2) R r_p(x,y,z) - \frac{\Delta N(x,y,z) - \Delta N^o}{\tau} - \frac{(f_1 + f_2) c \sigma \Delta N(x,y,z)}{n} \Phi \phi(x,y,z)$$

where $\Delta N = N_2 - N_1$ is the population inversion resulting from optical pumping, ΔN^o is the unpumped population inversion, R is the pumping rate, Φ is the photon number, $r_p(x,y,z)$ and $\phi(x,y,z)$ are the pump and laser distributions, c is the speed of light in a vacuum, σ is the emission cross section and n is the refractive index of the gain medium . Assuming there is no pump saturation the pumping rate and photon number are given by

$$R = \frac{P_p(1-e^{-\alpha l})}{h\nu_p} \qquad \Phi = \frac{2nlP_L}{ch\nu_s} \tag{2.38}$$

where P_p is the incident pump power and P_L is the average intracavity laser power. The pump and laser distributions are normalised in such a way that

$$\int r_p(x,y,z)dV = \int \phi(x,y,z)dV = 1 \tag{2.39}$$

The steady state solution for $\Delta N(x,y,z)$ can be found from equation (2.37), using $f = f_1 + f_2$ and assuming that ΔN^0 is equal to the unpumped population of the lower laser level we can write

$$\Delta N(x,y,z) = \frac{\tau f R r_p(x,y,z) - N_1^o}{1 + \frac{c\sigma\tau}{n} f\, \Phi\phi(x,y,z)} \tag{2.40}$$

The growth of the signal intensity propagating through the laser medium is related to the gain, g(x,y,z) by

$$\frac{dI(x,y,z)}{dz} = g(x,y,z)I(x,y,z) \tag{2.41}$$

The condition for lasing is that the round trip loss is equal to the round trip gain, this can

be described, if the losses are small, by the equation

$$\int_{roundtrip} dP_L(z) = 2\int_0^l \frac{dP_L(z)}{dz}dz = P_L(L+T) \qquad (2.42)$$

L gives the loss in the cavity and T is the transmission of the output mirror at the laser wavelength. $P_L(z)$ is the total single pass power, which can be expressed as

$$P_L(z) = \int_{-\infty}^{\infty}\int_{-\infty}^{\infty} I(x,y,z)dxdy \qquad (2.43)$$

Differentiating equation (2.43) with respect to z gives

$$\frac{dP_L(z)}{dz} = \int_{-\infty}^{\infty}\int_{-\infty}^{\infty} \frac{dI(x,y,z)}{dz}dxdy \qquad (2.44)$$

From equations (2.41), (2.42) and (2.44) we get

$$2\int_0^l\int_{-\infty}^{\infty}\int_{-\infty}^{\infty} g(x,y,z)I(x,y,z)dxdydz = P_L(L+T) \qquad (2.45)$$

The gain in the system, g, is given by the population inversion multiplied by the emission cross section, and hence expressing I(x,y,z) as equal to $(ch\nu_s/2n)\Phi\phi(x,y,z)$ and combining equations (2.40) and (2.45) we get the expression

$$2\int_0^l\int_{-\infty}^{\infty}\int_{-\infty}^{\infty} \frac{ch\nu_s}{2n}\frac{\sigma\tau fRr_p(x,y,z)-N_o^1\sigma}{1+\frac{c\sigma\tau}{n}f\Phi\phi(x,y,z)}\Phi\phi(x,y,z)dxdydz = P_L(L+T) \qquad (2.46)$$

To proceed further it is necessary to calculate the pump and laser distributions. In a waveguide we can assume that the spot sizes do not vary with distance through the

crystal so the pump and laser distributions are

$$r_p(x,y,z) = \frac{2\alpha}{\pi w_{px} w_{py}(1-e^{-\alpha l})} \exp\left(\frac{-2x^2}{w_{px}^2}\right) \exp\left(\frac{-2y^2}{w_{py}^2}\right) e^{-\alpha z} \tag{2.47}$$

$$\phi(x,y,z) = \frac{2}{\pi w_{sx} w_{sy} l} \exp\left(\frac{-2x^2}{w_{sx}^2}\right) \exp\left(\frac{-2y^2}{w_{sy}^2}\right) \tag{2.48}$$

Combining equations (2.38), (2.46), (2.47) and (2.48) yields

$$2\int_0^l \int_{-\infty}^{\infty} \int_{-\infty}^{\infty} \frac{ch\nu_s \Phi}{2n} \frac{\left[\frac{2\sigma\tau f P_p \alpha}{h\nu_p \pi w_{px} w_{py}} \exp\left(-\frac{2x^2}{w_{px}^2}\right) \exp\left(\frac{-2y^2}{w_{py}^2}\right) e^{-\alpha z} - N_1^o \sigma\right]}{\left[1 + \frac{2c\tau\sigma f \Phi}{n\pi w_{sx} w_{sy} l} \exp\left(\frac{-2x^2}{w_{sx}^2}\right) \exp\left(\frac{-2y^2}{w_{sy}^2}\right)\right]}$$

$$\cdot \frac{2}{\pi w_{sx} w_{sy} l} \exp\left(\frac{-2x^2}{w_{sx}^2}\right) \exp\left(\frac{-2y^2}{w_{sy}^2}\right) dx\,dy\,dz = \frac{ch\nu_l \Phi}{2nl}(L+T) \tag{2.49}$$

To simplify this expression the following substitutions can be made

$$B = \frac{2N_1^0 \sigma l}{L+T}, \qquad F = \frac{4P_p \tau\sigma(1-e^{-\alpha l})}{\pi h\nu_p w_{sx} w_{sy}(L+T)}, \qquad S = \frac{2c\sigma\tau\Phi}{n\pi w_{sx} w_{sy}}, \tag{2.50}$$

$$a_x = \frac{w_{px}}{w_{sx}}, \quad a_y = \frac{w_{py}}{w_{sy}}, \quad u = \frac{x}{w_{px}}, \quad v = \frac{y}{w_{py}}$$

The integration over z of the resulting equation gives

$$\frac{2fF}{\pi}\int_{-\infty}^{\infty}\int_{-\infty}^{\infty}\frac{\left[e^{-2u^2}e^{-2v^2}-\frac{Ba_xa_y}{fF}\right]e^{-2a_x^2u^2}e^{-2a_y^2v^2}}{\left[1+fSe^{-2a_x^2u^2}e^{-2a_y^2v^2}\right]}dudv = 1 \qquad (2.51)$$

F and S are the normalised pump and laser powers, and govern the input / output characteristics of the laser, which can therefore be calculated from equation (2.51). The normalised pump and laser powers are related to the actual pump and laser powers, P_p and P_l respectively, as shown below

$$P_p = \frac{\pi h\nu_p w_{sx} w_{sy}(L+T)}{4\sigma\tau(1-e^{-\alpha l})}\cdot F \qquad (2.52)$$

$$P_l = \frac{\pi h\nu_s w_{sx} w_{sy} T}{4\sigma\tau}\cdot S \qquad (2.53)$$

At threshold the normalised laser power is zero, and so equation (2.51) can be solved to give a threshold for the normalised pump power

$$F_{th} = \frac{\left[(1+a_x^2)(1+a_y^2)\right]^{1/2}(1+B)}{f} \qquad (2.54)$$

This enables a final calculation for the actual pump threshold power from equation (2.52)

$$P_{th}=\frac{\pi h\nu_p}{4\sigma\tau f}[(\overline{\omega_{px}^2}+\overline{\omega_{sx}^2})^{1/2}(\overline{\omega_{py}^2}+\overline{\omega_{sy}^2})^{1/2}][L+T+2N_1^0\sigma l] \qquad (2.55)$$

The slope efficiency for a quasi-three-level system is the same as that given in equation (2.35) except the loss term is now ($L+2N_1^0\sigma l$), and so it is evident that for

systems with significant reabsorption loss, i.e. the reabsorption loss term dominates the propagation loss term, the slope efficiency is not significantly changed in a waveguide relative to bulk.

2.4 Optical Amplifier Theory

The theory of optical amplifiers can be found in several textbooks [9, 10] so here I will only briefly outline some of the relevant points. Starting from the equation for unsaturated, small-signal, single pass power gain through a laser medium of length l, we can write [9, p.280]

$$G_0 = \frac{I(l)}{I(0)} = e^{g_0 l} \tag{2.56}$$

where G_0 is the gain, I(0) is the intensity of the signal at z=0, I(l) is the intensity at z=l, and g_0 is the unsaturated gain coefficient, given by [9, p.292]

$$\frac{1}{I}\frac{dI}{dz} = g_0(x,y,z) \tag{2.57}$$

In the case of a double pass amplifier, with normal incidence reflection of the signal back through the gain medium, the optical small-signal gain seen is

$$G_0 = e^{2g_0 l} \tag{2.58}$$

Derivation of Small-Signal Gain Coefficient for Waveguide Amplifiers

The analysis of the gain coefficient for a four level amplifier begins in a similar fashion to the quasi-three-level laser threshold calculations with the rate equations, which can be written, for a four level system as [8]

$$\frac{d\Delta N(x,y,z,t)}{dt} = Rr_p(x,y,z,t) - \frac{c}{n}\Phi\phi(x,y,z,t)\Delta N(x,y,z,t) - \frac{\Delta N(x,y,z,t)}{\tau} \tag{2.59}$$

$$\frac{d\Phi(t)}{dt} = \int_{amplifier} \frac{c}{n}\sigma\Delta N(x,y,z,t)\Phi\phi(x,y,z,t)dV - \gamma\Phi(t) \qquad (2.60)$$

where $\gamma\Phi(t)$ is a loss term, with $\gamma=1/\tau_c$, τ_c being the cavity lifetime. For an amplifier the loss term can be replaced by a term for the gain of the amplifier, g_0, which is given in terms of gain / unit length whereas γ is a loss per unit time and so we must write $g_0=\gamma/c$. The steady state solution to equation (2.59) can be rearranged to give

$$\Delta N(x,y,z) = \frac{\tau R r_p(x,y,z)}{1+\frac{c\sigma\tau}{n}\Phi\phi(x,y,z)} \qquad (2.61)$$

Substituting for ΔN in equation (2.60) yields the steady state equation

$$g_0 = \int_{amplifier} \frac{\frac{\sigma}{n}\phi\tau R r_p}{1+\frac{c\sigma\tau}{n}\Phi\phi(x,y,z)} dV \qquad (2.62)$$

The pumping rate, R, can be written as

$$R = \frac{P_p\eta_q(1-e^{-\alpha l})}{h\nu_p} \qquad (2.63)$$

where η_q is the fraction of absorbed photons which result in population of the upper laser level. For small signals the condition applies that

$$\frac{\Phi\phi(x,y,z)c\sigma\tau}{n} \ll 1 \qquad (2.64)$$

so we can write equation (2.62) as

$$g_0 = \frac{P_p \eta_q (1-e^{-\alpha l})\sigma\tau}{nh\nu_p} \int_{ampl} r_p(x,y,z)\phi(x,y,z)dV \qquad (2.65)$$

assuming spot sizes do not vary through the length of the amplifier, Equations (2.47) and (2.48) substituted into Equation (2.65) give

$$g_0 = \frac{P_p \eta_q \sigma\tau}{h\nu_p} \int_{ampl} \frac{4\alpha}{\pi^2 w_{px} w_{py} w_{sx} w_{sy} l} \exp\left(\frac{-2x^2}{w_{px}^2} - \frac{2x^2}{w_{sx}^2} - \frac{2y^2}{w_{py}^2} - \frac{2y^2}{w_{sy}^2} \right) e^{-\alpha z} dV \qquad (2.66)$$

integration of this equation with respect to x and y yields

$$g_0 = \frac{2\alpha P_p \eta_q \sigma\tau}{\pi h \nu_p l} \int_0^l \frac{e^{-\alpha z}}{(w_{px}^2 + w_{sx}^2)^{1/2}(w_{py}^2 + w_{sy}^2)^{1/2}} dz \qquad (2.67)$$

Integration over the length of the amplifier with respect to z, and using equation (2.56) gives a final expression for the small-signal gain exponent in a single pass amplifier

$$\ln(G_0) = \frac{2P_p \eta_q \sigma\tau(1-e^{-\alpha l})}{\pi h \nu_p} \cdot \frac{1}{(w_{px}^2 + w_{sx}^2)^{1/2}(w_{py}^2 + w_{sy}^2)^{1/2}} \qquad (2.68)$$

For a double pass amplifier there is a factor of two increase in the gain exponent, resulting from a change in the limits of the integration.

Saturation Behaviour

One limiting factor of real amplifier systems is that a large input signal may be able to saturate the population inversion, and hence reduce the gain observed. Again I will start with a formula taken from [9, p.292], giving the increase of intensity of a plane wave with distance through a gain medium

$$\frac{dI}{dz} = gI = \Delta N \cdot \sigma I \tag{2.69}$$

where g is the saturated gain coefficient. The population difference will saturate with increasing signal strength, in such a way that we can write

$$\Delta N = \Delta N_0 \left(\frac{1}{(1 + W\tau_{eff})} \right) \tag{2.70}$$

where W is the stimulated transition probability, and τ_{eff} is an effective lifetime for the transition, ΔN_0 is the unsaturated, small-signal, population inversion. The stimulated transition probability is proportional to the signal intensity inside the gain medium, and can be shown to be given by

$$W = \frac{\sigma I}{h\nu} \tag{2.71}$$

Rearranging equation (2.70) and combining with equation (2.69), it is possible to show that gain coefficient will saturate in the form

$$g = \frac{\Delta N_o \sigma}{1 + (\sigma\tau_{eff}/h\nu)I} = \frac{g_o}{1 + I/I_s} \tag{2.72}$$

where g_o is the unsaturated gain coefficient, I_s is known as the saturation intensity and is the signal intensity required to reduce the gain to half its small signal value, it can be written as

$$I_s = \frac{h\nu}{\sigma\tau_{eff}} \tag{2.73}$$

Two physical explanations of the saturation intensity are that it is the photon flux that corresponds to one photon per cross section per effective lifetime, it is also the intensity required to equalise the stimulated and spontaneous emission rates.

The input / output characteristics of an optical amplifier can be deduced from rearranging equation (2.69). For a double pass amplifier where the signal is reflected back through the gain medium, this equation becomes

$$\frac{1}{I^{+}(z)+I^{-}(z)}\frac{dI^{+}}{dz}\frac{dI^{-}}{dz} = g(I) = \frac{g_o}{1+I/I_s} \qquad (2.74)$$

where I^+, I^- relate to the intensities travelling in opposite directions i.e. the two passes of the signal through the gain medium. If we assume that the input intensity is I_i at z=0, and the output intensity is I_o then equation (2.74) can be simplified and then integrated to give

$$\ln\left(\frac{I_o}{I_i}\right)+2\frac{I_o-I_i}{I_s} = 2g_o l = \ln G_o \qquad (2.75)$$

where G_o is the unsaturated gain. Equation (2.75) can be rearranged to give the actual power gain of the amplifier under any input signal power

$$G = \frac{I_o}{I_i} = G_o \exp\left[-2\frac{I_o-I_i}{I_s}\right] \qquad (2.76)$$

This equation shows that the saturated gain is reduced with increasing extracted power (I_o -I_i). Equation (2.76) can be rearranged to give formulae relating the input or output intensities solely to the unsaturated and saturated gains and the saturation intensity

$$\frac{I_i}{I_s} = \frac{1}{2(G-1)} \ln\left(\frac{G_0}{G}\right) \qquad (2.77)$$

$$\frac{I_o}{I_s} = \frac{G}{2(G-1)} \ln\left(\frac{G_0}{G}\right) \qquad (2.78)$$

As the signal intensity is increased the gain saturates down to the limiting value of unity, or G=1, at which point the amplifier is essentially transparent to the signal. The amount of power that is extracted from the amplifier is given by I_o - I_i, which can be found from equations (2.77,2.78)

$$I_{extracted} = I_o - I_i = I_s \ln\left(\frac{G_0}{G}\right) \tag{2.79}$$

this quantity gives the amount of power actually supplied to the input signal by the amplifier. At low signal intensities, when the gain is near the small signal value, the extracted power and output power are nearly the same, as the gain begins to saturate the extracted power approaches the value

$$I_{available} = I_s \cdot \ln(G_0) \tag{2.80}$$

this is the limiting value which gives the maximum extractable power from the amplifier, or the maximum available power which the amplifier can give to the input signal. A problem with real amplifier systems is that in order to extract the maximum available power it is necessary to run the amplifier with a gain approaching that of unity, because from equation (2.76) the extracted power will decrease with increasing gain. This point can be demonstrated by defining the energy extraction efficiency to be

$$\eta_{ext} = \frac{I_{extracted}}{I_{available}} = \frac{\ln(G_0) - \ln(G)}{\ln(G_0)} = 1 - \left(\frac{G(dB)}{G_0(dB)}\right) \tag{2.81}$$

This value plotted against gain will be a straight line and so it is apparent that to extract half the available power it is necessary to lose half the dB gain of the amplifier.

The above theoretical analysis does not account for certain factors which could adversely affect the small-signal gain, and hence output powers, of the amplifier relative to the value predicted. Upconversion, excited state absorption of the pump light or temperature dependant shifts in the emission line positions may all have such an affect

on the amplifier gain. Pump saturation effects can lead to a change in the population inversion profile, hence reducing the signal / inversion overlap, which may also influence the measured small-signal gain, all these factors will be considered in Chapter 5.

References

1. D.L.Lee, Electromagnetic Principles of Integrated Optics, Wiley, 1986

2. A.Yariv, Optical Electronics, Holt-Sanders, 1985

3. H.Nishimara and T.Suhara, Optical Integrated Circuits, McGraw-Hill, 1989

4. H.Kogelnik and V.Ramaswamy, Applied Optics **13**, 1857, 1975

5. M.F.J.Digonnet and C.J.Gaeta, Applied Optics **24**, 333, 1985

6. W.A.Clarkson and D.C.Hanna, Journal of Modern Optics **36**, 483, 1989

7. W.P.Risk, Journal of the Optical Society of America B **5**, 1412, 1988

8. K.Kubodera and K.Otsuka, Journal of Applied Physics **50**, 653, 1979

9. A.E.Siegman, Lasers, University Science Books, 1986

10. O.Svelto, Principles of Lasers, Plenum, 1989

Chapter 3 - Experimental Techniques

3.1 Introduction

This chapter will describe the apparatus and techniques used for the characterisation of optical waveguides, as well as the waveguide laser and amplifier experiments. The experimental details for the bulk laser experiment will also be outlined.

3.2 Launching Light into Waveguides.

To perform the experiments described later in the chapter it is first necessary to launch light into the waveguide and to collect the light exiting it. Two methods were used to couple light into the waveguides; the first used microscope objectives, and the second cylindrical lenses. In both cases the lenses were mounted on three axis (xyz) positioners and the waveguide on a five axis (xyz$\theta\Phi$) positioner. The waveguide was aligned so that the end faces were perpendicular to the direction of the incoming light. The general arrangement for launching light into the waveguide using microscope objectives is shown in figure 3.1, below

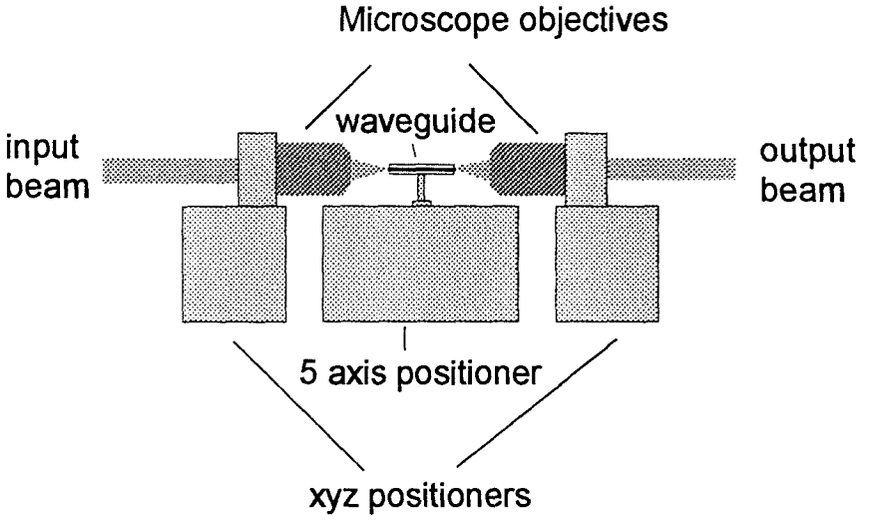

Figure 3.1 Launching light into waveguides using microscope objectives

From a distance of several centimetres from the crystal the input microscope objective was moved horizontally towards the guide, while observing the system of Lloyd's mirror fringes of the unlaunched pump beam at the position of the output objective. The optimum launch of the pump into the guide was when the Lloyd's fringes stopped separating as the objective was moved towards the guide before starting to converge. The best vertical alignment was similarly found to be where the fringes were at their most separated. The output objective could then be positioned to focus the light exiting the waveguide at the desired place.

In the case where cylindrical lenses were used to launch light into the waveguide the alignment procedure is similar to that used for microscope objectives, with a cylindrical lens being used to focus the light in the guided plane; this produces a thin line of light which matches the geometry of a planar waveguide. For laser and amplifier experiments, however, the optimum gain is achieved by focusing the pump radiation so as to optimise the launch in the guided plane, and focusing confocally through the length of the crystal in the unguided plane. A cylindrical lens should be chosen which focuses to a spot size w_y in the unguided direction such that the confocal parameter, b, is equal to the crystal length. This condition may be written as

$$b = \frac{2\pi w_y^2 n}{M^2 \lambda} = l \qquad (3.1)$$

where l is the crystal length, n is the refractive index, and λ is the wavelength. This is equivalent to collimating the pump beam through the length of the crystal. M^2 is a parameter giving the divergence of a beam relative to that of a diffraction limited beam which is focused to the same spot size. That is to say that a beam with an M^2 of 10, say, will be 10 times less diverging than a diffraction limited beam when focused to an equal spot size. A diffraction limited beam will have, therefore, an M^2 equal to one; the output from a broad stripe diode laser, for example, may have M^2s of 100 and 1 in orthogonal planes.

3.3 Detector Choice

For the experiments which will be described later in this chapter it is necessary to choose appropriate detectors; this is primarily determined by the wavelength to be detected as shown in table 3.1, below. Other considerations to be taken into account are the area, the sensitivity and the speed of the detector. At low light levels photodiodes are not very efficient and it is often better to use a photomultiplier, for example. For spectroscopic experiments it can be useful to use a photodiode array which can give a rapid coverage of a whole region of the spectrum, however in this case the resolution and spectral coverage will be partly determined by the groove density of the grating although the resolution is normally limited by the width of the monochromator slits.

Table 3.1

Wavelength Range	**Detector Type**	**Notes**	**Device Used**
~0.4 - 1.1μm	silicon photodiode (Si)	can be cheap, large area ~ 100mm^2	Radio Spares type RS-651-995, RS-303-674
~0.4 - 1.0μm	photomultiplier	more sensitive than Si for low light levels	
~0.8 - 1.9μm	germanium photodiode (Ge)	Can get fast response ~ 0.5ns	Hammamatsu type B2297-02
~1.5 - 2μm	indium gallium arsenide (InGaAs)	electrically cooled for longer wavelengths	EPITAXX Optoelectronic Devices
~1 - 3.8μm	indium antimonide (InSb)	liquid nitrogen cooled, high vacuum needed	EG&G Judson J10D series

Wavelength Range	Detector Type	Notes	Device Used
~1 - 5μm	indium arsenide (InAs)	liquid nitrogen cooled, high vacuum needed	EG&G Judson model J12D-M204-RO1M

In the case of neodymium and thulium doped laser host crystals the fluorescence lifetime of the upper laser level, for the 1μm and 2μm transitions respectively, is typically between 0.2ms and 5ms; the detectors used were fast enough to measure changes over time periods of this order.

3.4 Spectroscopy Experiments

Before describing in detail the spectroscopy experiments performed I shall give some consideration to practical methods for optimising the resolving power and optical throughput of light in spectrometers. One important concept to consider is that of geometric extent (geometric étendue) which characterises the ability of an optical system to accept light. The geometric extent of a system is a function of the area of the emitting source, S, and the solid angle into which light propagates from the source and is given by [1]

$$G = \pi S \sin^2 \Omega \qquad (3.2)$$

where Ω is the half angle of light collected by the focusing lens from a source. The geometric extent of a system is determined by the worst segment of the whole system, and so to optimise a system in terms of light collection and stray light reduction the geometric extent of each element in the system should be matched.

For light emitted from a waveguide the relatively complicated procedure required to match the geometric extents of the elements in a system, in order to allow efficient capture and propagation of all available light, is greatly simplified by collecting the light

and launching into the monochromator using microscope objectives. The numerical aperture can be expressed as [2]

$$N.A. = n \sin\Omega \tag{3.3}$$

so we can write equation (3.2) in the form

$$G = \pi S(NA)^2 \tag{3.4}$$

The problem now is reduced to that of collimating the light exiting the waveguide and focusing it into the monochromator using microscope objectives with an N.A. matching that of the monochromator.

One further important feature is the choice of grating used in a monochromator; the resolving power, R, of an instrument gives a measure of the ability to resolve between two adjacent spectral lines and can be written as

$$R = \frac{\lambda}{d\lambda} = kN \tag{3.5}$$

where k is the spectral order and N is the number of lines on the grating. Using a grating with as many lines/mm as possible therefore increases the resolving power of the system. It should be noted, however, that for the short focal length monochromators used the resolution is normally limited by the slit width which will allow transmission of sufficient light to be detected.

Absorption Spectroscopy

White light absorption spectra of the waveguides could be obtained by using the apparatus shown in figure 3.2. Light from a tungsten filament lamp was coupled into the waveguide in the manner described in section 3.2. Light transmitted through the waveguide was collimated using a microscope objective and focused into a monochromator using another microscope objective whose numerical aperture matched that of the monochromator. The monochromator used was an EG&G Princeton Applied

Research Model 1235 Digital Triple Grating Spectrograph[1], with a 1000 element Si diode array. The gratings were ruled with 150, 600 and 1200 lines/mm and blazed at 500nm, 1000nm and 250nm. A computer interfaced with the detector allowed direct readout of the spectra.

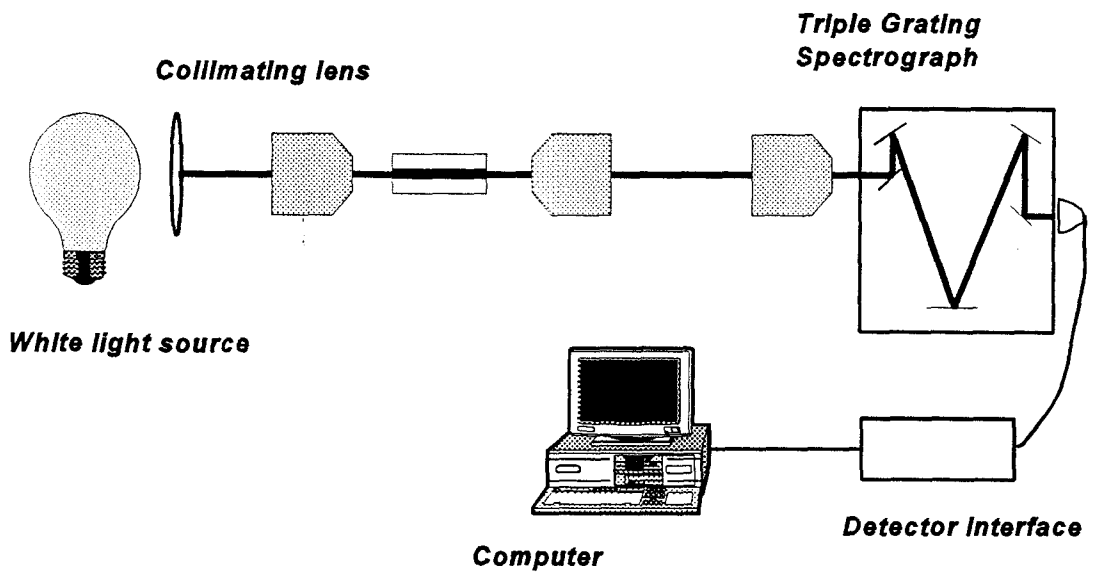

Figure 3.2 Experimental setup for measuring white light absorption spectra in waveguides

Fluorescence Spectroscopy.

The fluorescence spectra from waveguides can be measured in two different ways, depending on the wavelength at which the measurement is desired. For measurements at wavelengths below about 1100nm the experimental setup is similar to that used for absorption spectroscopy, but with the white light source being replaced with a pump laser tuned to the absorption band of the rare earth dopant. For

[1] This is so called as three gratings are mounted on a motorised rotation stage

measurements above 1100nm the experimental arrangement was that shown in Figure 3.3. The fluorescence was temporally modulated using an optical chopper with a 1/2 duty cycle, focused into a motor driven monochromator and detected with a photodiode, the output from which could be boosted using a lock in amplifier, and plotted on a chart recorder as fluorescence intensity against wavelength. The spectral resolution of the system could be analysed by looking at the spectral width of the pump light. The spectra were not adjusted for detector response, because the object was usually to compare the spectra in waveguides with that of a bulk sample, furthermore for the reasonably small spectral regions covered the detector response can often be assumed to be approximately constant.

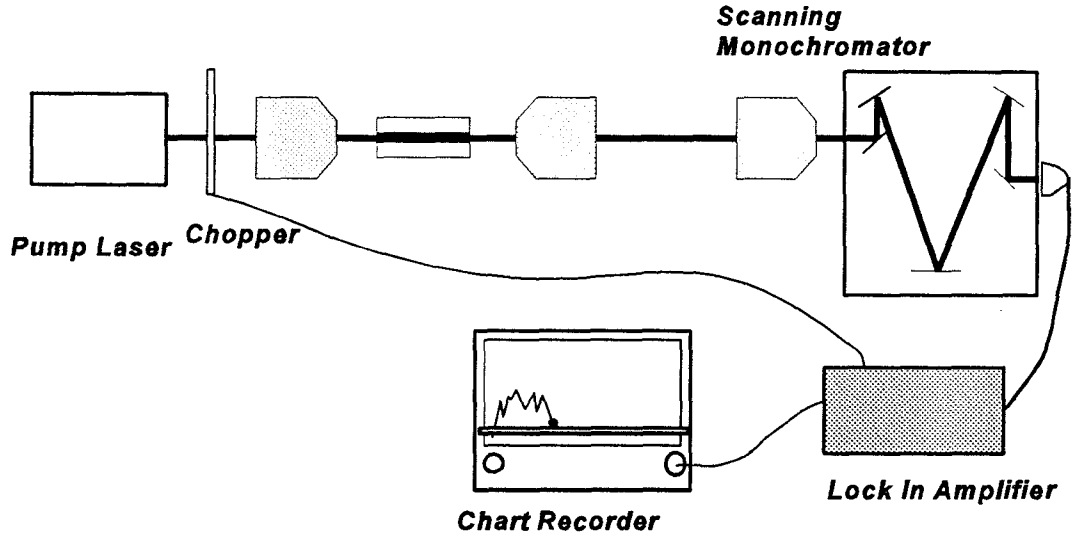

Figure 3.3 Experimental setup for fluorescence measurements

Determination of Emission Cross Section for Waveguides from Fluorescence Linewidth

Many methods of waveguide fabrication result in a broadening of absorption and emission lines relative to those in bulk samples. The emission cross section for a

transition is given by equation (3.6) [3]

$$\sigma_e = \frac{\eta\lambda_p^5}{\tau_f \left(\int \lambda I(\lambda) d\lambda\right) f 8\pi n^2 c} \cdot I(\lambda_p) \qquad (3.6)$$

where $I(\lambda)$ is the spectral fluorescence intensity, τ_f is the radiative lifetime of the upper laser level, η is the radiative quantum efficiency of the upper level, f is the fraction of the excited population in the Stark split level of the upper manifold, n is the refractive index and λ_p is the peak emission wavelength. Values of n, η, f and λ_p will be approximately the same in a waveguide as in a bulk material therefore the ratio between the stimulated emission cross sections for waveguides relative to bulk is simply given by

$$\frac{\sigma_{e(waveguide)}(\lambda_p)}{\sigma_{e(bulk)}(\lambda_p)} = \frac{\Delta\nu_{(bulk)}}{\Delta\nu_{(waveguide)}} \qquad (3.7)$$

where $\Delta\nu$ is the luminescence linewidth for each material, this enables a calculation of the emission cross section in a waveguide if it is known in the bulk material.

3.5 Fluorescence Lifetime Measurements

One important characteristic of rare earth doped lasers and amplifiers is the radiative lifetime of the upper laser level. Some methods of fabrication of optical waveguides in laser hosts can produce a material in which there is an alteration of the fluorescence lifetime relative to the bulk value, thus making a method of measuring the lifetime important in order to fully quantify device performance.

The lifetime of transitions which terminate in manifolds above the ground state can easily be measured. Pump light, tuned to the absorption band of the active ion, was passed through an optical chopper and launched into the guide in the same manner as used in the fluorescence spectroscopy measurements. Fluorescence from the end of the waveguide could then be imaged onto a photodiode using filters to cut out the pump light. The signal from the diode was stored using a Thurlby DSA 524 Digital Storage

Adaptor. The fluorescence decays in the form $V = V_0 e^{-t/\tau}$, where V is the voltage from the photodiode, and V_0 is the maximum voltage. The gradient of a graph of ln (V) against time will give τ, the fluorescence lifetime. The speed of the chopper should be such that its period is several times longer than the lifetime in order to allow the fluorescence to reach a steady state during each cycle.

For transitions which terminate on a level in the ground state manifold, which may be thermally populated, a slight variation on this technique must be used because fluorescence from the beginning of the guide may be reabsorbed towards the end and repopulate the emitting level. The resulting excited ion will then relax spontaneously emitting another photon which may then be reabsorbed and so on. The measured fluorescence lifetime of the whole sample is thus greater than that of an isolated ion. To prevent such radiation trapping it is necessary to pass through only a very short length of doped material which was achieved by passing the pump light and collecting the fluorescence perpendicular to the plane of the waveguide, as shown in figure 3.4, below. In such a case the pump and emitted light only passed through a few microns of doped material allowing a more accurate measurement of the lifetime.

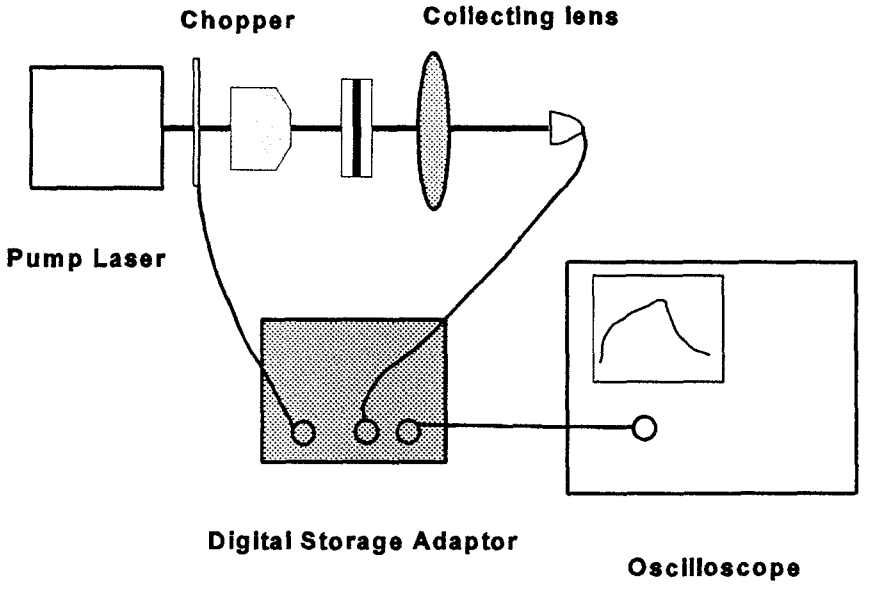

Figure 3.4 Fluorescence lifetime measurements for quasi-three-level transitions

3.6 Waveguide Transmission Measurements

A rough estimation of waveguide losses can be made from a simple transmission measurement of light through the guide. Laser light, tuned off any absorptions of the dopant ion, was launched into the waveguide using a microscope objective and imaged onto a power meter upon exiting the guide. The transmission is given by

$$T = \frac{P_o}{P_i} \cdot \frac{1}{T_i T_o} \cdot \frac{1}{(1-R_F)^2} \tag{3.8}$$

where P_o and P_i are the measured input and output powers, R_F is the Fresnel intensity reflectivity coefficient off the end faces of the crystal and T_i, T_o are the transmissions of the input and output objectives respectively. The overall transmission will have a component due to the waveguide loss and a component due to the efficiency of launching light into the waveguide. If one assumes a launch efficiency of 100% then the measured transmission value can be interpreted to give an upper limit on the waveguide loss.

3.7 Launch × Absorption Measurements

A measurement of the product of launch efficiency and resonant absorption can also be obtained from a transmission measurement. The pump light should be tuned onto the strongest absorption, and launched into the waveguide. The transmitted pump power can be measured on a power meter. The pump beam is then passed through the substrate (assuming the substrate is undoped and made of the same material as the guide). The launch × absorption is simply given by

$$L \times A = 1 - \frac{P_{wg}}{P_s} \tag{3.9}$$

where P_{wg} is the power measured through the waveguide, and P_s the power through the substrate. The transmissions of the microscope objectives and the Fresnel losses are the same for both the waveguide and substrate and hence cancel out. The value determined from such a measurement can be used to calculate how much of the incident pump

radiation is absorbed in the waveguide to enable, for example, a measure of the absorbed power threshold which can then be compared with the theory.

If the pump laser can be tuned off the absorption and a transmission measurement made then a figure for the absorption in the length of the guide can be found from equation (3.10)

$$A = \frac{1 - \frac{P_{wg}}{P_s}}{T} \tag{3.10}$$

where T is given in equation (3.8). This value of A, and equation (3.9) can then in turn be used to find the launch efficiency of pump light into the waveguide.

3.8 Waveguide Laser Experiments

The experimental arrangement used for waveguide laser experiments is similar to that used for fluorescence measurements, as shown in figure 3.5, overleaf. The laser resonator is formed using two thin dielectric mirrors held onto the polished end faces of the crystal by the surface tension of a drop of Fluorinert FC-70 fluorinated liquid. Light from the guide can be directly imaged onto a detector using colour filters to cut out any unabsorbed pump light. The output from the detector is viewed on an oscilloscope. The onset of lasing can be observed as a large increase in the signal and sharp spikes can be seen in place of the usual smooth fluorescence shape. The lasing threshold is found by reducing the incident pump power using the variable attenuator and adjusting the xyz positioner which controls the launch of light into the waveguide, so as to give the lowest power at which the guide still lases. Increasing the incident pump power and measuring the output power from the laser enables the slope efficiency of the laser to be measured.

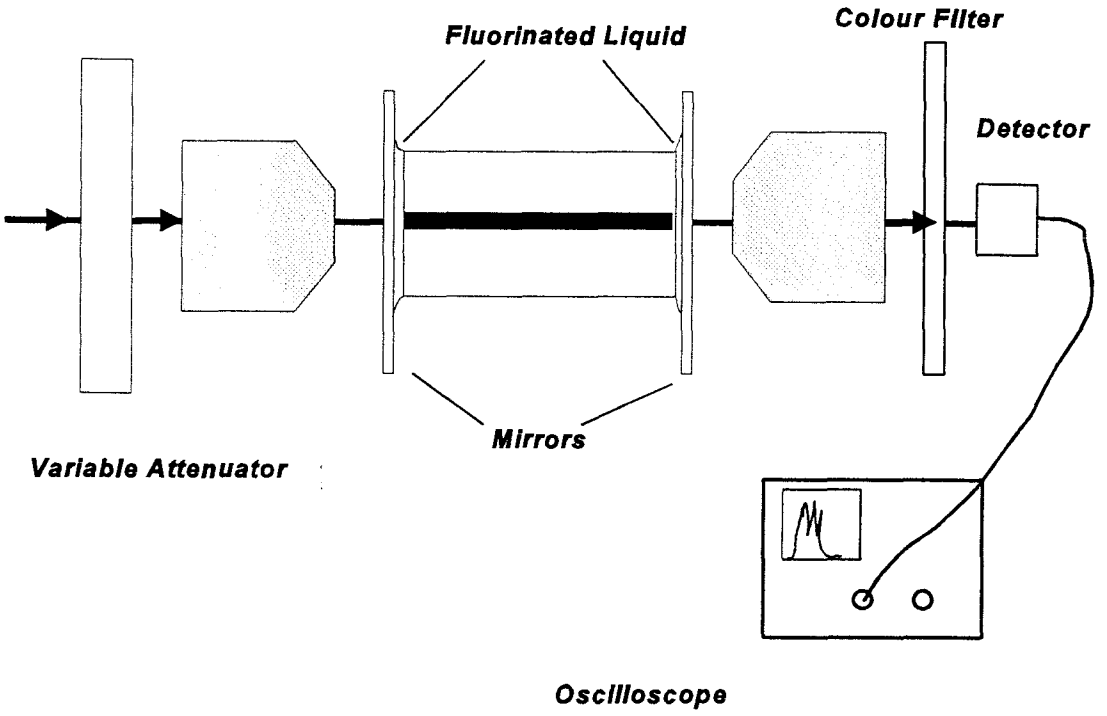

Figure 3.5 Configuration for waveguide laser experiments

Absorbed Power in a Waveguide Laser Cavity.

If mirrors are attached to the waveguide end faces (as described above) then a calculation of the absorbed power must take into account the launch × absorption in the waveguide together with any feedback which can result from reflection of the pump light back into the cavity off the mirrors. The absorbed power is given by

$$P_{abs} = P_{inc}\left[T_i\,LA + T_i\,LA(1-A)(1-T_o) + T_i\,LA(1-A)^2(1-T_o)(1-T_i) + T_i\,LA(1-A)^3(1-T_o)^2(1-T_i)+\ldots\right] \quad (3.11)$$

P_{abs} , P_{inc} are the absorbed and incident powers respectively, T_i is the transmission of the input mirror at the pump wavelength, T_o is the transmission of the output mirror, L is the

launch efficiency and A the absorption in the length of the guide. Three or four terms in the expression are typically required to be used, although this depends on the reflectivities of the mirrors at the pump wavelength.

3.9 Waveguide Amplifier Experiments

Two slightly differing double pass amplifier experiments were set up, one which could be used when the waveguide had end faces which were polished parallel to one another, the other in the case where one face was polished at a slight angle, in the horizontal plane, to the other end face. In both cases the Ti:sapphire pump radiation and the signal, from a diode pumped Nd:YAG laser were launched into the waveguide using cylindrical lenses. Retroreflection of the signal is provided by a thin mirror butt coupled to the face of the guide in the manner described for the waveguide laser experiments. In the case where the two end faces of the guide are polished parallel to one another extraction of the amplified signal is obtained using a Faraday isolator, as shown in figure 3.6.

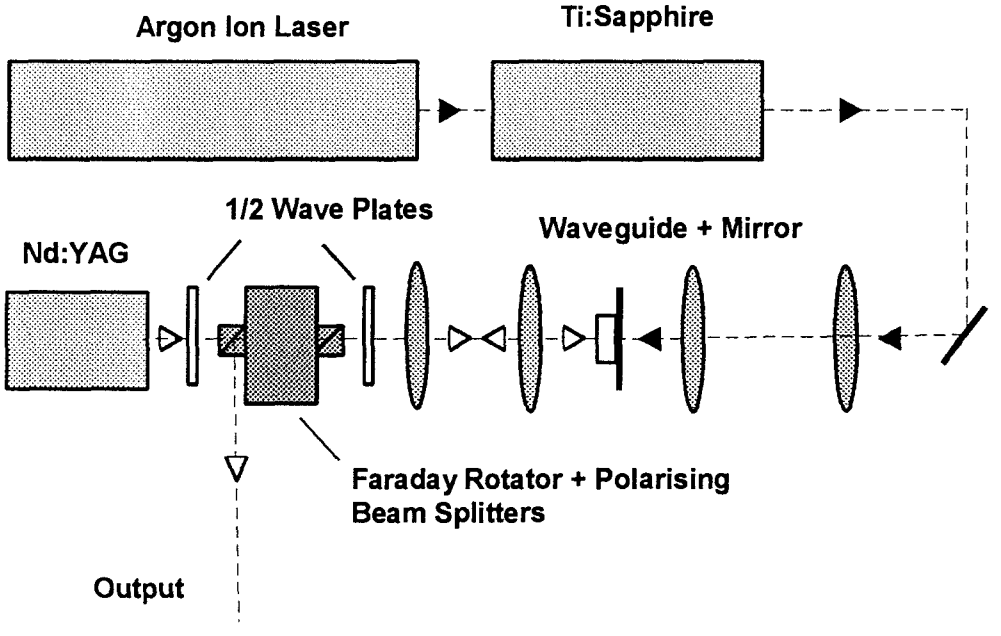

Figure 3.6 Double pass amplifier experiment for parallel polished waveguide

The linearly polarised signal beam passes through the Faraday rotator followed by a half wave plate, the amplified reflected signal passes back through the half wave plate and is therefore rejected by one of the polarising beamsplitters in the isolator.

In the case where the waveguide is wedge polished extraction of the amplified signal is somewhat simpler, as shown in figure 3.7.

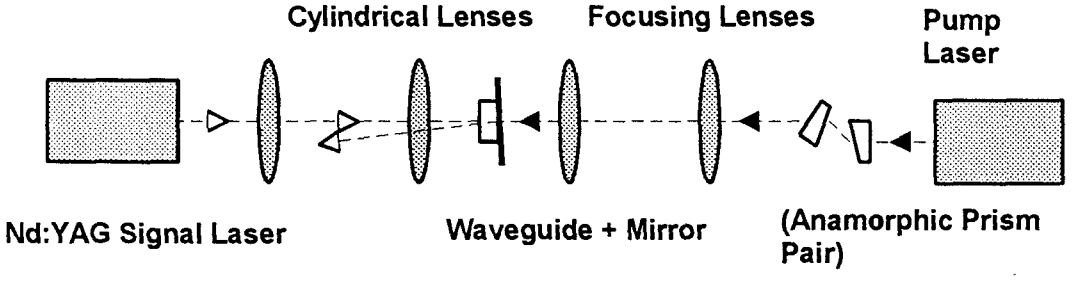

Figure 3.7 Double pass amplifier in a wedge polished waveguide

The guide should be polished at such an angle that there is spatial separation of the incident and reflected signal at the output plane of the waveguide, the amplified signal can then be picked off using a highly reflecting mirror.

Diode Pumped Amplifier

Using a 1.2W, high brightness, broad stripe diode laser as the pump source

required a slightly different pump focusing technique. The output of the diode was collimated in the plane parallel to the diode junction using a cylindrical lens, the output in this plane is about 34 times diffraction limited. In the other, diffraction limited, plane the output was collimated using a 6.5mm focal length diode collimating lens. The resulting beam was focused into the waveguide using a microscope objective. The signal focusing and output extraction were the same as for the Ti:sapphire pumped experiments.

3.10 Bulk Laser Experiments

Two bulk laser experiments were set up which differed slightly from each other. In one case the laser rod was uncoated requiring it to be Brewster angled to the incident pump beam, in order to eliminate reflections of the pump and signal, the latter would result in a loss in the cavity. In the second case the rod had one face coated with a mirror which was highly reflecting at the laser wavelength, the other face had a broad band antireflection coating covering both the pump and laser wavelengths. For the uncoated rod the experimental setup can be seen in figure 3.8.

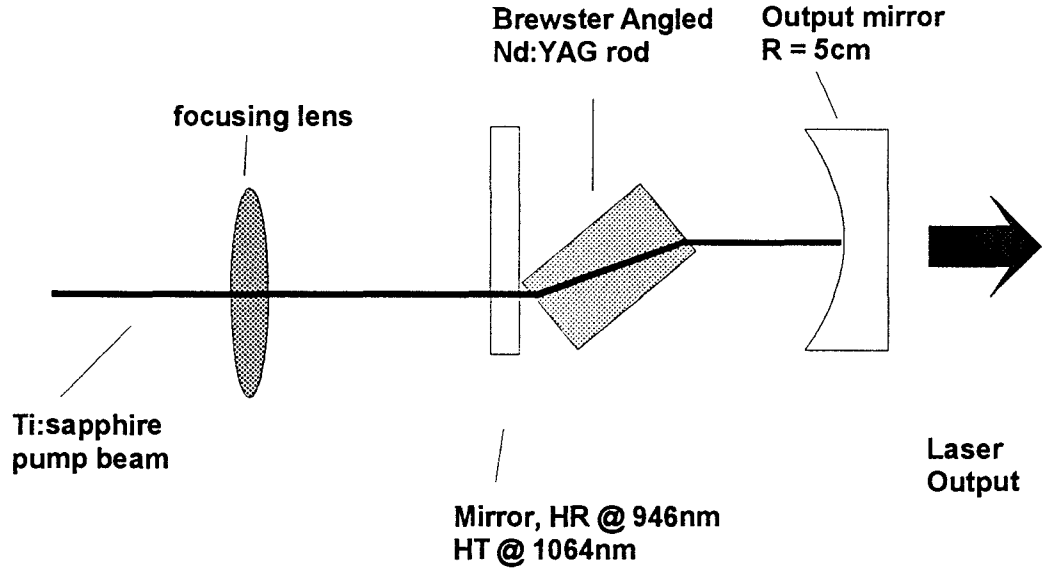

Figure 3.8 Experimental arrangement for the Brewster angled bulk laser

The laser cavity consisted of the neodymium doped YAG rod in a simple plano concave resonator. The rod was positioned so as to be Brewster angled to the incident pump beam, and hence to the resonating signal. The waist of the laser mode in such a resonator will be on the plane mirror [5] so the rod was placed as close as possible to this mirror in order to have the smallest possible spot sizes in the gain medium. The output mirror had a 5cm radius of curvature. The spot size of the laser mode, w_0, for a plano concave cavity is given by the equation below, after [5]

$$w_0^4 = \left(\frac{\lambda}{\pi}\right)^2 \cdot (R_2 - d) \cdot d \qquad (3.12)$$

where λ is the laser wavelength, d is the separation of the two mirrors and R_2 is the radius of curvature of the output mirror. Increasing the separation of the two mirrors toward the radius of curvature, R_2, therefore reduces the mode waist size. The pump beam was focused onto the plane highly reflecting mirror using a spherical lens, to the optimum waist spot size given in [6]

$$w_{p,\,opt} = \sqrt{\frac{\lambda l}{\sqrt{3}\pi n}} \qquad (3.13)$$

The experimental setup for the coated rod can be seen in figure 3.9, overleaf. Due to the antireflection coating there was no need to Brewster angle the rod in this case. The rod was positioned so that the end faces were perpendicular to the direction of the incoming pump light which enabled easier mounting of the rod in a copper heat sink resulting in more efficient heat extraction. The pump light was focused through the highly reflecting coated face to the same spot size as used in the previous experiment.

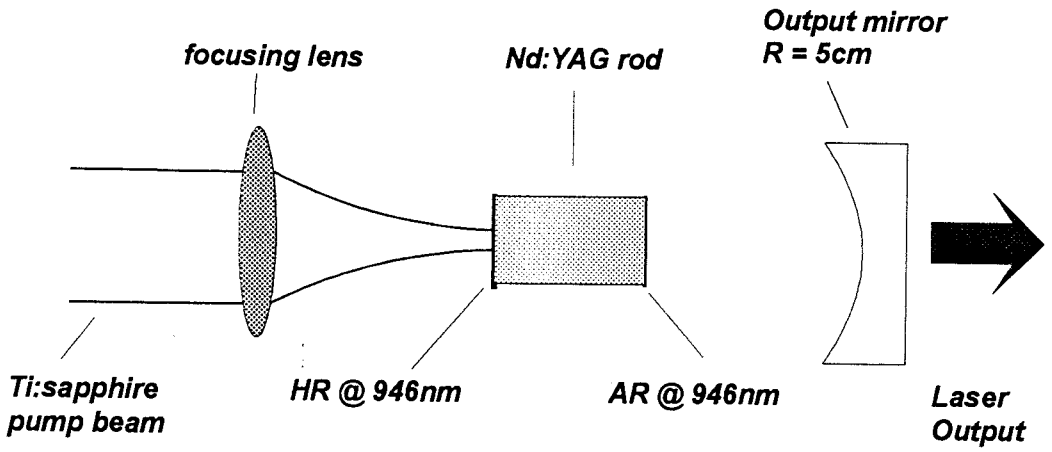

Figure 3.9 Experimental arrangement for the bulk laser with coated faces

References

1. Instruments S.A. Inc, Jobin Yvon/Spex Division, Guide for Spectroscopy, 1994

2. E.Hecht, Optics, Second Edition, p. 171, Addison-Wesley Publishing Company, 1987

3. B.F.Aull and H.P.Jenssen, IEEE Journal of Quantum Electronics, **QE-28**, 925, 1988

4. D.S.Sumida and T.Y.Fan, Optics Letters **19**, 1343, 1994

5. O.Svelto, Principles of Lasers, Chapter 4, Plenum, 1989

6. M.F.J.Digonnet and C.J.Gaeta, Applied Optics **24**, 333, 1985

Chapter 4 - Tm^{3+} Doped Waveguide Lasers

4.1 Introduction

Rare earth doped solid state lasers are of particular importance in spectral regimes where semiconductor diode lasers have not been made to operate efficiently. For this reason the triply ionised thulium ion doped into laser host materials is of great interest due to having optical transitions at wavelengths around 1.8 - 2.0μm and in the blue region of the spectrum [1-6]. Lasers operating at such wavelengths have uses in the fields of medicine and laser radar for the infrared transitions [7,8,9], and optical data storage for the lower wavelength transitions [10].

The transition at 2.012μm in Tm:YAG terminates on a Stark level with an energy of 588cm^{-1} in the ground state manifold [11] which at room temperature has a thermal population of about 1.6%. Due to the low loss nature of guides fabricated by liquid-phase epitaxy (LPE), operation of a laser on this quasi-three-level transition in a waveguide should result in an improvement in terms of threshold over similar bulk lasers, without significantly degrading output performance.

In this chapter I will present experimental results for laser operation at 2.012μm of liquid-phase epitaxially-grown Tm:YAG planar waveguides.

The final part of this chapter will deal with results for epitaxially-grown Tm:YSO waveguide lasers operating at 1.884μm.

4.2 Spectroscopy of LPE Grown Tm^{3+} Doped YAG

The partial energy level diagram of Tm:YAG, shown in figure 4.1, shows the important absorption and emission lines for laser operation around 2.0μm. The cross-relaxation process shown for two adjacent thulium ions can result in two signal photons being emitted for each absorbed pump photon [12]. The waveguides were co-doped with gallium and lutetium, the former to increase the refractive index difference between

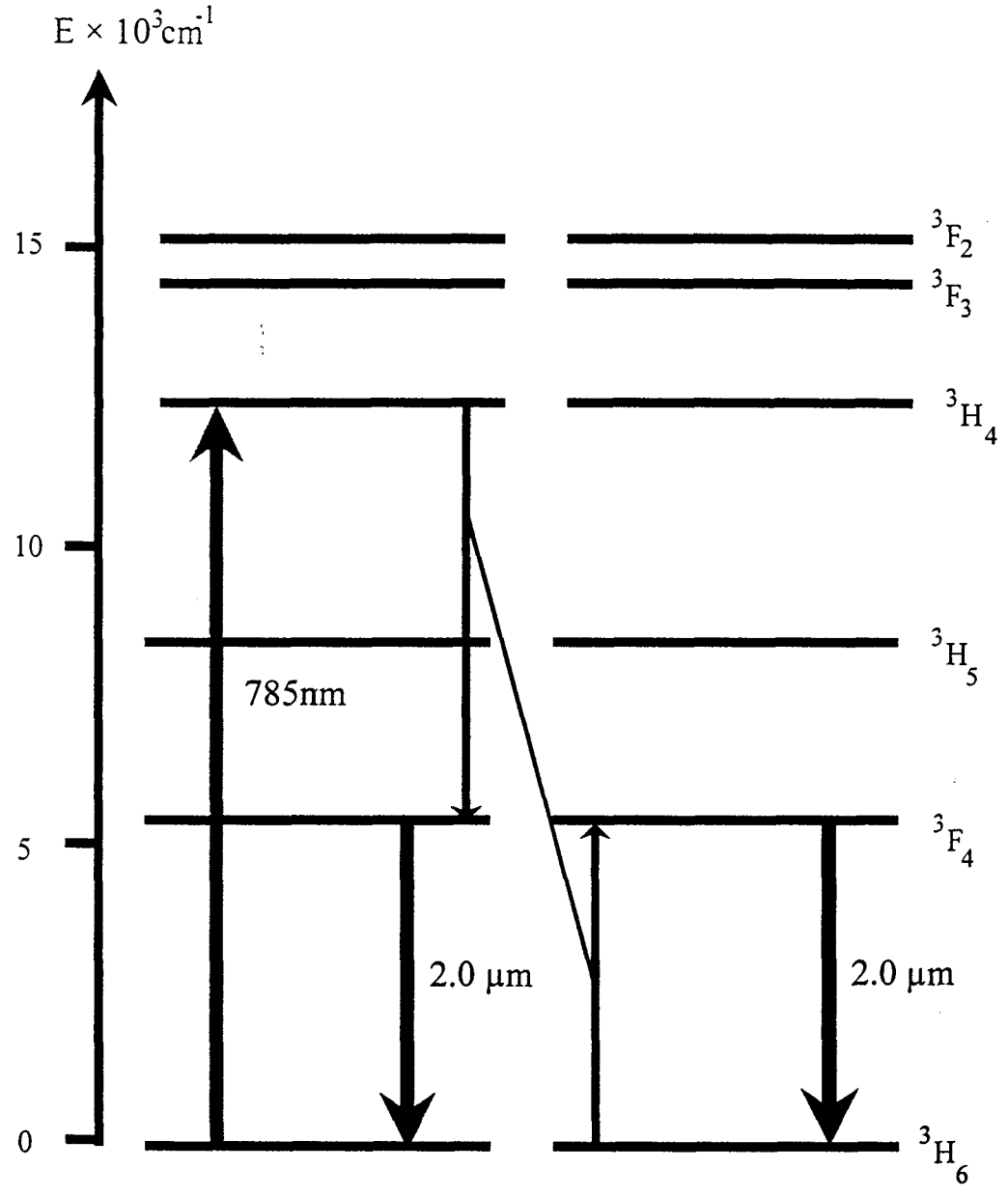

Figure 4.1 Partial Energy Level Diagram for the Tm^{3+} ion showing the absorption and emission wavelengths for Tm:YAG.

the active layer and substrate, the latter compensates for the lattice mismatch due to the large gallium ion substituting for yttrium in the crystal lattice.

Absorption Spectra

The white light absorption spectrum of a Tm:YAG epilayer (figure 4.2), which was measured by evaluating the relative absorption of a white light source in the epilayer compared to that in undoped material, shows the two peaks in the absorption around 785nm which correspond to a transition from the $^3H_6$ ground state manifold to $^3H_4$ level, as shown in figure 4.1. The absorption at 785nm allows efficient pumping using a Ti:sapphire laser or an AlGaAs laser diode. The strong absorption at 680nm corresponds to the $^3H_6$ - $^3F_3$ transition.

Fluorescence Spectroscopy

The fluorescence spectra around 2μm from the $^3F_4$ - $^3H_6$ transition, shown in figure 4.3, exhibits the broadening of spectral linewidths with increasing Ga doping. The spectra have been normalised so as to have the same area under the graph; this allows the relative cross sections to be deduced directly from the heights of the emission peaks as described in Chapter 3. The more highly-Ga-doped guide exhibits broader linewidths and hence has lower peak emission cross sections which will have a detrimental effect on threshold for laser operation. It should be noted, however, that this effect and that of increasing waveguide loss with Ga concentration [9] are not significant enough to negate the improvements over a bulk system due to the guidance effect. The waveguides with no Ga doping will confine the light weakly and so may offer little of the advantage associated with the geometry. The position of the various peaks in the spectra are slightly shifted in the case of the Ga doped waveguide. The epitaxial growth process alone has little effect on the linewidth relative to bulk materials [14] resulting in a negligible decrease in the peak emission cross section for waveguides without Ga doping.

The relatively smooth shape of the fluorescence curve over a range of ~ 400nm

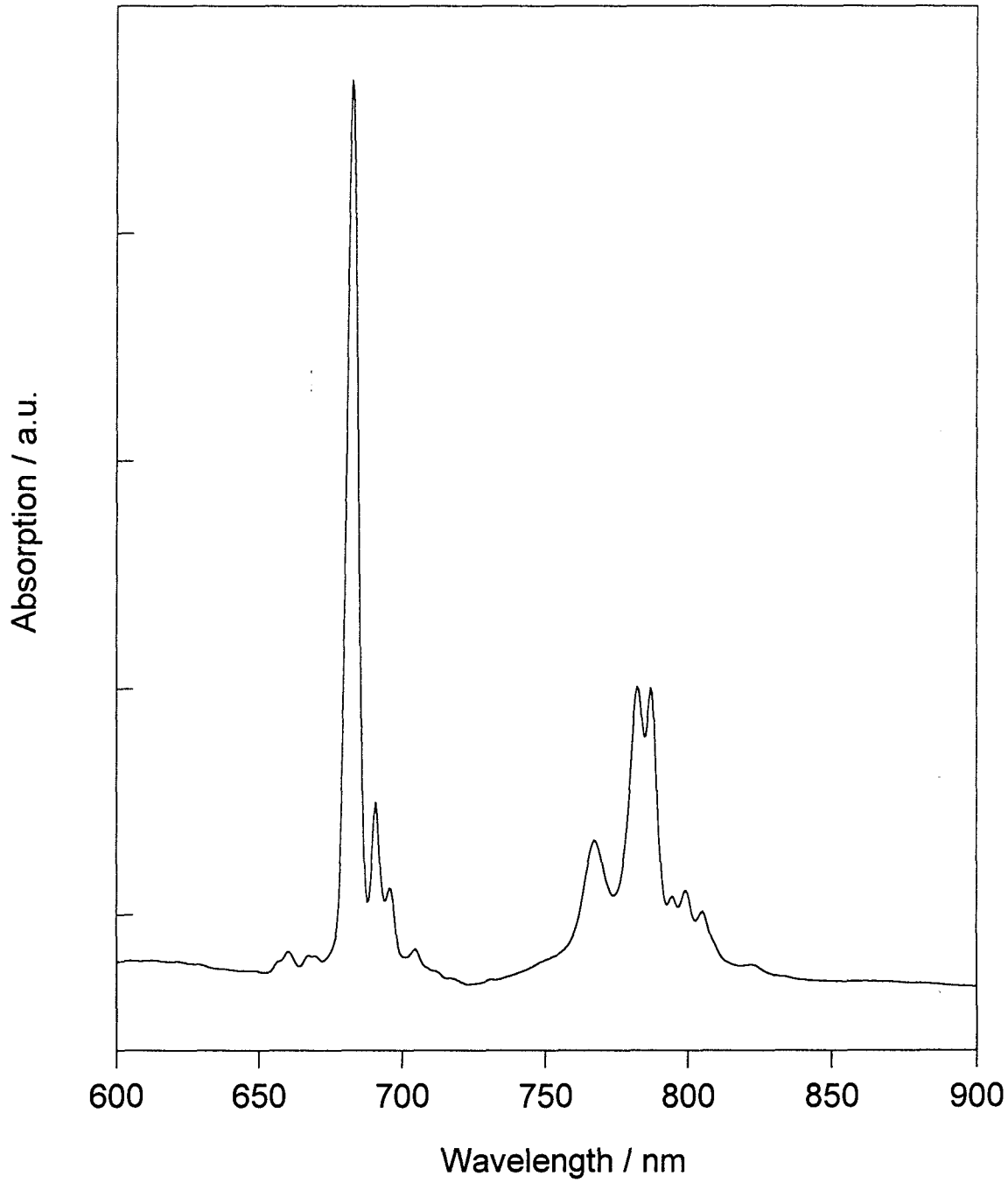

Figure 4.2 White light absorption spectrum of 6.6at% Tm epilayer showing the $^3H_6$ - $^3H_4$ absorption around 785nm

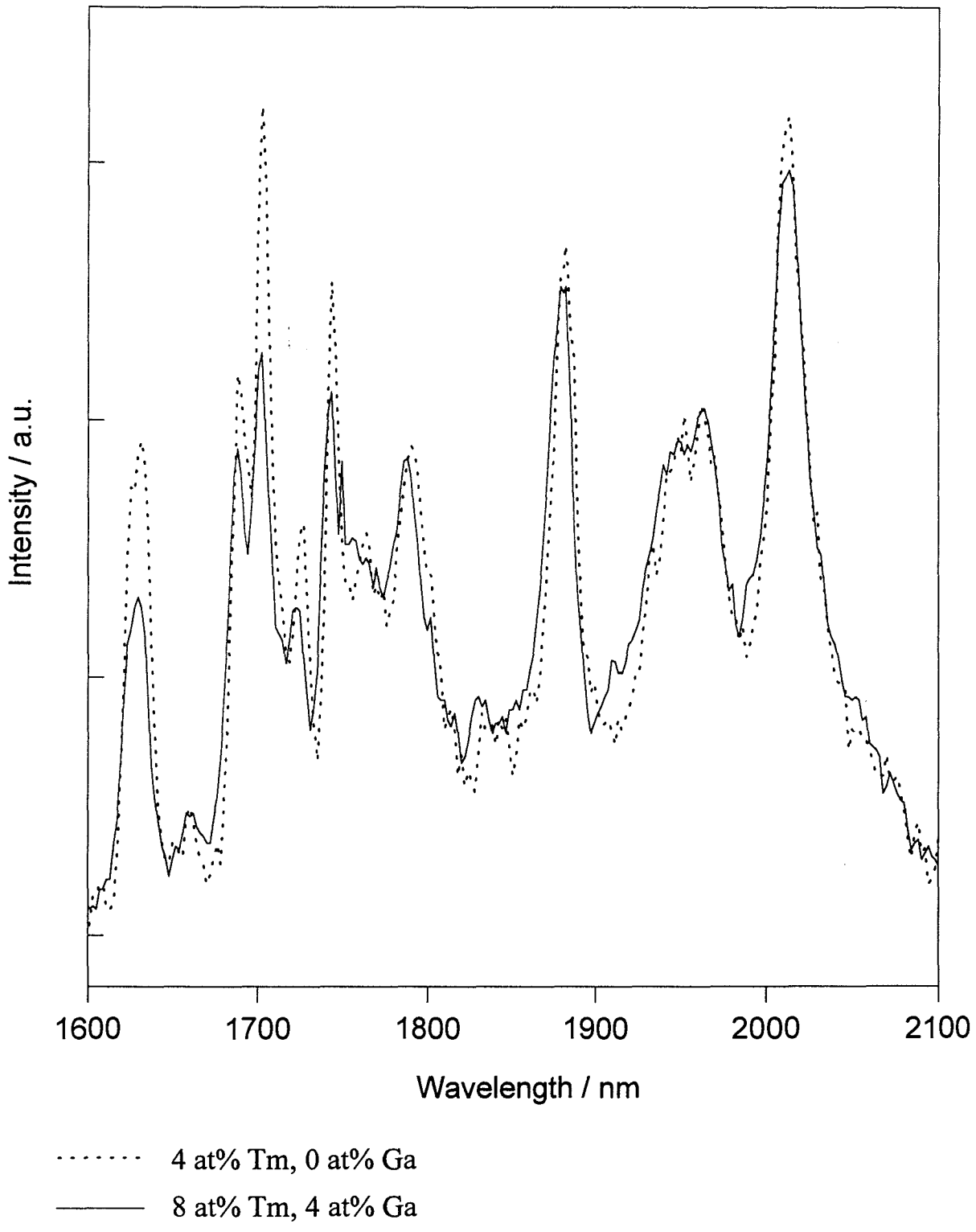

Figure 4.3 Fluorescence from $^3F_4$ - $^3H_6$ manifolds in Tm:(Ga):YAG epilayers.

suggests the possibility of broad tunability of a Tm:YAG laser on the $^3F_4$ - $^3H_6$ transition; this is a result of the overall bandwidth of the fluorescence being less than the number of possible transitions between Stark levels (117) multiplied by the linewidth of a single transition (~10nm) [15]. Absorptions at wavelengths between ~ 1.5 - 1.9μm, due to population in the lower level, limit the range over which tunability is possible. A bulk laser has been tuned, however, between 1.90μm and 2.16μm [15].

4.3 Fluorescence Lifetime Measurements

In order to understand the effect that doping the crystal with Tm and Ga has on a system it is necessary to measure the fluorescence lifetime of the $^3F_4$ state. Due to the thermally induced population in the Stark split state of the $^3H_6$ manifold which is the lower level for the 2μm transition it was necessary to use the procedure described in section 3.6 for quasi-three-level transitions. Lifetimes were measured for waveguides with various Tm and Ga doping levels, the results are shown in table 4.1, below.

Table 4.1

	0% Ga	4% Ga	12% Ga
0.5% Tm	3.1 ms	-	-
4% Tm	2.4 ms	-	-
6.6% Tm	-	-	2.8 ms
8% Tm	1.3 ms	2.1 ms	-
13% Tm	-	1.3 ms	-

Experimental errors are ± 0.1ms

Although the table is far from complete, due to guides with other doping levels being sandwiched between large pieces of YAG which prevented transmission and collection of light through their top and bottom faces, it is possible to deduce that increasing Tm concentration has the effect of shortening the lifetime while an increase in Ga concentration increases the lifetime.

4.4 Tm:YAG Waveguide Lasers at 2.012μm. [16]

Laser operation was achieved in epitaxially grown Tm:Ga:Lu:YAG waveguides with a variety of doping levels; the results for the more important of these will be discussed in the remainder of this section. As a result of the cross relaxation process described in section 4.2, whereby two photons can populate the upper laser level for each absorbed pump photon, the maximum theoretical slope efficiency for a 2μm Tm:YAG laser pumped at 785nm is 78% due to the ratio of the pump and laser wavelengths. Room temperature bulk lasers have been operated with slope efficiencies of 59% [15] and thresholds in the order of 200mW [15,17].

Highly Ga Doped Waveguides.

The first waveguides grown by LETI in Tm:YAG were doped with 4.75, 6.6 or 10at% Tm, 35at% Lu and approximately 12at% Ga. The best diode pumped lasing result for these guides was obtained in a waveguide which had a 6.6at% Tm doping level, and was 14.6μm thick with a length of 4mm.

With a 1W SDL 2362 diode array as the pump source, tuned to the strongest absorption around 785nm, the launch × absorption (as defined in Chapter 3) was measured to be 0.515 when using a ×10 microscope objective to launch light into the guide. The absorption through the length of the guide was measured to be 0.56 which allows the launch efficiency to be calculated to be 92%. The pump spot sizes were measured to be 2.1μm in the guided plane and 17μm in the unguided plane. A silicon filter was used to cut out the unabsorbed pump light enabling a measurement of the laser output power.

The laser cavity was formed by two mirrors which were highly reflecting at 2.0μm and had negligible reflectivity at the pump wavelength. The absorbed power threshold was measured to be 29.5mW. With the output mirror replaced by a mirror with a 2% transmission at the laser wavelength the threshold was 50.1mW and the slope efficiency was 34%. With a 15% output coupler the threshold rose to 139mW and the

slope efficiency to 49%. A plot of output power versus absorbed pump power for operation with the 2% and 15% output couplers is shown in figure 4.4.

When pumped with a Ti:sapphire laser, using two mirrors reflecting 99.1% of the 2.0μm emission the best results were obtained in a guide with 6.6at% Tm, a thickness of 17.69μm and a length of 4mm. The absorbed power threshold was 8.6mW with a 31% slope efficiency. The wavelength of the laser was measured to be 2.012μm using an Applied Photophysics f/3.4 monochromator.

Although a large Ga doping level will result in good confinement of waveguide modes the decrease in emission cross section and the increase in loss associated with a large amount of Ga will degrade laser performance. Guides were grown, therefore, with lower levels of Ga doping.

4% Ga Doped Waveguides

Waveguides were grown at LETI doped with 4at% Ga, and without any Lu, this resulted in a lattice mismatch between the active layer and substrate but this was not large with only the small amount of Ga present ($\Delta a \sim \pm 3$Å). These waveguides had thulium doping levels of between 4at% and 13 at%, with depths between 6.7 and 23.3μm. The best results under diode pumping conditions were obtained in a guide which had 8at% Tm doping, a thickness of 23.3μm and a length of 4mm. The launch × absorption was calculated to be 0.366, the absorption in 4mm of guide was 0.57 giving a launch efficiency of 64%. An AsGa filter was used to cut out the unabsorbed pump light.

Using two mirrors which transmitted 0.26% at the laser wavelength, around 2.0μm, the absorbed power threshold was 15.1mW. With a 2% output coupler which was highly reflecting at the pump wavelength the threshold was 22.8mW and the slope efficiency was 46%. With a 15% output coupler replacing the 2% output coupler the threshold was 39.1mW and the slope efficiency was 64% as shown in figure 4.5. A

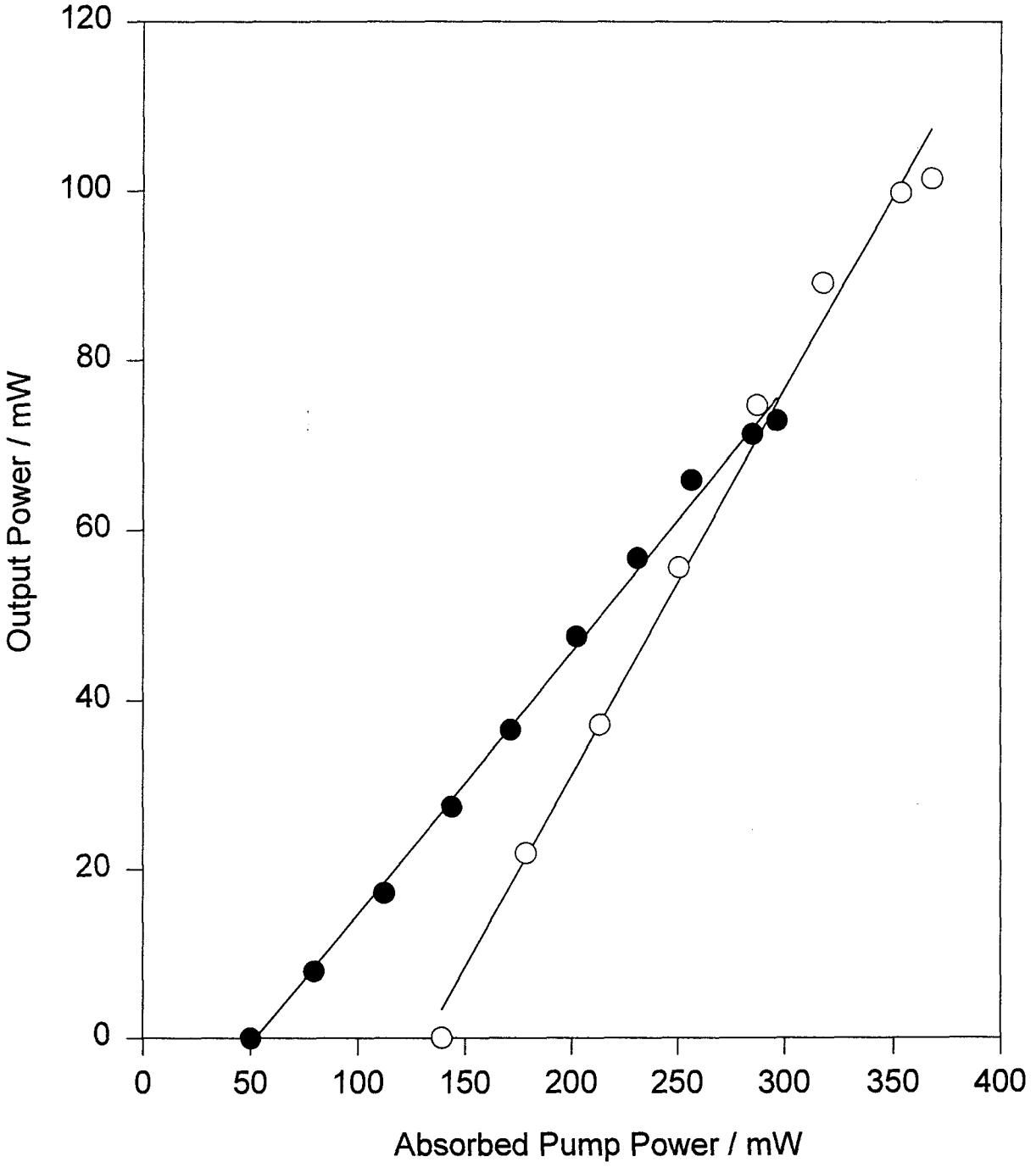

● 2% output coupler : slope efficiency = 34%

○ 15% output coupler : slope efficiency = 49%

Figure 4.4 Laser output power vs absorbed pump power for a 4mm long, 6.6at% Tm, ~12% Ga, 35 at% Lu YAG epilayer pumped by a 785nm AlGaAs diode array

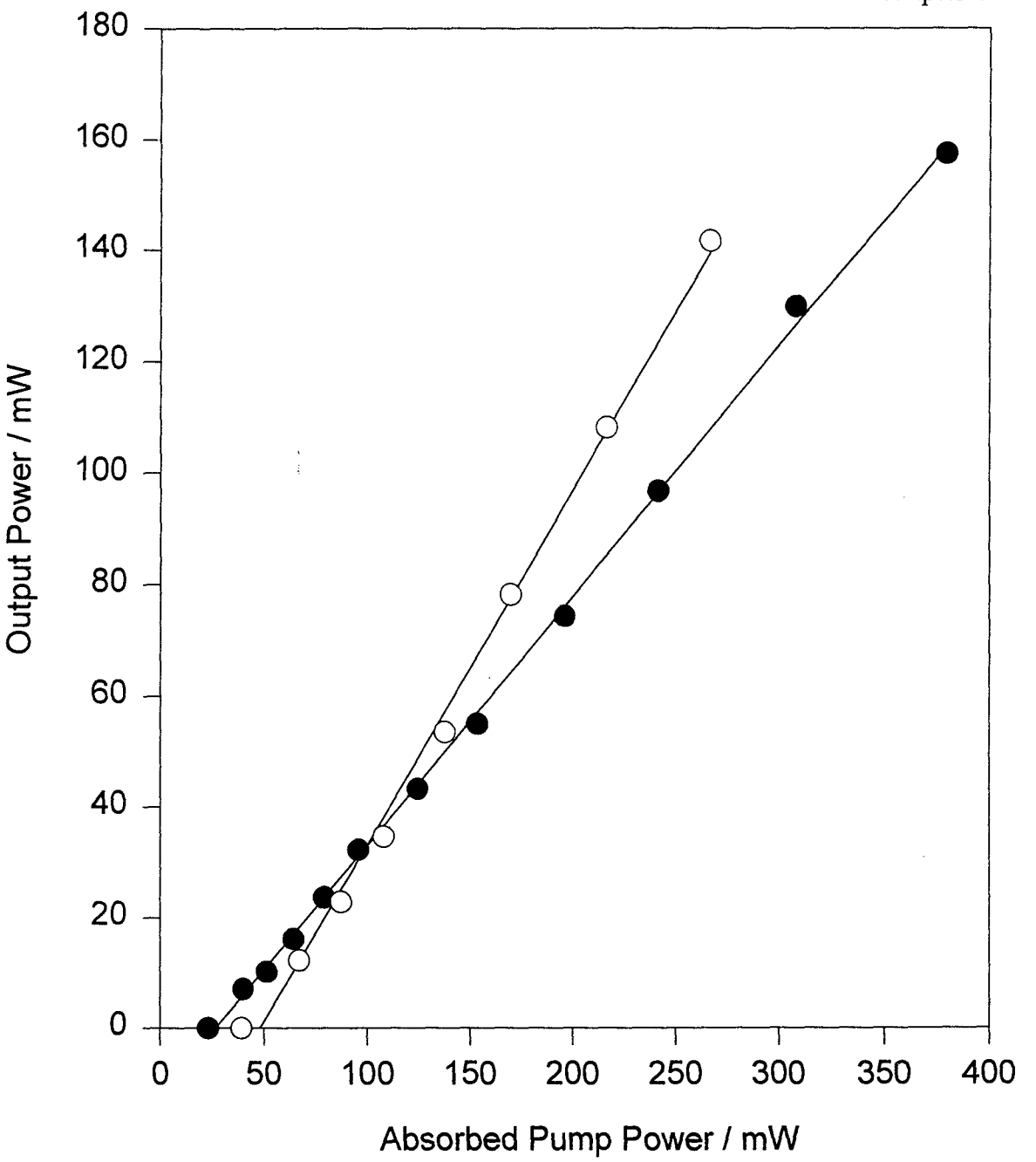

● 2% output coupler : slope efficiency = 46%

○ 15% output coupler : slope efficiency = 64%

Figure 4.5 Laser output power vs absorbed pump power for a 785nm AlGaAs diode pumped laser in a 4mm long, 8 at% Tm, 4 at% Ga YAG epilayer

maximum output power of 142mW was obtained for 266mW of absorbed pump power.

The best results for the 4% Ga doped waveguides when pumped with a Ti:sapphire laser were obtained in the same guide that gave the best performance under diode pumping. The launch × absorption was measured to be 0.6, which is considerably higher than that obtained in the diode pumped experiments, due to an improved launch for the Ti:sapphire pump light. Results in terms of absorbed power, however, would be expected to be comparable under both pumping schemes. Using the two 0.26% transmission mirrors, as used for the diode pumped results, the absorbed power threshold was 7mW. With the 15% output coupler replacing one of the mirrors the absorbed power threshold was 45.2mW and the slope efficiency 68%, as shown in figure 4.6. It should be noted that the slope efficiency of the laser with respect to incident power on the crystal, when using the 15% output coupler, was 40%. This compares to a value of 27% for diode pumping.

0% Ga Doped Waveguides

Waveguides were grown which were not codoped with Ga, guidance being achieved as a result of the refractive index difference between the active layer and substrate due to thulium doping alone. Several guides were fabricated with differing thulium concentrations and thicknesses (4-8at%Tm, 7-20μm). The best results were obtained in a waveguide which had an 8at% Tm doping level, a length of 4mm and was 17.2μm thick. The launch × absorption of the pump was measured to be 0.302 when using an AlGaAs diode laser pump. With two 0.26% reflectivity mirrors forming the laser cavity the absorbed power threshold was 28.4mW; replacing one of the mirrors with a 2% output coupler resulted in a rise of threshold to 53.3mW, a slope efficiency with respect to absorbed power was measured to be 20%, as shown in figure 4.7. No lasing was observed at the pumping levels available when using the 15% output coupler.

Under Ti:sapphire pumping conditions, using one 0.26% reflectivity mirror and one 15% output coupler the absorbed power threshold was 191mW and the slope

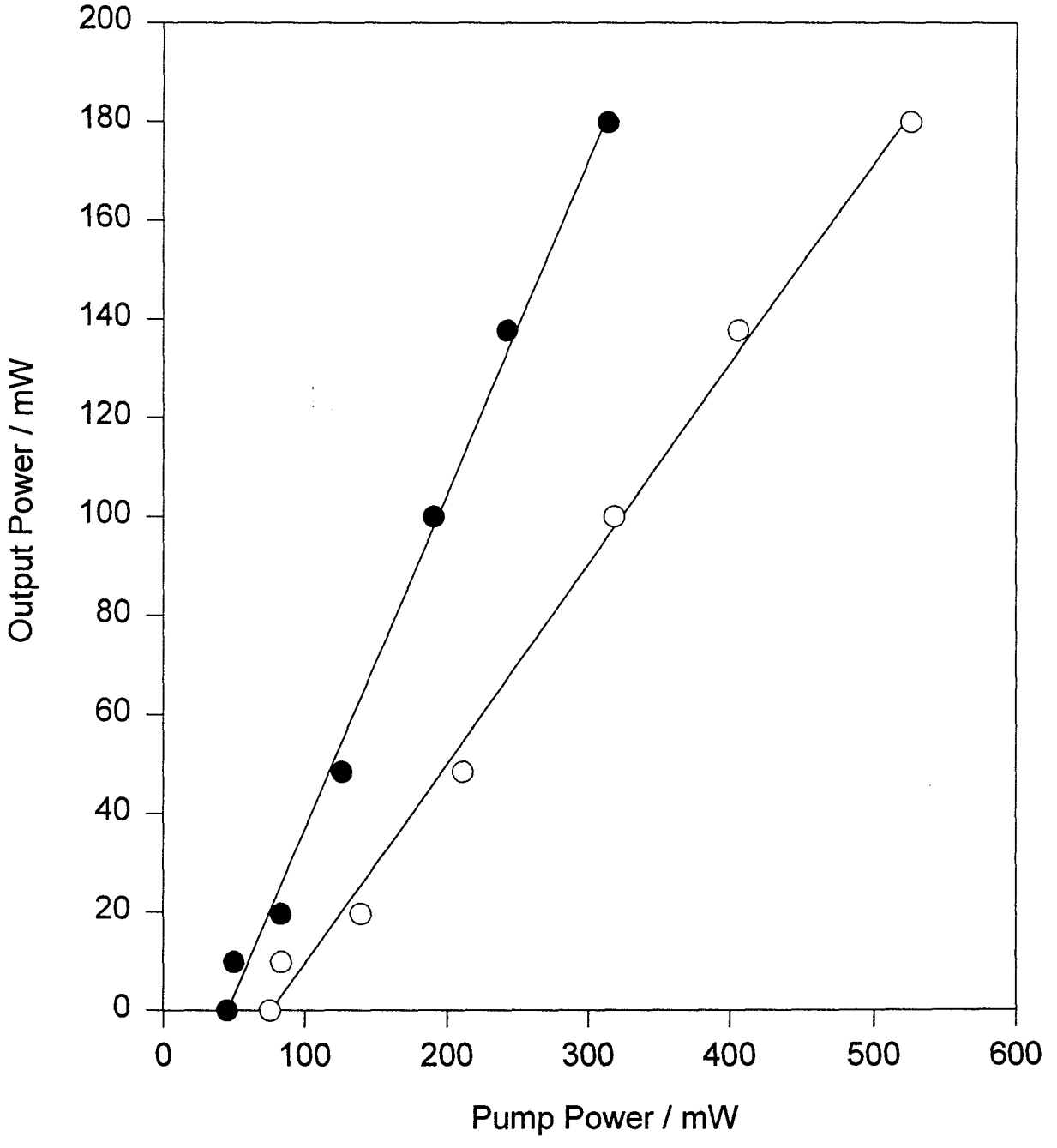

● Absorbed power slope efficiency = 68%

○ Incident power slope efficiency = 40%

Figure 4.6 Input / output characteristics for a Ti:sapphire pumped laser in a 4mm long, 8 at% Tm, 4 at% Ga, YAG epilayer with 15% output coupling

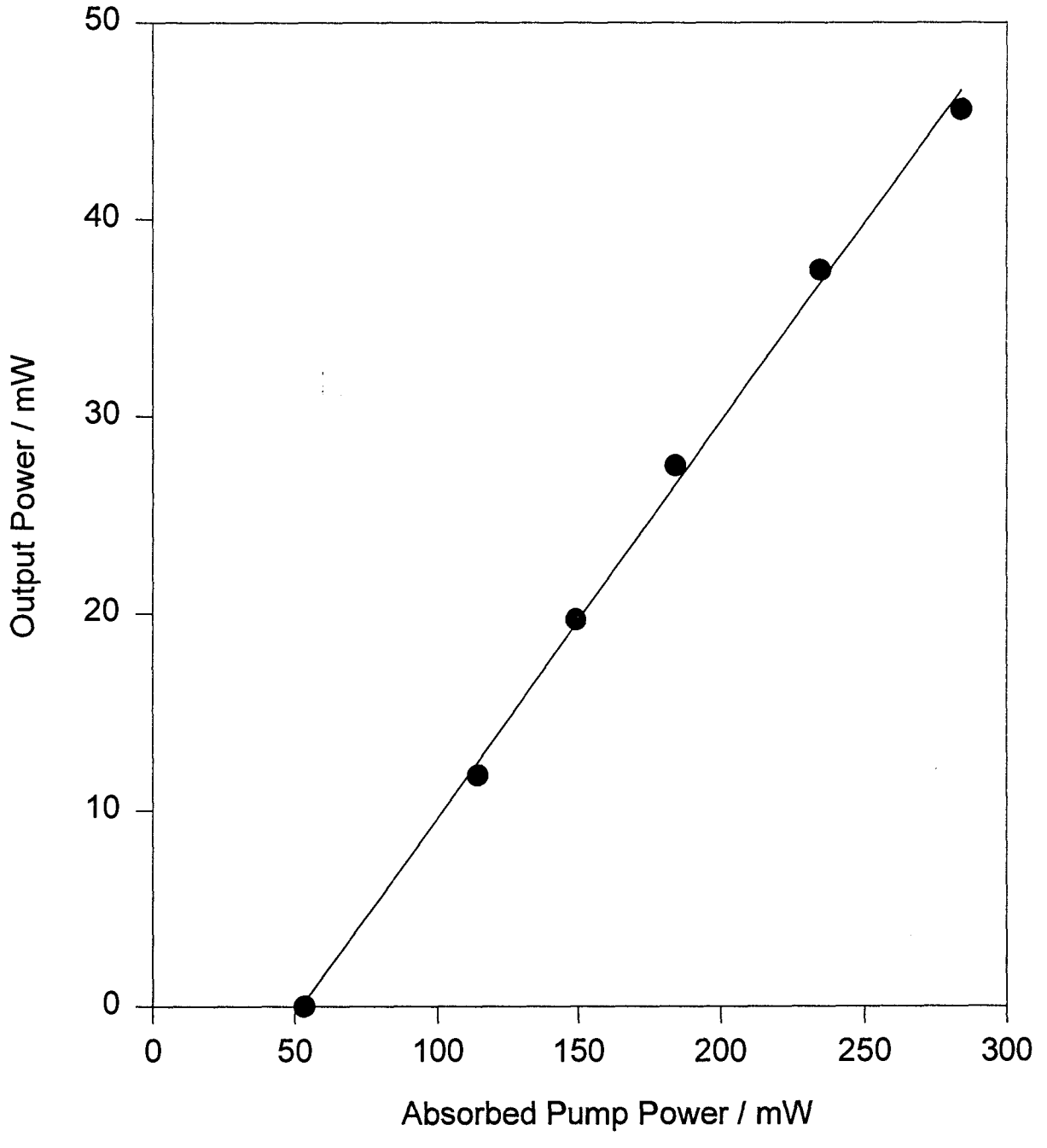

Figure 4.7 Laser output power vs absorbed pump power for a 4mm long, 8at% Tm, 0 at% Ga, YAG epilayer pumped by a 785nm AlGaAs diode array

efficiency was 17%.

4.5 Tm:YSO Waveguide Lasers at 1.884μm [18]

Liquid-phase epitaxy has, to date, been used to produce low loss, good quality planar waveguides and waveguide lasers in YAG with a variety of rare earth dopants [16,19-21]. The technique had not previously been extended to producing laser waveguides in any other host materials. Yttrium orthosilicate (YSO) is a laser host material of interest when doped with thulium due to having a larger absorption cross section around 790nm than Tm:YAG, 1.3×10^{-24} m^2 compared to 7.5×10^{-25} m^2 [22]. The large absorption cross section allows the possibility of fabricating very compact devices for side pumped lasers or amplifiers or microchip lasers for example. The Tm:YSO system is less three-level [23] than that of YAG resulting in a reduced reabsorption loss at the laser wavelength. The fluorescence lifetimes, however, are shorter than for YAG, ~1.6ms for 1 at% Tm doping and ~0.6ms for 10at% Tm [22], this is partly compensated for by the larger emission cross section, with a peak around 5.5×10^{-25} m^2 [22].

As a test of the potential for using liquid phase epitaxy to produce low threshold lasers in YSO, Tm^{3+} doped layers were grown by LETI on Czochralski grown ⟨010⟩ orientated YSO substrates. Waveguides were grown with thulium concentrations of between 1.7at% and 4.5at%. The lattice mismatch between the active layer and substrate increases with increasing thulium concentration [24] requiring the layers to be codoped with germanium to reduce this effect. Layers were grown with thicknesses from 5.2μm to 26.8μm.

The fluorescence lifetimes for the $^3F_4$ - $^3H_6$ transition were measured, at LETI, to be 1.6ms for 1.7at% Tm, 1.1ms for a 4.5at% Tm doped sample and 1.5ms for a 2.6at% Tm, 1.4% Ge doped waveguide. These lifetimes are in good agreement with values measured in bulk samples [22,25].

The waveguides were cut and polished so that light propagated along the D_1 or

D_2 direction. The experimental techniques were the same as for the Tm:YAG laser experiments, using a Ti:sapphire pump laser. The best laser results were obtained in a sample with 2.6at% Tm, 1.7at% Ge which was 9.8μm deep with a 8.0μm pure YSO cladding layer. Two samples were prepared from this melt, one with the two polished faces perpendicular to the D_1 axis (sample A, 5mm long), the other with the faces perpendicular to the D_2 axis (sample B, 4mm long). Propagation of light was, therefore, along the D_1 axis and the D_2 axis respectively, as depicted in figure 4.8.

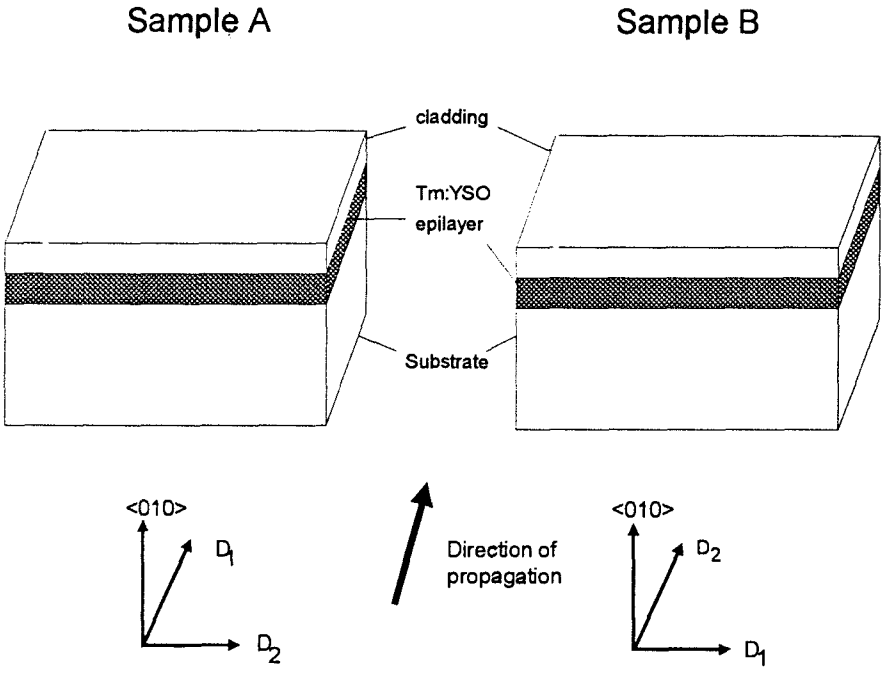

Figure 4.8 The orientations of Tm:YSO samples A and B

For Sample A the launch × absorption was measured to be 0.67 using a ×5 microscope objective for pump light polarised parallel to the ⟨010⟩ axis. Using two highly reflecting mirrors to form the laser cavity the absorbed power threshold was 59.8mW. Replacing one of the highly reflecting mirrors with a 2% output coupler resulted in a rise of threshold to 121mW. The maximum output power was 11.1mW for 362mW of absorbed pump power, corresponding to a slope efficiency of about 5%.

In Sample B the launch × absorption was 0.70, again using a ×5 microscope objective, with the pump light polarised parallel to the D_1 axis. Sample B was cut to a shorter length than Sample A due to the higher absorption cross section for light polarised parallel to the D_1 axis compared to the ⟨010⟩ axis [24]. A cavity was formed with two highly reflecting mirrors and the absorbed power threshold was measured to be 62.4mW. Figure 4.9 shows the laser output power against absorbed pump power with a 2% output coupler replacing one of the highly reflecting mirrors; the threshold was measured to be 78.0mW. The maximum output power was 36mW for 442mW of absorbed power. The pump wavelength was 792nm, measured on the EG&G Triple Grating Spectrograph. The laser wavelength was 1884nm, measured on an Applied Photophysics f/3.4 monochromator and the output was unpolarised.

While these results are inferior in terms of both threshold and slope efficiency to those achieved in Tm:YAG they compare well with bulk Tm:YSO lasers where thresholds of 176mW and slope efficiencies of 17% have been obtained [25] showing the promise of the liquid-phase epitaxial technique for fabricating waveguides in different crystal host materials such as YSO.

4.6 Summary

The thresholds and slope efficiencies of all the Tm:YAG waveguides tested are tabulated below, all guides were 4mm long. "P_{th}" is the absorbed power threshold, "O/C" denotes the output coupling used, and "slope" is the slope efficiency of the laser.

Table 4.2

Dopants	Depth /μm	Pump	O/C / %	P_{th} / mW	Slope / %
6.6%Tm, ~12%Ga, 35%Lu	14	AlGaAs diode	HR	29.5	-
"	"	"	2	50.1	34
"	"	"	15	139	49

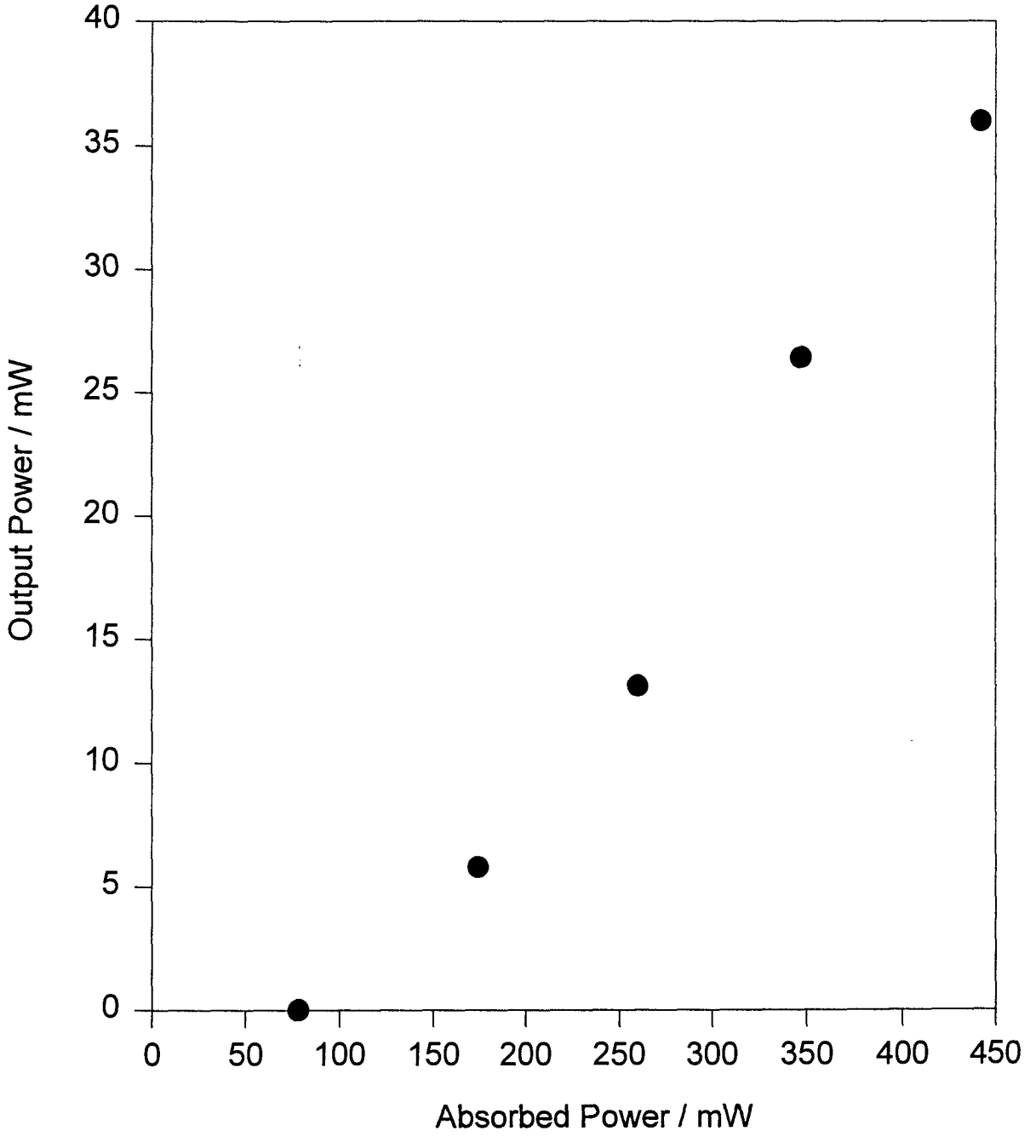

● 2% output coupler : slope efficiency = 13%

Figure 4.9 Laser output power vs absorbed pump power for a 4mm long Tm:YSO waveguide laser with a 2% output coupler (Sample B)

Dopants	Depth /μm	Pump	O/C / %	P_{th} / mW	Slope / %
6.6% Tm, ~12% Ga, 35% Lu	14	Ti:sapphire	1.8	8.6	31
8% Tm, 4% Ga	23.3	AlGaAs diode	HR	15.1	-
"	"	"	2	22.8	45
"	"	"	15	39.1	64
"	"	Ti:sapphire	HR	7.0	-
"	"	"	15	45.2	68
8% Tm, 4% Ga	14.1	"	"	72.2	44
13% Tm, 4% Ga	16.8	"	"	95.5	39
4% Tm, 2% Ga	13.6	"	"	42.7	45
"	23.8	"	"	73.6	48
8%Tm, 0% Ga	17.2	AlGaAs diode	HR	28.4	-
"	"	"	2	53.3	20
"	"	"	15	did not lase	-
"	"	Ti:sapphire	"	191	17

The results presented above show that improvements can be obtained over previous bulk laser results at 2μm in Tm:YAG in terms of both threshold and slope efficiency by a move to a planar geometry. A Ti:sapphire pumped Tm:YAG bulk laser has been operated with a threshold of about 200mW and a 59% slope efficiency [15]. Diode pumped bulk lasers have operated with a 77mW threshold and a 36% slope efficiency [26] and with a threshold of about 200mW and a 49% slope efficiency [17].

Waveguides, grown by LPE, with 4% Ga codoping showed better laser performance at 2μm than other guides grown with 12%, 2% and 0% Ga resulting in slope efficiencies of up to 68% with respect to absorbed power. The guide with 4% Ga gave the best trade off between the additional confinement of waveguide modes offered by Ga doping and the decrease in peak cross sections and increase in waveguide loss associated with it. A 4% Ga doping level is not necessarily the optimum and a different amount may enable optimisation of the 2μm laser.

The extension of the liquid-phase epitaxial technique to the growth of other low loss rare earth doped laser host crystal waveguides is a potentially important result. Liquid-phase epitaxy has been used, for the first time, to grow planar waveguides in the YSO host crystal, which were doped with Tm^{3+}. Lasers operating around 1.8μm in Tm:YSO planar waveguides have been realised with results comparable to that achieved in bulk crystals in terms of slope efficiency and with lower absorbed power thresholds.

If liquid-phase epitaxy can be used to fabricate low loss waveguides in other host materials such as low phonon energy fluoride crystals, for example, then possibilities exist for the fabrication of a new range of planar waveguide devices, such as room temperature upconversion lasers which could operate in the blue region of the spectrum for thulium doped materials.

References

1. J.N.Carter, R.G.Smart, A.C.Tropper and D.C.Hanna, Journal of Non Crystalline Solids, **140**, 10, 1992

2. J.P.de Sandro, J.K.Jones, D.P.Shepherd, M.Hempstead, J.Wang and A.C.Tropper, IEEE Photonics Technology Letters, **8**, 2, 209-211, 1996

3. G.J.Kintz, R.Allen and L.Esterowitz in Conference on Lasers and Electro-Optics, Vol. 2, 1988 OSA Technical Digest Series, Optical Society of America, Washington, D.C., 1988, paper FB 2

4. S.G.Grubb, K.W.Bennett, R.S.Cannon and W.F.Humer, Electronics Letters, **28**, 1243, 1992

5. T.Hebert, R.Wannemacher, R.M.Macfarlane and W.Lenth, Applied Physics Letters, **60**, 21, 2592, 1992

6. B.P.Scott, F.Zhao, R.S.F.Chang and N.Djeu, Optics Letters, **18**, 2, 113, 1993

7. K.F.Gibson and W.G.Kernohan, Journal of Medical Engineering & Technology **17**, 2, 51-57, 1993

8. I.Melngailis, W.E.Keicher, C.Freed, S.Marcus, B.E.Marcus, A.Sanchez, T.Y.Fan and D.L.Spears, Proceedings of the IEEE **84**, 2, 227-267, 1996

9. T.J.Kane, W.J.Kozlovsky, R.L.Byer and C.E.Byvik, Optics Letters **12**, 4, 239-241, 1987

10. J.Webjörn, D.Nam, S.Siala and R.Waarts, Optics & Photonics News, **8**, 4, 16-

20, 1997

11. J.B.Gruber, M.E.Hills, R.M.Macfarlene, C.A.Morrison, G.A.Turner, G.J.Quarles, G.J.Kintz and L.Esterowitz, Physical Review B, **40**, 14, 9464, 1989

12. T.Becker, R.Clausen, G.Huber, E.W.Duczynski and P.Mitzscherlich, Tunable Solid State Lasers, Vol. 5 of OSA Proceedings Series, Optical Society of America, Washington D.C., 1989, p.150

13. A.C.Large, D.C.Hanna, D.P.Shepherd, A.C.Tropper, I.Chartier, B.Ferrand and D.Pelenc, OSA Proceedings on Advanced Solid State Lasers, A.Pinto and T.Y.Fan eds., Optical Society of America, Washington D.C., 1993, Vol. 15, p.258

14. D.P.Shepherd, A.C.Large, D.C.Hanna, A.C.Tropper, I.Chartier, B.Ferrand and D.Pelenc, Applied Physics Letters **63**, 1, 7-9, 1993

15. R.C.Stoneman and L.Esterowitz, Optics Letters, **15**, 9, 486, 1990

16. A.Rameix, C.Borel, B.Chambaz, B.Ferrand, D.P.Shepherd, T.J.Warburton, D.C.Hanna and A.C.Tropper, submitted to Optics Communications 1997

17. P.J.M.Suni and S.W.Henderson, Optics Letters, **16**, 11, 817, 1991

18. A.Rameix, C.Borel, B.Ferrand, C.Wyon, D.P.Shepherd, T.J.Warburton, A.C.Tropper and D.C.Hanna, in Conference on Lasers and Electro-Optics Europe, Optical Society of America, Washington, D.C., 1996, paper CFD1

19. I.Chartier, B.Ferrand, D.Pelenc, S.J.Field, D.C.Hanna, A.C.Large, D.P.Shepherd and A.C.Tropper, Optics Letters, **17**, 11, 810, 1992

20. D.Pelenc, B.Chambaz, I.Chartier, B.Ferrand, C.Wyon, D.P.Shepherd, D.C.Hanna, A.C.Large and A.C.Tropper, Optics Communications, **115**, 491, 1995

21. D.P.Shepherd, D.C.Hanna, A.C.Large, A.C.Tropper, T.J.Warburton, C.Borel, B.Ferrand, D.Pelenc, A.Rameix, P.Thony, F.Auzel and D.Meichenin, Journal of Applied Physics, **76**, 11, 7651, 1994

22. C.Li, R.Moncorgé, J.C.Souriau and C.Wyon, Optics Communications, **101**, 356, 1993

23. A.A.Kaminskii, Laser Crystals, Springer Series in Optics Sciences, **14**, p. 145, Springer, Berlin, 1981

24. G.Buisson and C.Michel, Materials Research Bulletin, **3**, 193, 1968

25. C.Borel and J.C.Souriau, Materials Research Society Proceedings, **329**, 253, 1994

26. T.Yokozaura and H.Hara, Applied Optics, **35**, 9, 1424, 1996

Chapter 5 - Nd:YAG Planar Waveguide Amplifiers

5.1 Introduction

Rare earth doped solid state lasers have applications in diverse areas such as materials processing [1], laser radar [2,3,4], medicine [5], optical communications [6], free-space communications [7,8], and non linear frequency conversion [9,10]. For the high power operation often required it may be preferable to use a master oscillator power amplifier configuration rather than a simple high power laser source. Such a system permits careful design of the low power master oscillator in terms of beam quality, pulse shape and repetition rate allowing high fidelity modulation of a signal without the degrading effects associated with high power lasers. High power operation of the system is achieved using an optical power amplifier.

Guided wave amplifiers, such as the erbium-doped silica fibre amplifier have already been shown to play a key role in optical communications and in sensor applications. In this chapter I will report on investigations into the use of thin film planar waveguides as high gain optical amplifiers. Planar waveguide amplifiers can offer advantages over both bulk crystal and fibre devices; the confinement of the pump and signal radiation leads to high gains for lower pump powers than would be necessary in a bulk system and the larger cross sections for crystal waveguides relative to glass fibres allows for the fabrication of more compact devices in these materials.

Laser diodes are the preferred pump source for high power laser and amplifier devices due to their compactness, high power outputs and high efficiencies. The planar geometry is uniquely compatible with the elliptical beam shape from broad stripe diodes and diode bars enabling a simplification of some of the focusing techniques needed relative to those in a bulk device where complicated resonator designs or beam shaping techniques are often required to optimise performance [11,12,13]. The slab geometry of a planar system, together with the fact that cooling can be applied very close to the pumped region should allow for good heat removal, essential for high power operation

of a device.

As a first step towards proving some of these features the performance of Nd:YAG waveguides as amplifiers have been investigated the results for which will be reported in the remainder of this chapter. The waveguides investigated were fabricated by liquid-phase epitaxy (LPE) and thermal bonding.

5.2 Comparison of Thermally Bonded and Liquid-Phase Epitaxially Grown Nd:YAG waveguides

In this section I will briefly outline some of the properties of the two waveguides used in the experiments. The thermally bonded waveguide was fabricated by ONYX OPTICS, California whereas the LPE guide was grown by collaborators at LETI, Grenoble, France. Some of the physical properties of the waveguides are outlined in Table 5.1, below. Both waveguides had a pure YAG cladding layer.

Table 5.1

	Dopants	Length	Depth	Δ n	υ-parameter	~ Loss
LPE Grown	1at% Nd, 12at% Ga, 35at% Lu	5mm	3.8 μm	1.4×10^{-3}	5.1 @ 1.064μm	[1]0.15dB /cm
Thermally Bonded	1at% Nd	5mm	20 μm	0.48×10^{-3}	4.9 @ 1.064μm	[2]2.1dB / cm

In the above table Δn is the refractive index difference between the active layer and substrate, the υ-parameter is given by equation (2.20); a symmetric waveguide will be single mode at a given wavelength if the υ-parameter $\leq \pi$.

---

[1] See ref [14]

[2] This value may be as low as 0.7dB / cm, see Appendix B

Another factor of interest is the spectral characteristics of the two waveguides as any broadening of the fluorescence lines will result in a decrease of the peak emission cross section relative to that in a bulk sample. Figure 5.1 shows the emission spectra around 1.06μm of a bulk Nd:YAG sample together with those of the thermally bonded waveguide, an epitaxially grown Nd:YAG waveguide and the epitaxially grown Nd:Ga:Lu:YAG waveguide used for the amplifier experiments. All the spectra were taken using the same instrumentation and with the same spectral resolution. The thermal bonding process shows little sign of broadening the lines relative to a those in the bulk sample hence the emission cross section will be approximately the accepted bulk crystal value of $3.5\times10^{-23}m^2$ at 1.064μm. Liquid-phase epitaxy itself can be seen to have a slight effect on the emission line width, resulting in a small decrease in the peak emission cross section. Co-doping with gallium, to the level used here results in a marked broadening of the fluorescence lines and a corresponding decrease in the peak emission cross section at the laser wavelength to a value of 50% that of a bulk Nd:YAG sample. The broadening is inhomogeneous and can be attributed to crystal field variations at the Nd ion in the mixed crystal [15]. There is also a slight shift (~0.3nm) in the position of the peak of the fluorescence. It should be noted, however, that it should be possible to grow waveguides of the same depth as used here with a lower gallium concentration which would result in less broadening of the fluorescence and hence an improvement in the peak cross section.

5.3 Epitaxially Grown Nd:YAG Planar Waveguide Amplifiers

The epitaxially grown waveguide used in these experiments had one of its faces polished at an angle of around 0.5° to the other in the plane of the guide, which was to allow spatial separation of the reflected signal beam from the input signal after a double pass of the amplifier. The experimental setup was that described in section 3.9. Two pump sources were used for these experiments, a Ti:sapphire laser and a broad stripe diode laser, I shall begin by describing the Ti:sapphire pumped amplifier.

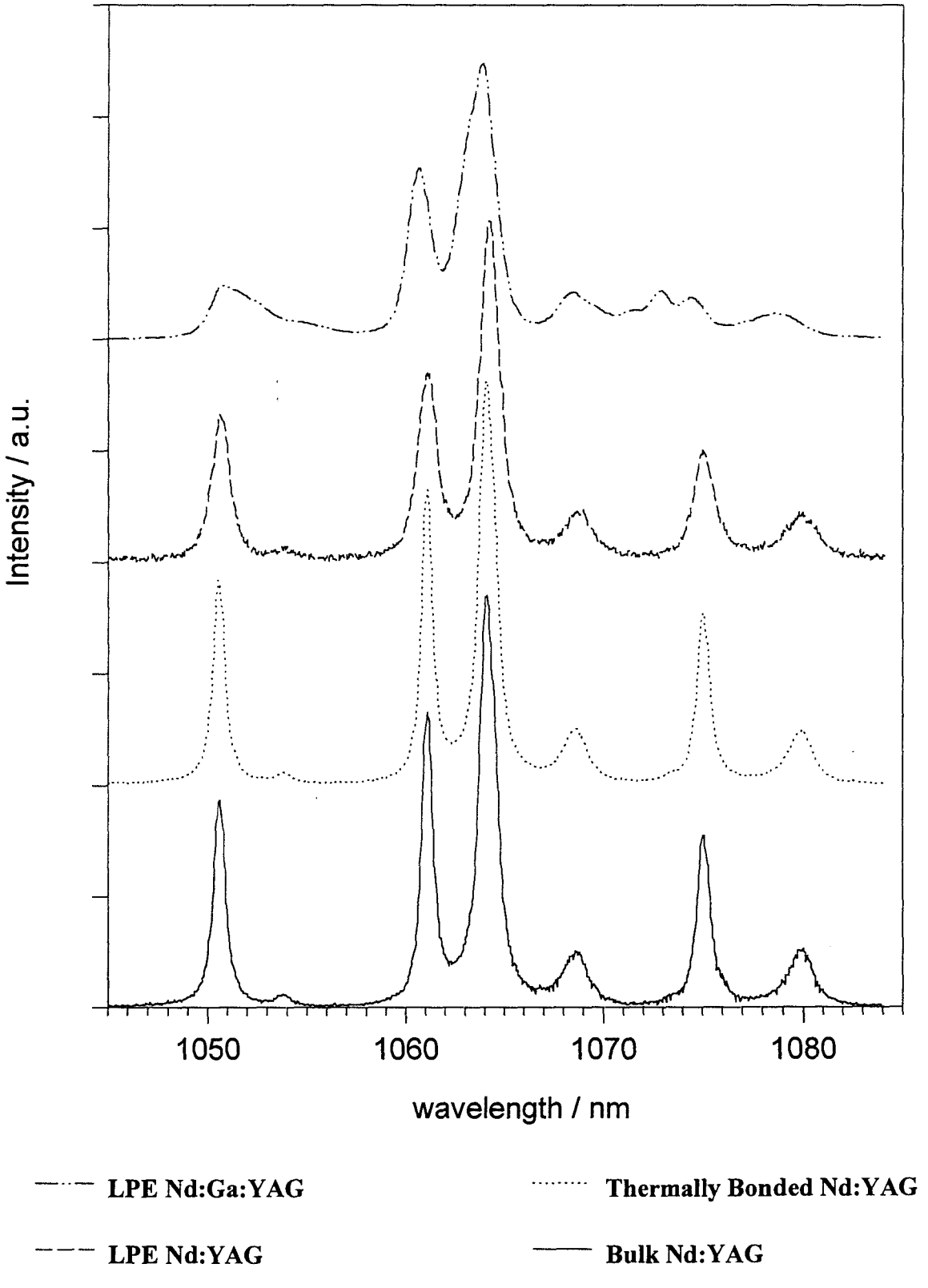

Figure 5.1 Fluorescence spectra of bulk and planar waveguide Nd:YAG

Ti:sapphire Pumped Amplifier

The preliminary experiments used the Ti:sapphire pump source as a test of the potential for using waveguides pumped by 4W broad stripe diode lasers as amplifiers. A broad stripe diode laser output consists of two lobes; if these lobes are separated and then polarisation coupled together the resulting beam will have M^2 of ~70 by ~1 in the two orthogonal planes [16]. From equation 3.1 the spot size required for confocal focusing through the length of the crystal is given by

$$w_y^2 = \frac{M^2 \lambda l}{2\pi n} \tag{5.1}$$

where λ is the pump wavelength, l is the crystal length and n is the refractive index. This gives a spot size in the unguided plane of 157μm. The pump beam was therefore focused into the waveguide, using an anamorphic prism pair and a 25cm focal length cylindrical lens to a spot size of 160μm in the unguided plane and to 2μm in the guided direction using a 12.7mm focal length cylindrical lens. Using equation (5.1) the calculated optimum spot size for the signal in the unguided direction, which maximised the small-signal gain was found to be ~30μm, this was achieved using a 20cm focal length cylindrical lens. The signal provided by a single frequency Nd:YAG laser was launched into the waveguide using a 22mm focal length lens. The relatively large width of the pump beam allowed for signal to double pass through this region, despite the spatial separation of the input and output. The output beam was picked off using a highly reflecting mirror.

The small-signal gain exponent is plotted against absorbed pump power in figure 5.2, the maximum small-signal gain is 226, equivalent to 23.5dB, for 250mW of absorbed pump power. The initial small-signal gain / watt of absorbed pump power was found to be 107dB / W; this is less than the theoretically expected value of 196dB / W. Reasons for the reduction in observed small-signal gain relative to theory are suggested in section 5.5. It should be noted, however, that these results suggest small-signal gains

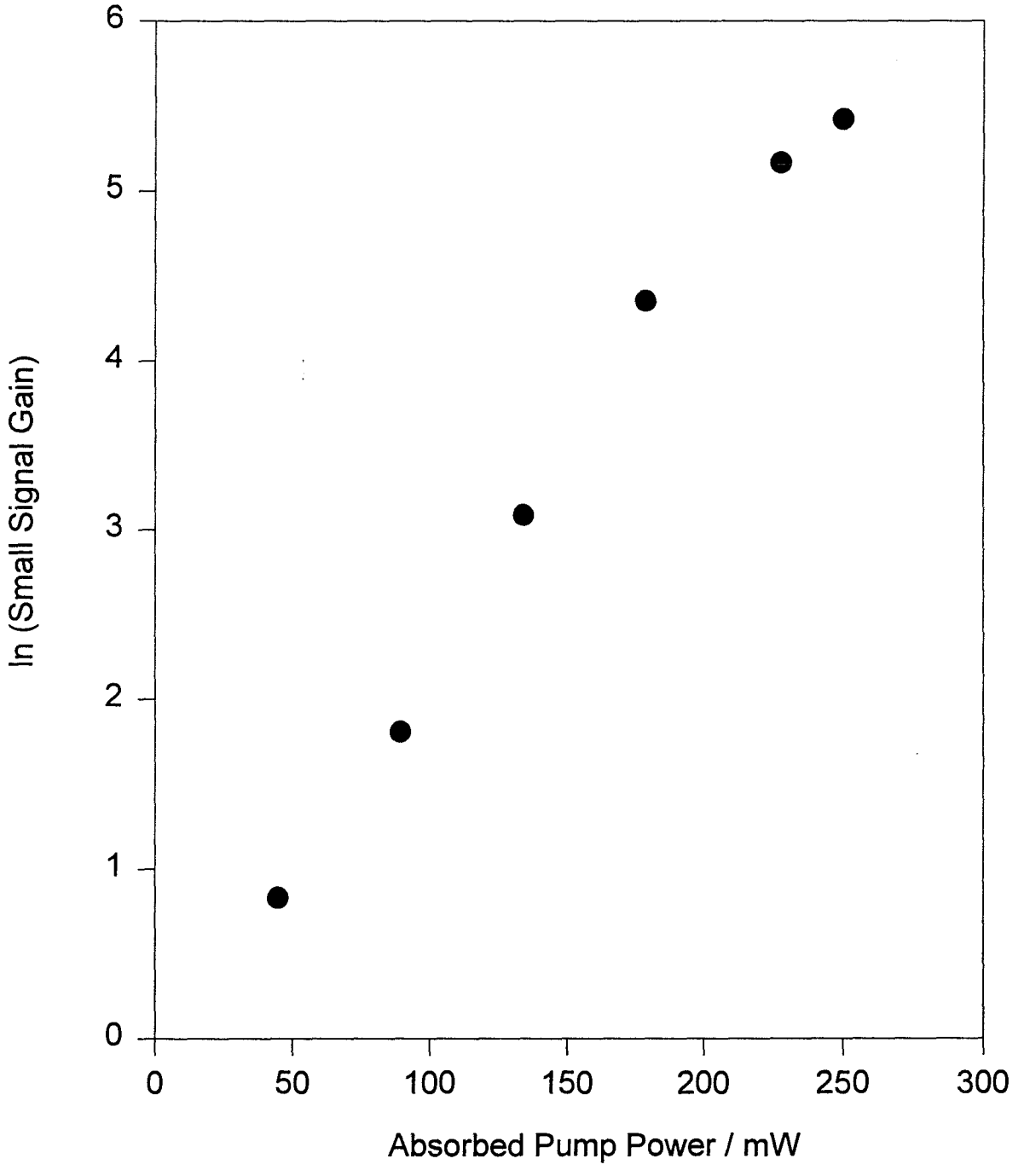

Figure 5.2 ln(small signal gain) vs absorbed pump power for Ti:sapphire pumped epitaxially grown Nd:YAG double pass amplifier

in the order of 200dB should be possible with a 4W broad stripe diode pump source, even if only half of the diode output power is absorbed in the waveguide.

Diode Pumped Amplifier [17]

Due to the unavailability of any 4W diodes the alternative pump source used for the double pass amplifier was a 1.2W SDL model 2360-P1 high brightness broad stripe diode. This diode has an emitting region of 1μm by 100μm perpendicular to and parallel to the plane of the junction respectively. The output from the diode has an M^2 of about 1 in the plane perpendicular to the junction and 34 in the orthogonal plane [18] which corresponds to the unguided plane of the waveguide. The spot size required in the unguided plane for confocal focusing of the pump can be calculated from equation (5.1) to be 110μm.

The pump light was collimated in the plane perpendicular to the junction, otherwise known as the fast plane, using a 6.5mm focal length spherical lens. In the other, slow, direction the pump was collimated using a 20cm focal length cylindrical lens. Final focusing into the waveguide was achieved by using a × 10 microscope objective. Careful adjustment of the cylindrical collimating lens achieved the pump spot size of ~ 110μm in the plane of the waveguide. The signal, from the 1mW single frequency Nd:YAG laser was focused using 12.7 and 250mm cylindrical lenses to produce spot sizes of 2μm × 32μm in the waveguide.

The maximum absorbed pump power was 505mW, from 1W of diode output. At this pump level the measured small-signal gain was 456 (26.6dB) corresponding to ~53dB / W of absorbed pump power. Saturation of the small-signal gain could be observed even for signal powers below 1mW as shown in figure 5.3.

In order to investigate the output extraction efficiency of the amplifier the single frequency Nd:YAG signal laser was replaced by a higher power, diode pumped bulk Nd:YAG laser system. This enabled signal powers approaching 90mW to be launched

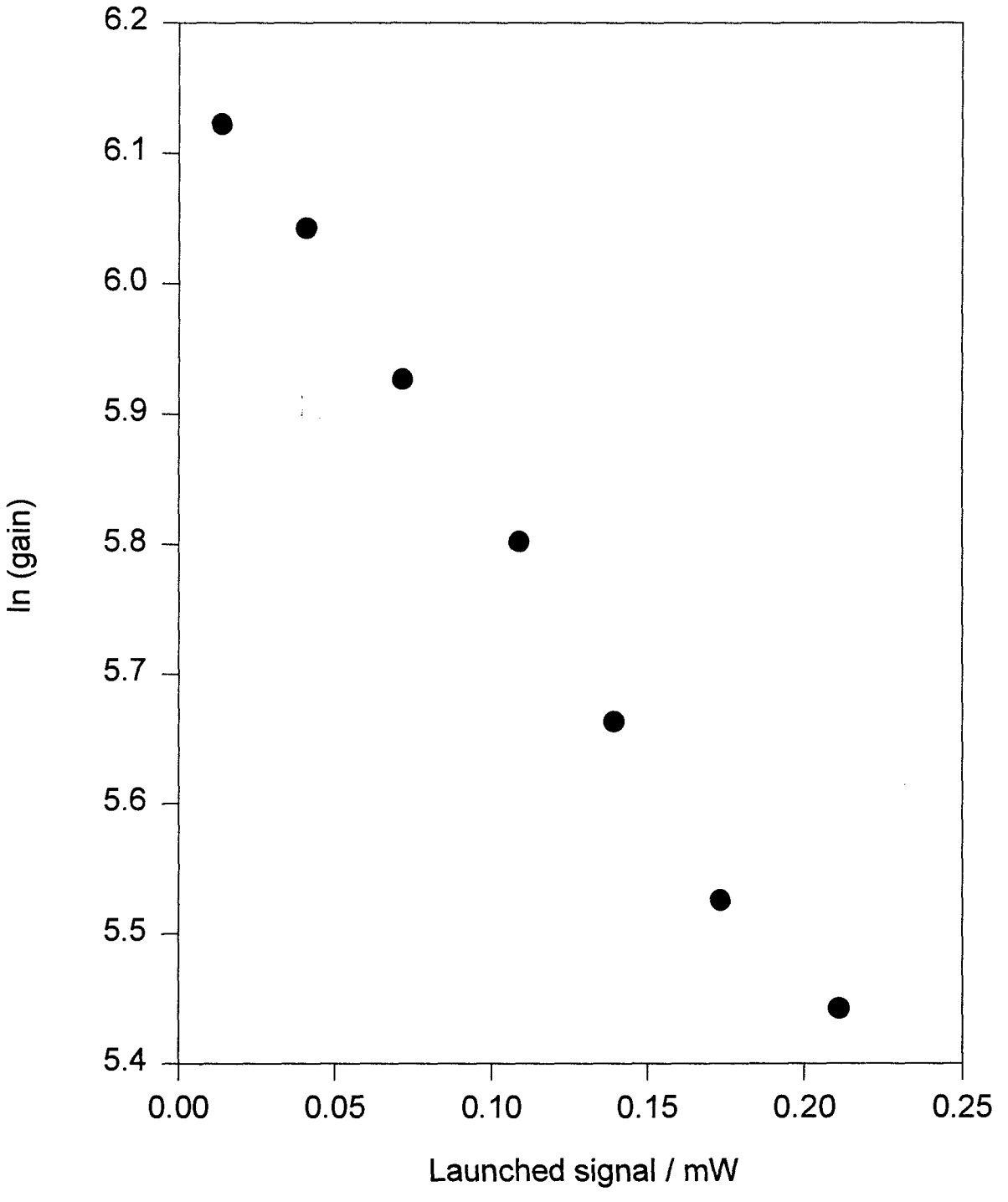

Figure 5.3 ln(gain) vs launched signal power for diode pumped epitaxially grown double pass Nd:YAG amplifier

into the waveguide. Using this signal source output powers of 290mW were measured for 89mW of launched signal power, figure 5.4, this corresponds to 201mW of extracted power for only 552mW of absorbed pump power. Even at lower signal powers of 1-8mW outputs of 50-100mW are obtained. The available power which can be extracted from an amplifier is given by equation (2.80), repeated below

$$I_{available} = I_s \cdot \ln(G_0)$$

where I_s is the saturation intensity and G_0 is the small-signal gain. The maximum possible power which can be extracted from this amplifier is therefore ~ 420mW. Our result, however, might well be improved by using a signal spot size better matching that of the pump and by having the signal retro-reflected at normal incidence.

The maximum small-signal gain measured was 686 (28.4dB) giving a small-signal gain / W of pump power similar to that found using the single frequency pump source. Figure 5.5 shows a plot of the gain in dB against absorbed pump power at a signal level of 0.52μW (some way above the small-signal level), it is interesting to note that the gain tails off rapidly from the initial straight line plot as the pump intensity is increased. The initial gain / unit pump power is ~90 dB / W which is some way below the theoretical value of ~ 278dB / W, according to equation (2.68), partly as a result of the slightly saturated nature. These results demonstrate the efficient performance possible in a planar waveguide amplifier, especially when one considers the peculiar path the signal beam takes through the pumped region. There is however some discrepancy between the theoretical small-signal gain, calculated using equation (2.68), and that obtained experimentally which will be addressed in section 5.5. It should be noted, however, that these results compare very favourably with bulk amplifiers where with 2.6W of absorbed pump power a cw small-signal gain of only 50 was obtained in a broad stripe diode pumped Nd:YLF amplifier [19]

5.4 A Thermally Bonded Nd:YAG Waveguide Amplifier

Thermal bonding is a potentially important new method of waveguide fabrication

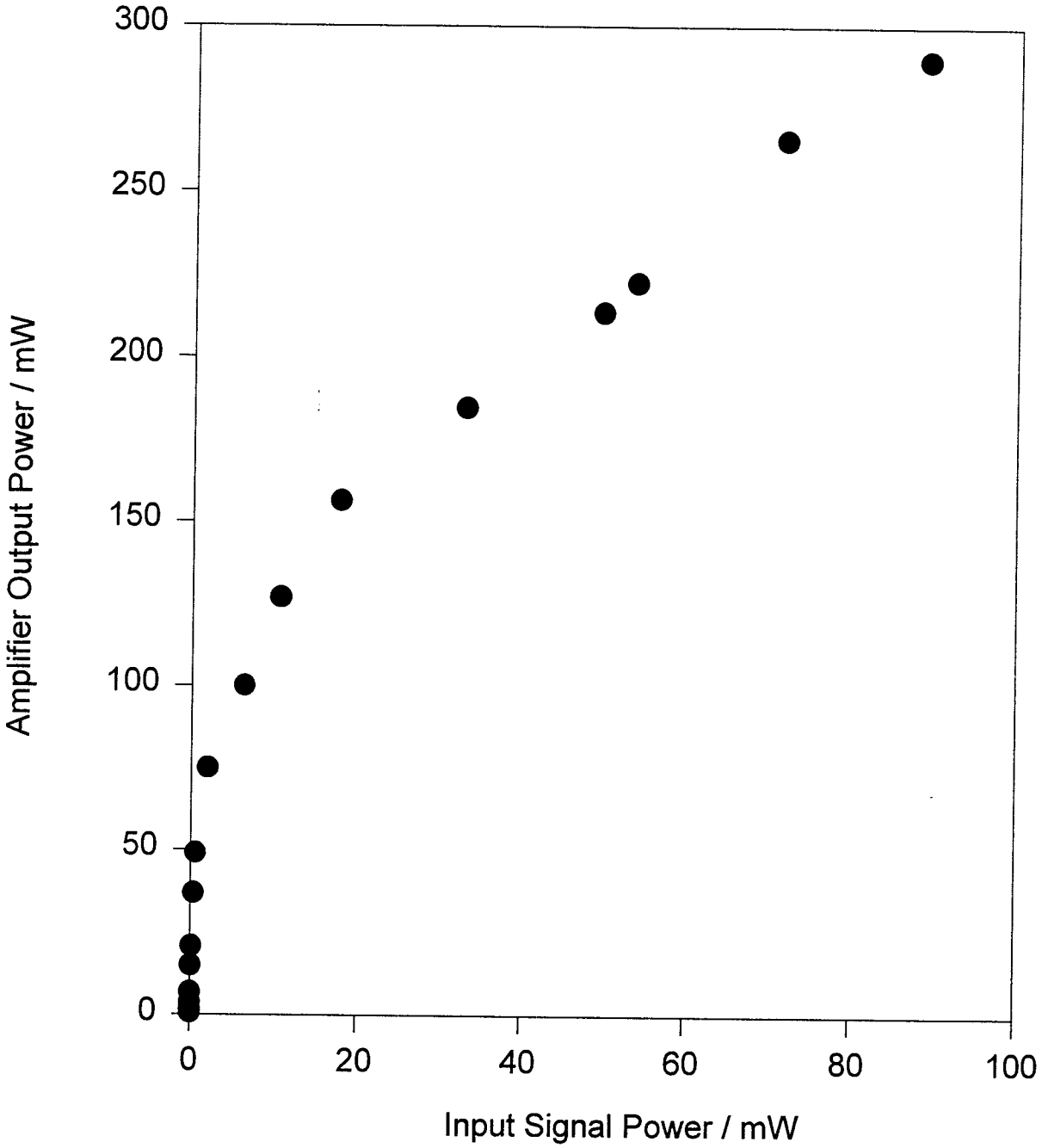

Figure 5.4 Output power vs launched signal power for diode pumped epitaxially grown Nd:YAG double pass amplifier with 552mW of absorbed pump power

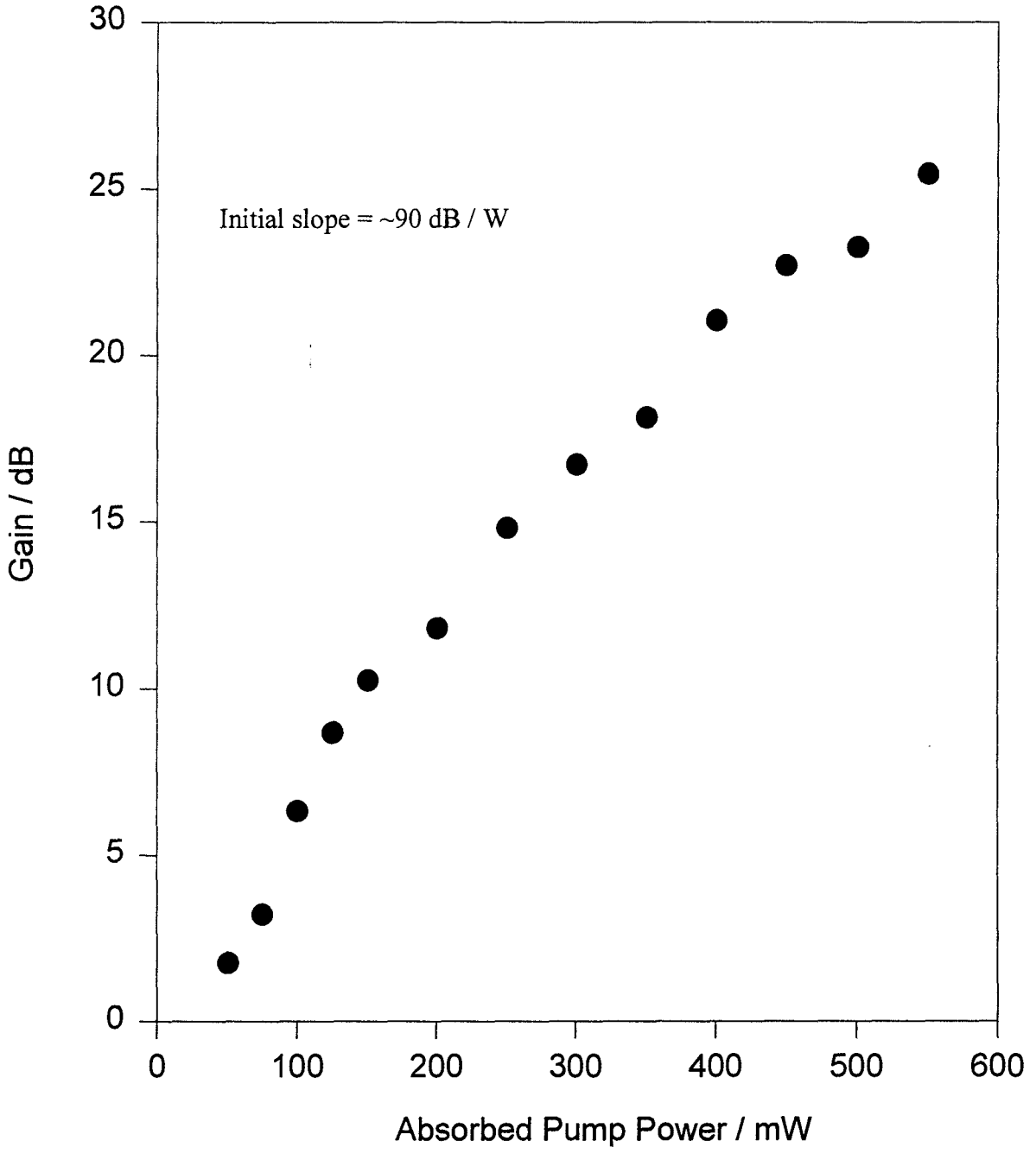

Figure 5.5 Gain (dB) against absorbed pump power for diode pumped epitaxially grown Nd:YAG double pass amplifier

due to its commercial availability and the simplicity of the procedure which, so the manufacturers claim, can be used to bond virtually any two crystalline materials or even to bond crystals to glasses. Appendix B describes laser experiments in a Nd:YAG waveguide fabricated using this method, from which the losses were estimated to be ≤2.1dB / cm. A loss of this order is surprisingly low considering the conceptual simplicity of the thermal bonding procedure, further reinforcing the suggestion that this could be a powerful new way to fabricate optical waveguides. It should still be noted, however, that these losses are quite high relative to other fabrication processes[3] which may inhibit the use of thermally bonded waveguides as low threshold lasers. There is some potential for the application of waveguides manufactured in such a manner as amplifiers where the tolerances on waveguide loss are somewhat lower than for lasers; a 2dB loss may be overlooked when gains in the order of 100 dB per watt of pump power are being considered. The waveguide used in the experiments described in this section was 1at% Nd doped, 20μm deep and sandwiched between two slabs of undoped YAG.

A double pass amplifier was set up using the thermally bonded Nd:YAG waveguide as the gain medium, in the manner described in section 3.9, with the two end faces of the waveguide polished parallel to one another. The pump source was a Ti:sapphire laser and the signal source was the 1mW single frequency diode pumped Nd:YAG laser used for some of the epitaxial amplifier experiments. The pump and signal beams were focused to spot sizes of 30μm in the unguided plane, which is equivalent to confocal focusing over a double pass of the crystal for the signal. The amplified output was extracted via the Faraday rotator and half wave plates as described in section 3.9.

In order to prevent lasing at 1.064μm an angled YAG wedge was butt coupled to the face of the waveguide through which the signal was launched, this was attached

---

[3] cf LPE Nd:YAG loss ~ 0.05dB / cm [20]
Ion implanted Nd:YAG loss ~ 1dB / cm [21]

to the waveguide face in the same manner as the dielectric mirror. The wedge served to couple any reflected light out of the waveguide preventing feedback which could lead to parasitic lasing, as shown in figure 5.6.

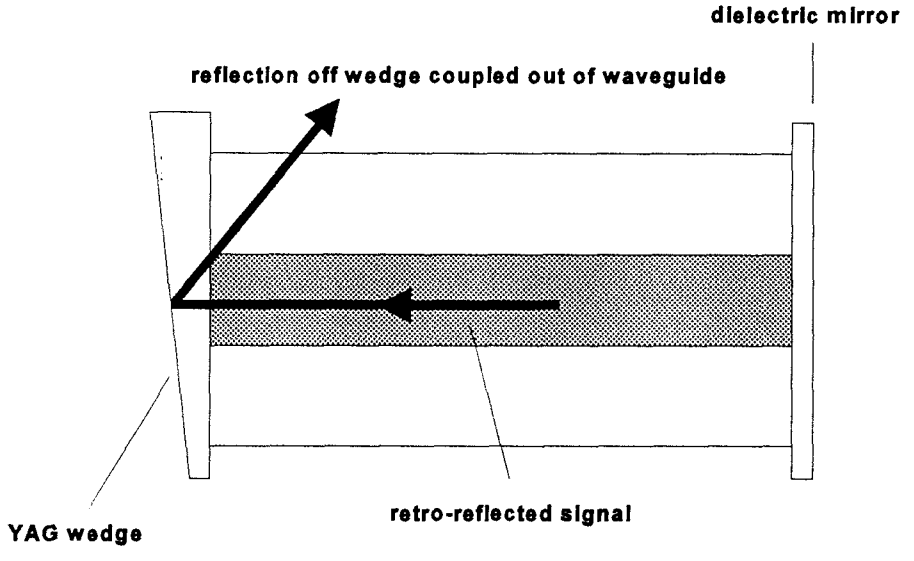

Figure 5.6 Coupling of retroreflected light out of the waveguide using a YAG wedge

The pure YAG was approximately index matched to the Nd:YAG in the core of the waveguide resulting in very little feedback from the front face of the wedge back into the guide and this allowed higher pump powers to be used without lasing. The lasing threshold was only 172mW of absorbed power in a cavity formed by one highly reflecting mirror and the Fresnel reflection from the opposite face [Appendix B]. It would improve the amplifier performance to have the end face of the waveguide antireflection coated at the signal wavelength.

In the double pass configuration the maximum small-signal gain observed was 229 (23.6dB) for 249mW of absorbed pump power, figure 5.7. With a signal power of <0.1mW launched into the waveguide an output of 7mW was extracted via the Faraday

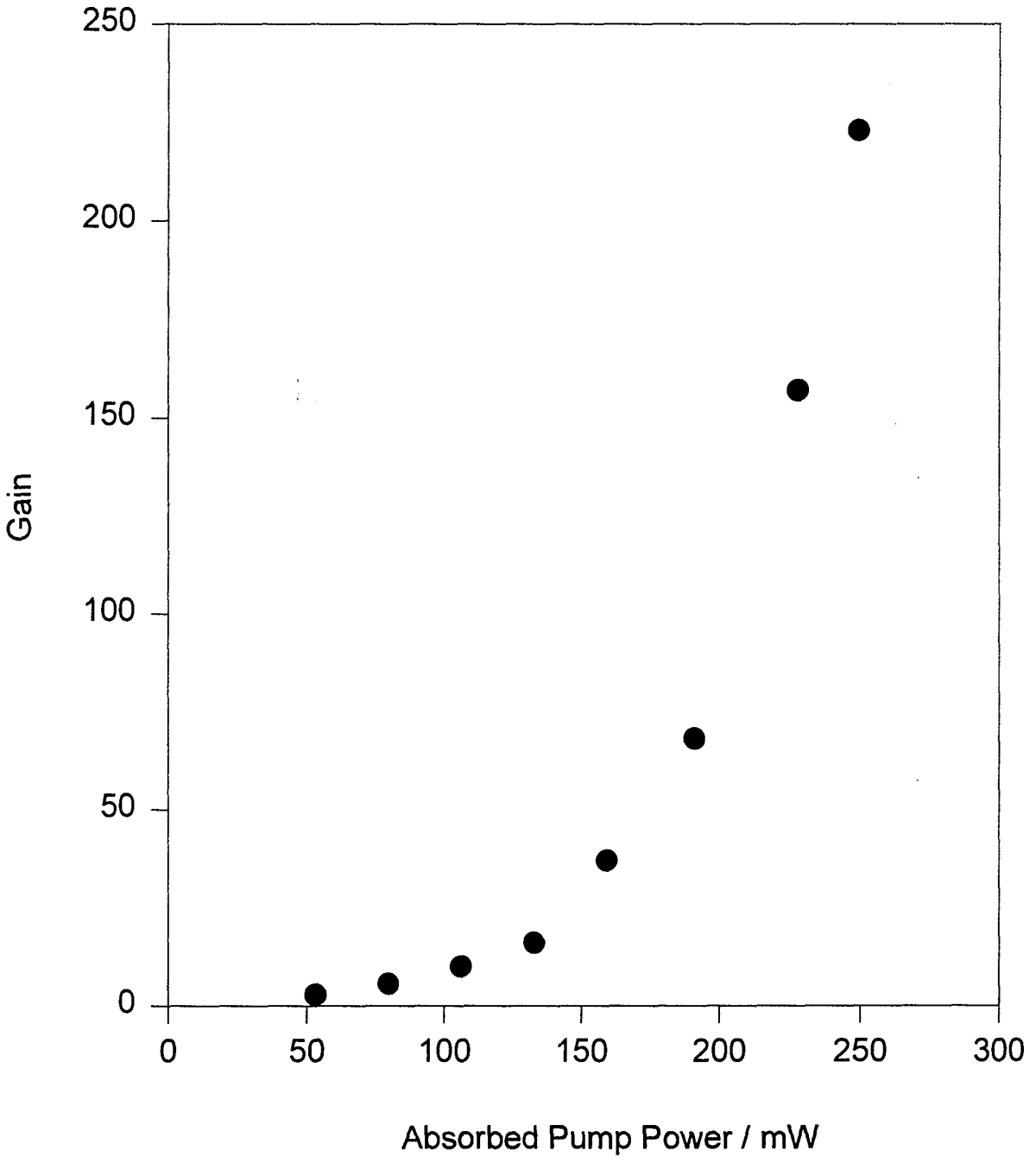

Figure 5.7 Small signal gain vs absorbed pump power for Ti:sapphire pumped thermally bonded Nd:YAG double pass amplifier

rotator. Theoretical analysis dictates, according to equation (2.68), that the small-signal gain should be equal to ~ 300 dB / W of absorbed pump power, however the experiments suggest a gain of 98 dB / W, figure 5.8. In all the amplifiers described in this chapter it has been observed that the theoretical small-signal gain, expressed in dB, is a factor of a few times larger than that experimentally observed, even at relatively low pump levels, furthermore the slope of the gain against pump power graph seems to tail off from its initial value at higher pump powers.

5.5 Comparison of Theoretical and Experimental Small-Signal Gain

There are several factors which may explain the discrepancy between the theoretical gain expected, from the analysis of Chapter 2, and that found experimentally as described in the previous sections of this chapter. The theory used so far has been a fairly simple one which neglects any effects due to upconversion, pump saturation, amplified spontaneous emission, temperature dependent shift in the spectral line position or indeed any consideration of the overlap between the pump and signal beams. I shall briefly discuss these factors one by one in a qualitative manner.

Excited state absorption (ESA) from the $^4F_{5/2}$ pump level to the excited $^4G_{7/2}$ manifold due to pumping the Nd^{3+} ion at 807nm (see figure 6.1) may, together with an energy transfer process between two ions in the upper laser level, lead to depopulation of this level. The depopulation of the upper laser level due to upconversion or ESA will lead to a decrease in the population inversion compared to that expected in the theory used, resulting in an overestimation of the gain.

Another factor to consider is the overlap of the signal with the pump, or more correctly the population inversion. It is fairly evident that for the epitaxial amplifier described earlier the unusual path described by the signal beam through the pumped region will result in a reduction in the overlap relative to the case where the signal is reflected at normal incidence. Even for slight angles between pump and signal there may be, however, some considerable reduction in the overlap. Pump saturation may also play

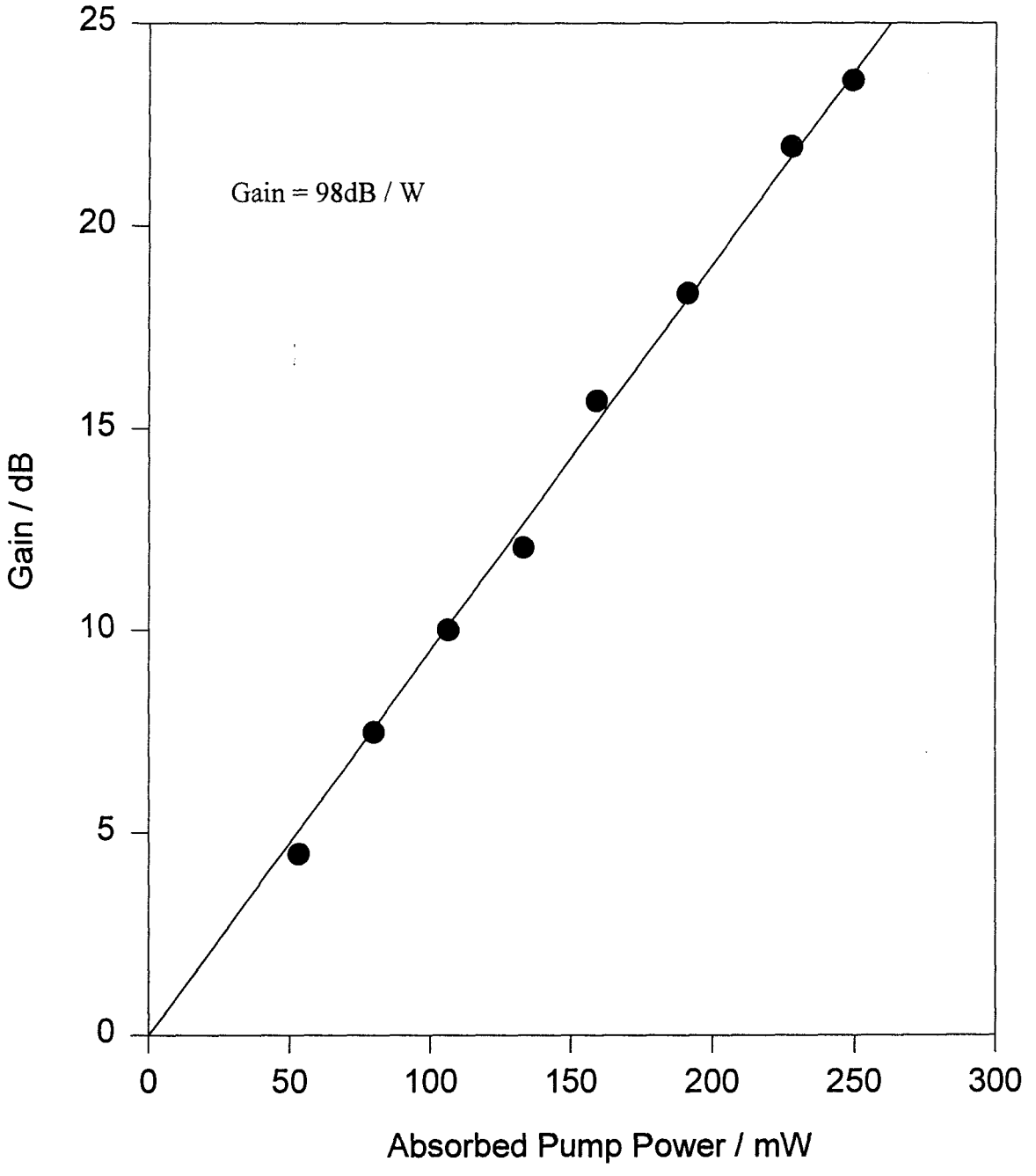

Figure 5.8 Gain (dB) vs absorbed pump power for Ti:sapphire pumped thermally bonded double pass amplifier

a part in decreasing the overlap for both the amplifier configurations considered here. The pump saturation intensity is given by equation (5.2)

$$I_{p,sat} = \frac{h\nu_p}{\sigma_a \tau} \tag{5.2}$$

where h is Planck's constant, ν_p is the frequency of the pump light, σ_a is the absorption cross section at the pump wavelength and τ is the radiative lifetime of the upper laser level. For both the Ti:sapphire and diode pumped experiments the pumping intensity is greater by a factor of 1.5 or more than the pump saturation intensity, this has the effect of beginning to saturate the population inversion which in turn leads to a change in the inversion profile which at low powers followed the pump beam shape. This change in population inversion profile will increase with increasing pump power above the saturation intensity and will result in a decreased overlap between the signal and population inversion which again leads to an overestimation in the theoretical gain.

At high gains there may be some clamping of the gain with respect to pump power by amplified spontaneous emission (ASE). Spontaneous emission from one part of the waveguide may be amplified in the rest of the guide which can then lead to saturation of the gain. The threshold above which ASE plays a dominant role in depopulating the inversion is given by equation (5.3), for an amplifier with a highly reflecting mirror on one end face [22]

$$\frac{[\ln G^2]^{1/2}}{G} = \frac{\Omega}{4} \tag{5.3}$$

where G is the gain and Ω is the solid angle into which light emitted from one end of the amplifier sees the full amplifier gain, given for a planar waveguide by equation (5.4).

$$\Omega = \frac{\pi D}{4l}\left(\frac{NA}{n}\right) \tag{5.4}$$

where D is the width of the inverted region, l the waveguide length, n the refactive index and N.A. is the numerical aperture. Above such a gain amplified spontaneous emission significantly reduces the experimental gain relative to theory. This limit can be evaluated for the thermally bonded and epitaxial waveguides of this chapter, and corresponds to values for G of 39dB and 31dB respectively.

The positions of the spectral lines in Nd doped samples are partly temperature dependent, with an energy shift in the 1.064μm emission line in Nd:YAG of 0.04cm^{-1} / °C at room temperature [23]. Under the diode pumping conditions for the epitaxial amplifier, for example, the temperature increase in the guided region may be around 10°C relative to the heat sink [24]; the resulting frequency lineshift of 12 GHz will decrease the spectral overlap between the signal and emission in the gain medium decreasing the measured small-signal gain.

In an attempt to reduce the above factors an experiment was set up using larger signal spot sizes than previously employed, in the thermally bonded waveguide at absorbed pump powers no greater than 150mW. The pump beam, from a Ti:sapphire laser was focused to a spot size of 55μm in the unguided direction using a 250mm focal length cylindrical lens. The signal, from the diode pumped Nd:YAG laser was focused to a 50μm spot size using a 200mm focal length lens. The pump and signal spot sizes were measured on a calibrated Big Sky Corporation Beam View Analyser. The pump saturation intensity for Ti:sapphire pumping at 807nm is around 120 MW / m^2, the maximum pump intensity used in this experiment was ~ 95MW / m^2 which is some way below the pumping intensity used for the earlier experiments.

Several experiments were carried out in both single and double pass amplifier configurations and lasing experiments, the results for which are shown in figure 5.9. The plot has been adjusted to give results in terms of single pass gain, i.e. the gain exponents measured in the double pass amplifier and over a round trip in the laser have been divided by two. The different sets of results indicate a good degree of internal consistency

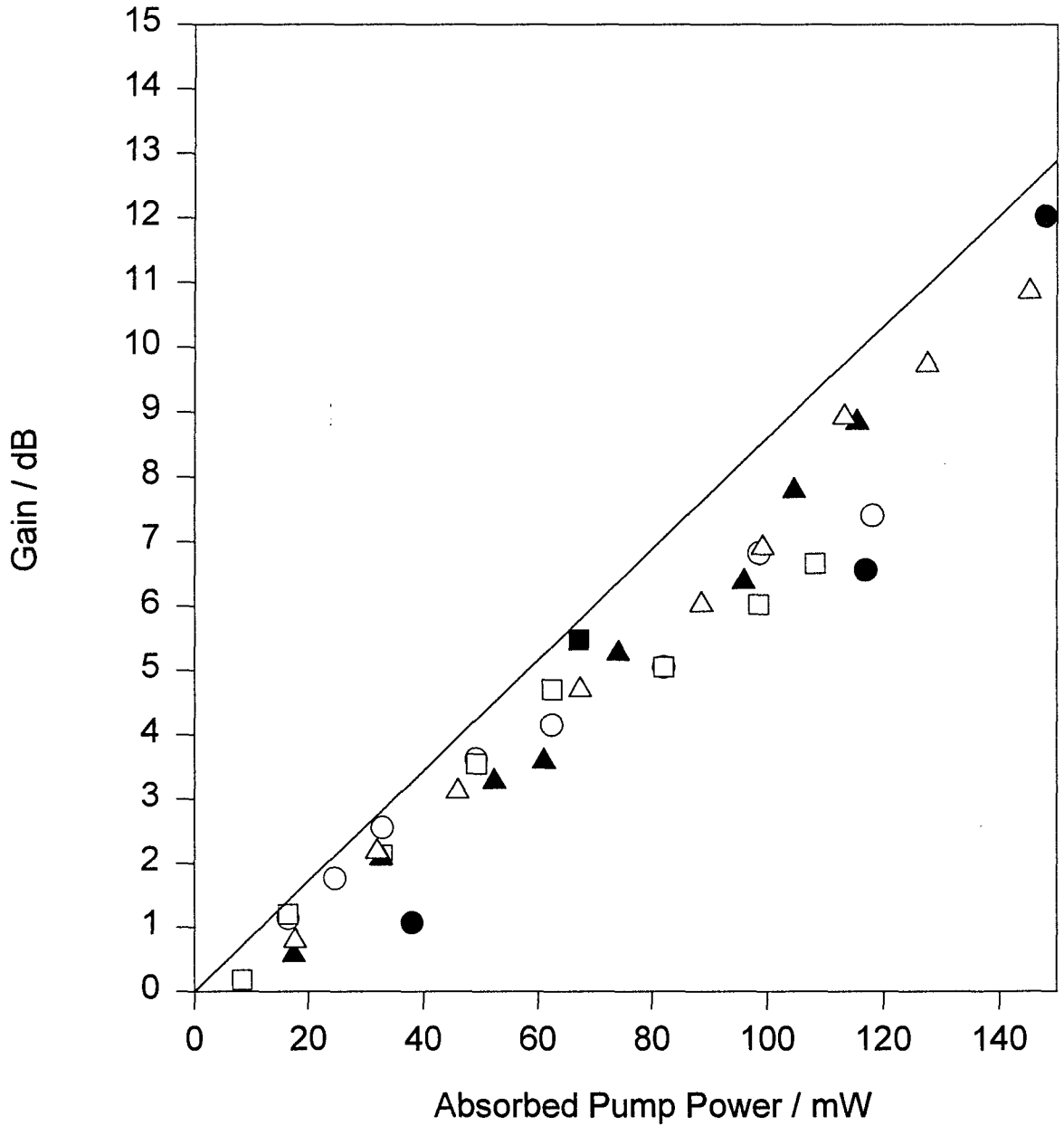

○ single pass, set 1

■ double pass, set 1

□ single pass, set 2

▲ double pass, set 2

△ single pass, set 3

● laser

—— theoretical small signal gain (dB)

Figure 5.9 Gain (dB) vs absorbed pump power for a variety of Ti:sapphire pumped amplifier / laser configurations in thermally bonded Nd:YAG waveguide

between different experiments, and a close relationship to the theory, represented by the solid line. The theory presented in Chapter 2 gives a value of gain against pump power of 86 dB / W, this compares reasonably with the experimental average value of 72 dB / W. Due to the low pump power and low gain nature of this experiment most of the factors considered earlier, which could lead to a reduction in the small-signal gain, can be assumed to be negligible. The difference between the theoretical gain and that observed experimentally can therefore be considered a measure of the overlap integral between the signal and population inversion.

5.6 Effect of Pump and Signal Overlap on Small-Signal Gain

In the low pump power limit, where saturation of the population inversion can be ignored, the profile of the population inversion follows that of the pump beam. The overlap integral between the pump and signal in a planar waveguide can be written as

$$\eta_{total} = \eta_{guided} \cdot \eta_{unguided} \tag{5.5}$$

where η_{total} is the total overlap integral, η_{guided} is the overlap in the guided direction and $\eta_{unguided}$ is the overlap in the unguided direction. From Appendix A the overlap of two waveguide modes is given by

$$\eta_{guided} = \int_{-d/2}^{d/2} \frac{\cos^2(k_s x)}{\sqrt{N_s}} \cdot \frac{\cos^2(k_p x)}{\sqrt{N_p}}\, dx \tag{5.6}$$

where N_s and N_p are normalising constants, k_s and k_p are the transverse wavenumbers in the waveguide region for the signal and pump respectively and d is the depth of the waveguide. This can be evaluated and for the waveguides considered in this chapter gives values of 0.994 for the thermally bonded guide and 0.993 for the epitaxial guide. This requires only a slight adjustment of the theory which predicts the overlap to be that of two Gaussian beams with the same spot size, giving an overlap of 1.

In the unguided direction of a planar waveguide the overlap integral is that of two Gaussian beams, which may have an angular tilt between them, θ, or an initial offset between the axes of the pump and signal, Δ_o, as shown in figure 5.10.

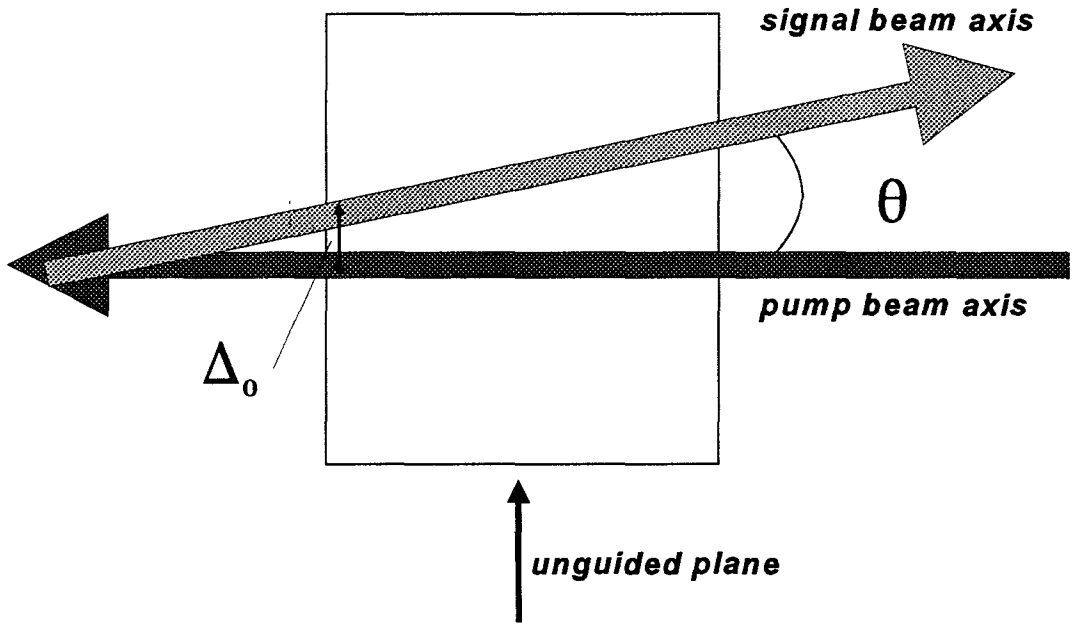

Figure 5.10

The expression for the overlap integral in such a case is derived in Appendix A and is given by equation (5.7)

$$\eta(z) = \frac{2(w_s w_p)^{1/2}}{(2w_p^2+2w_s^2)^{1/2}} \exp\left[-\Delta(z)^2\left(\frac{2}{w_s^2}-\frac{4}{w_s^4(2/w_s^2+2/w_p^2)}\right)\right] \qquad (5.7)$$

where $\Delta(z)=\Delta_0 + z\tan\theta$. To find the average overlap integral through the length of a device this equation must be integrated with respect to length. It is apparent that for a beam with zero offset or angular tilt (i.e. $\Delta = 0$ throughout the length of the device) this expression reduces to that of two Gaussian beams with spot sizes w_s and w_p.

5.7 Application of Overlap Integrals to Amplifier Experiments

Low Gain Thermally Bonded Amplifier

In the thermally bonded amplifier experiments there is an uncertainty in the angular tilt between the pump and signal beams resulting from the experimental configuration. By comparing the theoretical analysis of reduction in overlap due to tilt with the experimentally observed small-signal gain, it is possible to infer the approximate size of the tilt angle needed to explain the result. Figure 5.11 shows the variation in average overlap over the length of the waveguide against the tilt angle, θ. From the experimental results presented in section 5.4 the measured small-signal gain is 84% of the value given by the theory, this suggests the overlap in the unguided plane between pump and signal is 84%. From figure 5.11 it is possible to deduce that this overlap would result from a tilt angle of 7.8 mrad, equivalent to 0.45°. An angular tilt between the pump and signal beams of this size is quite feasible in the experimental setup, suggesting that the difference between the theoretical and experimental small-signal gains, in the low pump power, low gain, limit is indeed a measurement of the overlap integral.

Ti:sapphire Pumped Epitaxially Grown Amplifier

In the epitaxial amplifier, pumped using the Ti:sapphire laser the experimental small-signal gain per unit pump power was found to be 107 dB / W for low pump powers. The theory suggests that the small-signal gain should be 196 dB / W, according to equation (2.68). The experiment was set up so that the first pass of the signal was collinear with the pump while the second pass would be at an angle of 1° to the pump due to the angle polished face. These factors result in an overlap of 0.552 if the signal is on axis with the pump on the first pass. It may be preferable, however, if the signal were to have a slight offset to the pump on its first pass, which would decrease the overlap on this pass but improve it on the second pass. The optimum offset, which maximises the overlap, can be found to be around 20μm for this amplifier. An offset of this size will result in an overlap of 0.568 between the pump and signal. Figure 5.12 shows how the overlap changes with distance through the waveguide on the second pass

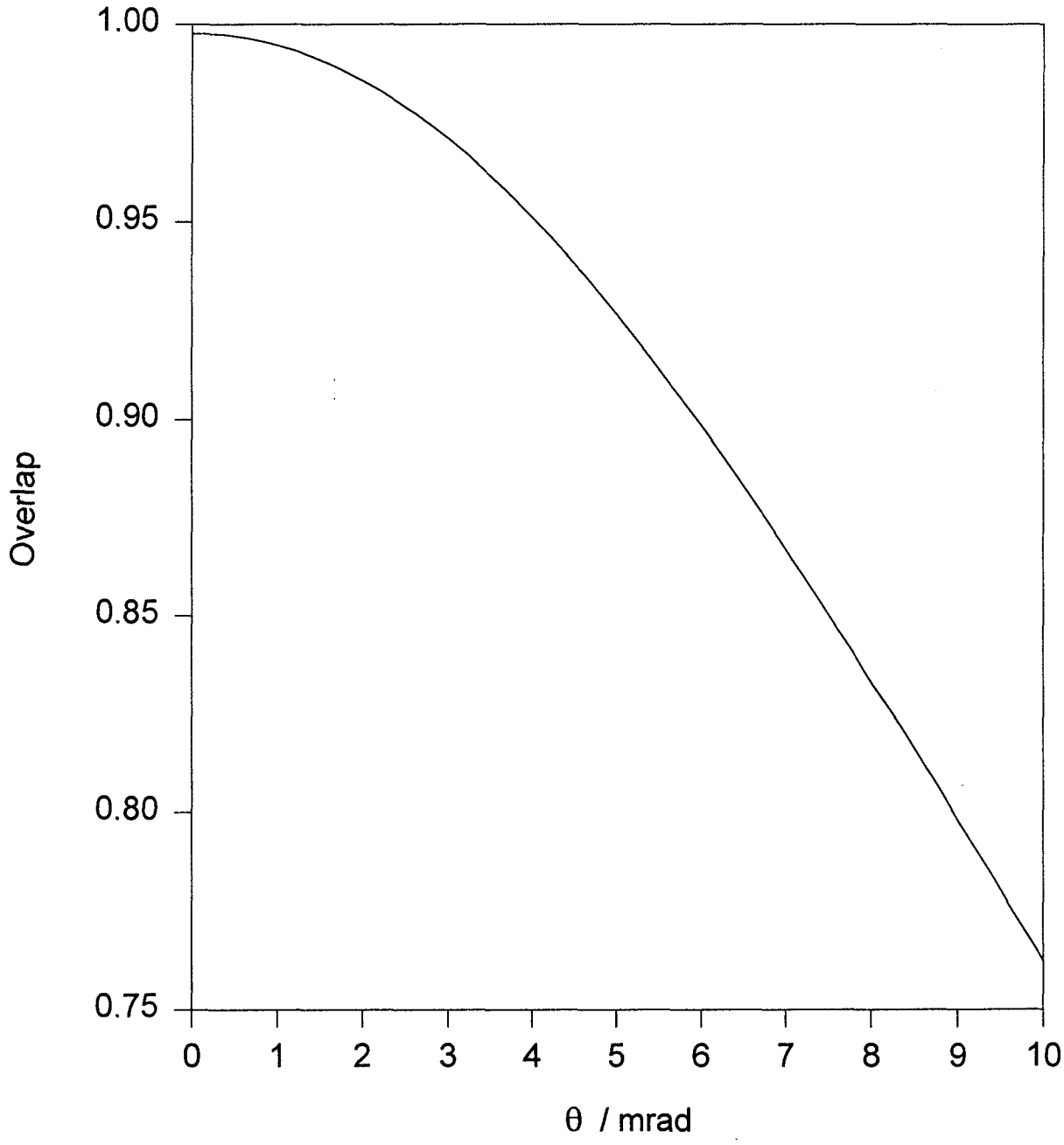

Figure 5.11 Variation of pump / signal overlap with angular tilt for thermally bonded amplifier

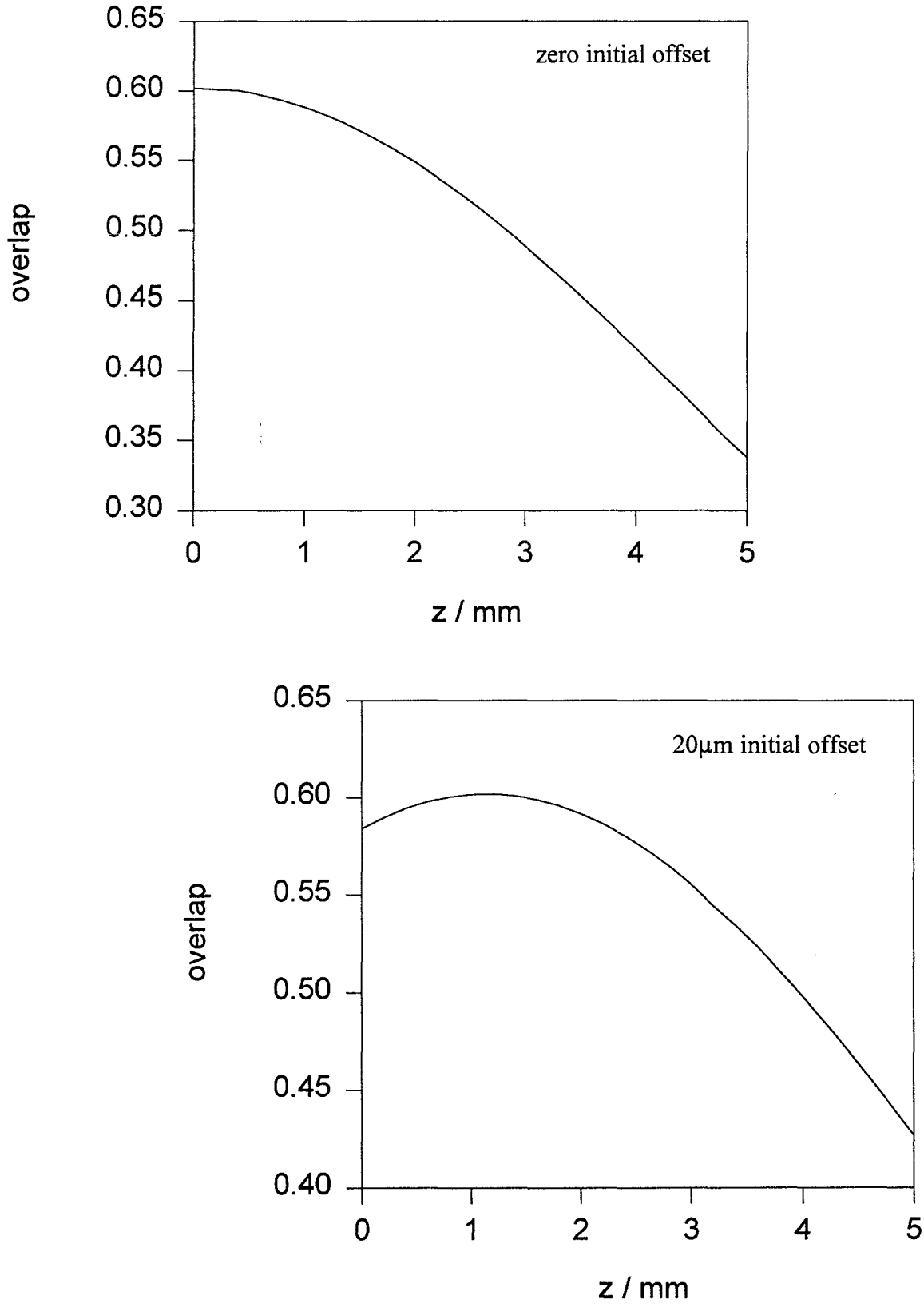

Figure 5.12 Overlap Integral against distance through crystal on the second pass of the amplifier in the epitaxially grown waveguide

of the amplifier for the cases of no offset and for a 20μm offset.

If one assumes that the difference between the experimental gain, found to be 107dB / W for low pump powers, and the theoretical gain calculated using equation (2.68) (196 dB / W) to be as a result of overlap alone then this would suggest an overlap integral of 0.55, which is in excellent agreement with the expected value of 0.568 if one assumes that the signal was indeed at an offset of 20μm with the pump.

This analysis of the effect that overlap integral has on the small-signal gain of an optical amplifier can be extended not only to other waveguide amplifiers, but also to bulk devices. In bulk systems, where there is no confinement of pump or signal radiation the overlap will be the product of two tilted Gaussian beams, in the two orthogonal planes. This extra degree of freedom in the tilt may result in worse overlaps than in the waveguide case, and could explain the reduction in experimental gains relative to the theory for such devices.

5.8 Summary

Double pass amplifier experiments have been performed in Nd:YAG planar waveguides at 1.064μm. The waveguides were fabricated by liquid-phase epitaxy (LPE) and by thermal bonding.

The LPE grown waveguide was 3.8μm deep, was codoped with gallium and lutetium and had a pure YAG substrate and cladding layer. Using a Ti:sapphire pump source, focused so as to simulate pumping with a 4W broad stripe diode laser, small-signal gains of 226 (23.5dB) were measured with 250mW of absorbed pump power. With a 1.2W broad stripe diode laser as the pump source small-signal gains of 686 (28.4dB) were obtained for ~550mW of absorbed pump power. Outputs of 290mW were extracted from this amplifier with 90mW of launched signal power.

The thermally bonded waveguide was 20μm deep with a pure YAG substrate and

cladding layer. Using a Ti:sapphire pump source, focused so as to optimise the gain, small-signal gains of 229 (23.6dB) were measured with ~250mW of absorbed pump power.

Discrepancies between the experimentally observed small-signal gain and that predicted by equation (2.68) were found to be attributable to the overlap between the pump and signal beams in the low pump power, low gain limit. In the higher power, higher gain limit discrepancies could be due to a number of additional factors such as upconversion, amplified spontaneous emission or as a result of pump saturation.

The results presented in this chapter show much of the potential for using planar waveguides for high gain optical amplifiers. The results show significant improvement, in terms of small-signal gain, over similar amplifiers in bulk neodymium doped crystals and due to certain unique features of the planar geometry these advantages may be added to as the amplifiers operate under higher pump power conditions.

References

1. K.Du, J.Biesenbach, D.Ehrlichmann, U.Habich, U.Jarosch, J.Klein, P.Loosen, J.Niehoff and R.Wester, Optical and Quantum Electronics **QE-27**, 1089-1102, 1995

2. T.J.Kane, W.J.Kozlovsky, R.L.Byer and C.E.Byvik, Optics Letters **12**, 4, 239-241, 1987

3. S.W.Henderson, P.J.M.Suni, C.P.Hale, S.M.Hannon, J.R.Magee, D.L.Burns and E.H.Yuen, IEEE Transactions on Geoscience and Remote Sensing **31**, 1, 4-15, 1993

4. I.Melngailis, W.E.Keicher, C.Freed, S.Marcus, B.E.Marcus, A.Sanchez, T.Y.Fan and D.L.Spears, Proceedings of the IEEE **84**, 2, 227-267, 1996

5. K.F.Gibson and W.G.Kernohan, Journal of Medical Engineering & Technology **17**, 2, 51-57, 1993

6. Govind P.Aggrawal, Nonlinear Fiber Optics, Academic Press Inc., 1989

7. M.A.Krainak and A.W.Yu, IEEE Journal of Quantum Electronics **32**, 1, 1996

8. K.Baker, A.Yu and M.Krainak, IEEE Photonics Technology Letters **5**, 260-262, 1993

9. M.D.Selker, T.J.Johnstone, G.Frangineas, J.L.Nightingale and D.K.Negus, in Postdeadline Digest of Conference on Lasers and Electro-Optics ,Optical Society of America, Washington, DC, 1996, paper CPD21-2

10. K.I.Martin, W.A.Clarkson and D.C.Hanna, Optics Letters **21**, 12, 875-877, 1996

11. T.M.Baer, D.F.Head, P.Gooding, G.J.Kintz and S.Hutchinson, IEEE Journal of Quantum Electronics **QE-28**, 1131-1138, 1992

12. H.Plaessman, S.A.Ré, J.J.Alonis, D.L.Vecht and W.M.Grossman, Optics Letters **18**, 1420-1422, 1993

13. W.A.Clarkson and D.C.Hanna, Optics Letters **21**, 6, 375, 1996

14. D.C.Hanna, A.C.Large, D.P.Shepherd, A.C.Tropper, I.Chartier, B.Ferrand and D.Pelenc, Applied Physics Letters **63**, 1, 7-9, 1993

15. R.K.Watts, W.C.Holton, Journal of Applied Physics **45**, 873, 1974

16. D.W.Hughes, A.A.Majidabadi, J.R.M.Barr and D.C.Hanna in OSA Proceedings on Advanced Solid-State Lasers, Optical Society of America, Washington, DC 1993, Vol. 19, p.200-202

17. D.P.Shepherd, C.T.A.Brown, T.J.Warburton, D.C.Hanna, A.C.Tropper and B.Ferrand, submitted to Applied Physics Letters, 1997

18. SDL Product Catalogue

19. G.J.Friel, W.A.Clarkson and D.C.Hanna, in Conference on Lasers and Electro-Optics, Vol.9, 1996 OSA Technical Digest Series, Optical Society of America, Washington, DC, 1996, p.144

20. I.Chartier, B.Ferrand, D.Pelenc, S.J.Field, D.C.Hanna, A.C.Large, D.P.Shepherd and A.C.Tropper, Optics Letters **17**, 11, 810-812, 1992

21. S.J.Field, D.C.Hanna, D.P.Shepherd, A.C.Troppper, P.J.Chandler, P.D.Townsend and L.Zhang, IEEE Journal of Quantum Electronics **QE-27**, 428-433, 1991

22. O.Svelto, Principles of Lasers, Plenum, 1989, p.68-70

23. T.Kushida, Physical Review **185**, 2, 500-508, 1969

24. C.T.A.Brown, Optoelectronics Research Centre, *private communication*, 1996

Chapter 6 - In-Band Pumping of 946nm Nd:YAG Lasers

6.1 Introduction

In the desire to find gain media for high average power solid state lasers an important factor which should be considered is the pump defect. This is the energy difference between the pump and laser wavelengths and has the effect of putting an upper limit on the possible slope efficiency of the laser and a lower limit on the amount of thermal energy which must be dissipated in the laser medium. A traditionally important rare earth doped laser transition is that at 1.064μm in Nd:YAG due to its large emission cross section, a strong absorption at a diode pumpable wavelength and the good thermal characteristics of the host crystal. At high powers, however, the large energy difference between the 807nm pump radiation and the laser emission around 1μm can result in thermal lensing and birefringence degrading output performance [1,2,3]. Such problems associated with neodymium doped lasers have led to much recent interest in ytterbium doped materials, particularly Yb:YAG [4,5,6] which can be pumped at 941nm or 968nm to obtain laser action at 1.03μm or 1.05μm, this shows a significant improvement in terms of pump defect to Nd:YAG pumped at 807nm.

As an alternative to the more conventional operation of Nd:YAG lasers or to Yb:YAG lasers in this chapter I will present results on an in-band pumped 946nm Nd:YAG laser. In such a scheme pumping occurs at 869nm directly into the upper laser level and lasing is on the quasi-three-level transition to the upper Stark level in the ground state manifold, as shown in figure 6.1. In-band pumping has previously been demonstrated in an early diode pumped Nd:YAG laser operating on the 1.064μm transition [7] although with a low efficiency. In this chapter I will describe what we believe to be the highest efficiency yet reported for a 946nm Nd:YAG laser offering future possibilities for high power, high efficiency diode pumped Nd:YAG lasers using this pumping scheme.

Whereas for many high power laser applications the more commonly used

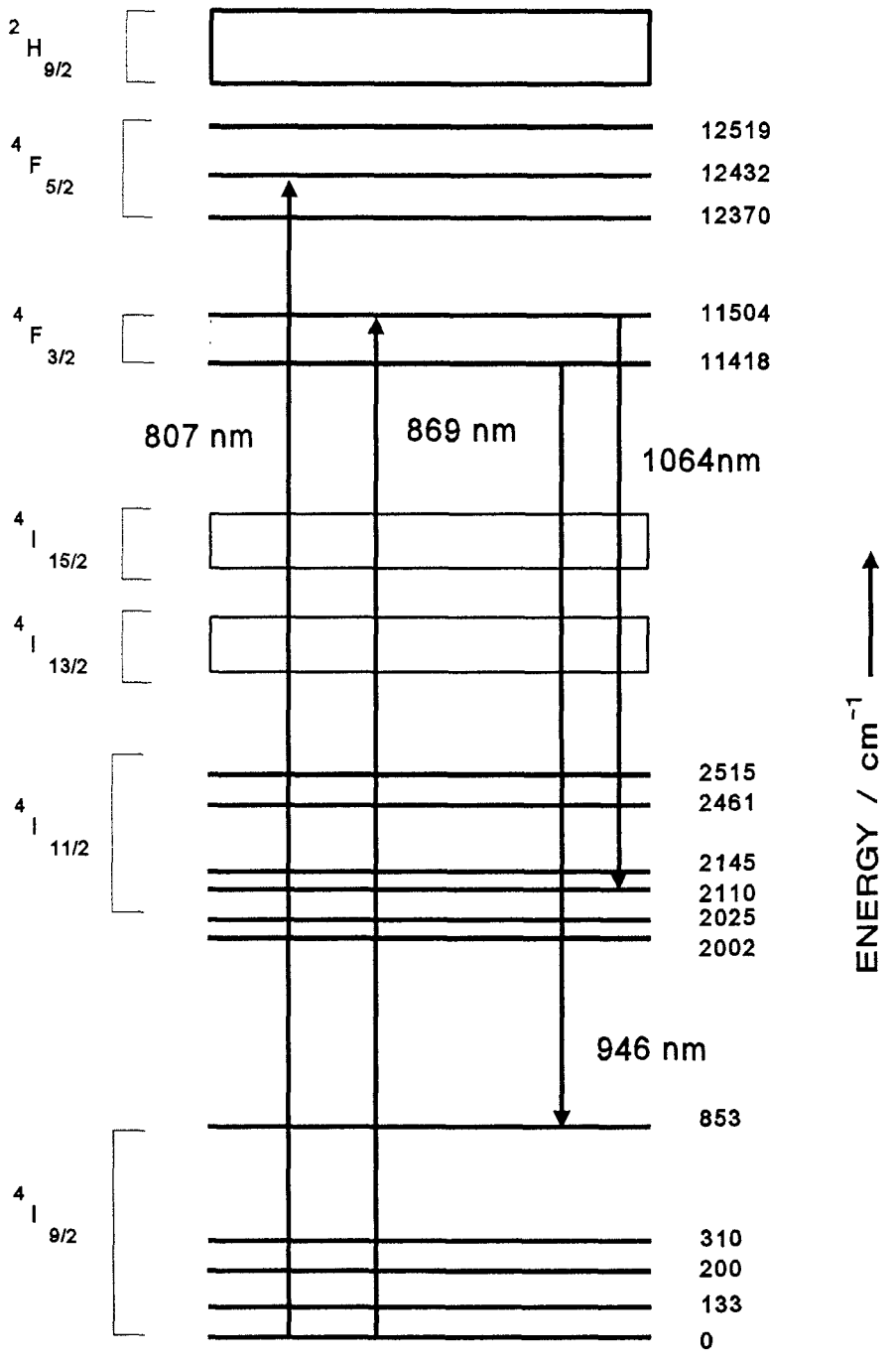

Figure 6.1 Partial energy level diagram of Nd:YAG showing absorption and emission lines

neodymium transition has been around 1 micron, due to its large emission cross section and four level nature, the 946nm emission wavelength of Nd:YAG is of interest in itself [8,9,10] as a pump source for ytterbium doped lasers [11] and due to the possibility of frequency doubling into the blue region of the spectrum for applications such as optical data storage, medical diagnostics and visual displays.

In this chapter I will compare in-band pumped 946nm Nd:YAG lasers with Yb:YAG lasers and consider the benefits that in-band pumping can offer over conventionally pumped 946nm lasers. In the final part of this chapter I will present laser results of an in-band pumped 946nm bulk Nd:YAG laser.

6.2 Comparison Between In-Band Pumped 946nm Nd:YAG Lasers and Yb:YAG Lasers

At high pump intensities solid state lasers exhibit thermal lensing due to a temperature-dependent change in the refractive index, a stress-dependent change in the refractive index and a distortion at the end face of the rod which is approximately proportional to the expansion coefficient of the host material [12]. The resulting degradation of output beam quality and laser efficiency has led to a search for rare earth doped lasers with a low energy defect between the pump and signal radiation, which reduces the amount of heat needed to be dissipated by the laser rod. A common solution to such a problem has been to work with ytterbium doped materials which can be pumped at pump and signal wavelengths which result in a much lower pump defect, furthermore having only one excited state manifold there are no complications with excited state absorption or upconversion in these materials. One of the most attractive features of ytterbium doped lasers for high power diode pumped operation is the breadth of the pump bands which eliminate the necessity for careful temperature tuning of the diode pump laser wavelengths. Although Yb:YAG may seem, on these criteria at least, to be a preferable laser host for high power lasers there are certain reasons why Nd:YAG, especially if in-band pumped, may be a better choice. Table 6.1 lists some of the relevant parameters for room temperature in-band pumped 946nm Nd:YAG lasers

and 1.03μm Yb:YAG lasers pumped at 941nm or 968nm.

Table 6.1

	946nm Nd:YAG	1.03μm Yb:YAG
Thermal loading	$\Delta\lambda$ = 76nm	941nm pump $\Delta\lambda$ = 89nm 968nm pump $\Delta\lambda$ = 62nm
Emission cross section	5.1×10^{-24} m^2 [13]	1.8×10^{-24} m^2 [14]
Absorption cross section	4.2×10^{-24} m^2 [13]	941nm : 0.7×10^{-24} m^2 968nm : 0.6×10^{-24} m^2 [4]
FWHM of absorption line	~ 1nm	941nm : 18nm 968nm : 4nm
Lower laser level energy	853 cm^{-1}	612 cm^{-1}
Fractional population in lower laser level at R.T.	0.7%	4.4%
Absorption cross section at laser wavelength	4.0×10^{-24} m^2 [15]	1.8×10^{-24} m^2
Upper laser level lifetime	230 μs	951 μs [14]

The 946nm transition in Nd:YAG has advantages over Yb:YAG due to a much lower population in the lower laser level, together with an advantage in absorption and emission cross sections together with a similar pump defect when in-band pumped. It should be noted, however, that a lack of concentration quenching in the case of Yb:YAG allows for much greater doping levels than would be optimal in the Nd:YAG system. It can be concluded that for very high power laser operation Yb:YAG may well be a better system than the 946nm transition in Nd:YAG due to the broad pump bands and lack of upconversion, excited state absorption and concentration quenching. The Nd:YAG transition is still important, however, due to applications specific to its particular wavelength.

6.3 Modelling of 946nm Nd:YAG Lasers

Using the theory presented in Chapter 2 in this section I will compare in-band pumped 946nm Nd:YAG lasers with conventional lasers pumped at 807nm. The disadvantage of in-band pumping is due to the absorption cross section at the pump wavelength, which is around 3½ times lower than that at 807nm. Figure 6.2 is a white light absorption spectrum of a 1at% Nd doped YAG sample which shows the relative absorptions at 807nm and 869nm. As a result of this a longer length of rod will be needed to absorb the same amount of incident pump power. Due to the quasi-three-level nature of the 946nm transition a longer rod length has the effect of increasing the reabsorption loss at the laser wavelength which adversely effects the laser threshold and will reduce the slope efficiency, although the latter will be compensated for by the lower pump defect in the in-band pumped case.

The optimum crystal length, l_o, that minimizes the threshold in terms of incident power can be calculated and is a result of a trade off between increasing absorbed power and increasing reabsorption loss with rod length and is given in equation 6.1 [16]

$$\alpha e^{-\alpha l_o}\left(\frac{2\sigma N_1^0}{\alpha} + L + T + 2N_1^0\sigma l_o\right) - 2N_1^0\sigma = 0 \qquad (6.1)$$

where α is the absorption coefficient at the pump wavelength, σ is the absorption cross section at the laser wavelength, N_1^0 is the lower laser level population, L is the fixed cavity loss and T the output coupling.

If we consider two 946nm lasers, one pumped at 807nm and the other in-band pumped at 869nm each with a 5% output coupler, both have the optimum length given by [16] which results in a round trip reabsorption loss at room temperature of ~3.7% for the 807nm pumped case whereas the loss for the in-band pumped laser is close to 10%. Such an increase in loss will have the effect of increasing the laser threshold. Nevertheless using an analysis based on that described in Chapter 2 the output of optimised 807nm pumped and in-band pumped 946nm lasers has been modelled. Figure

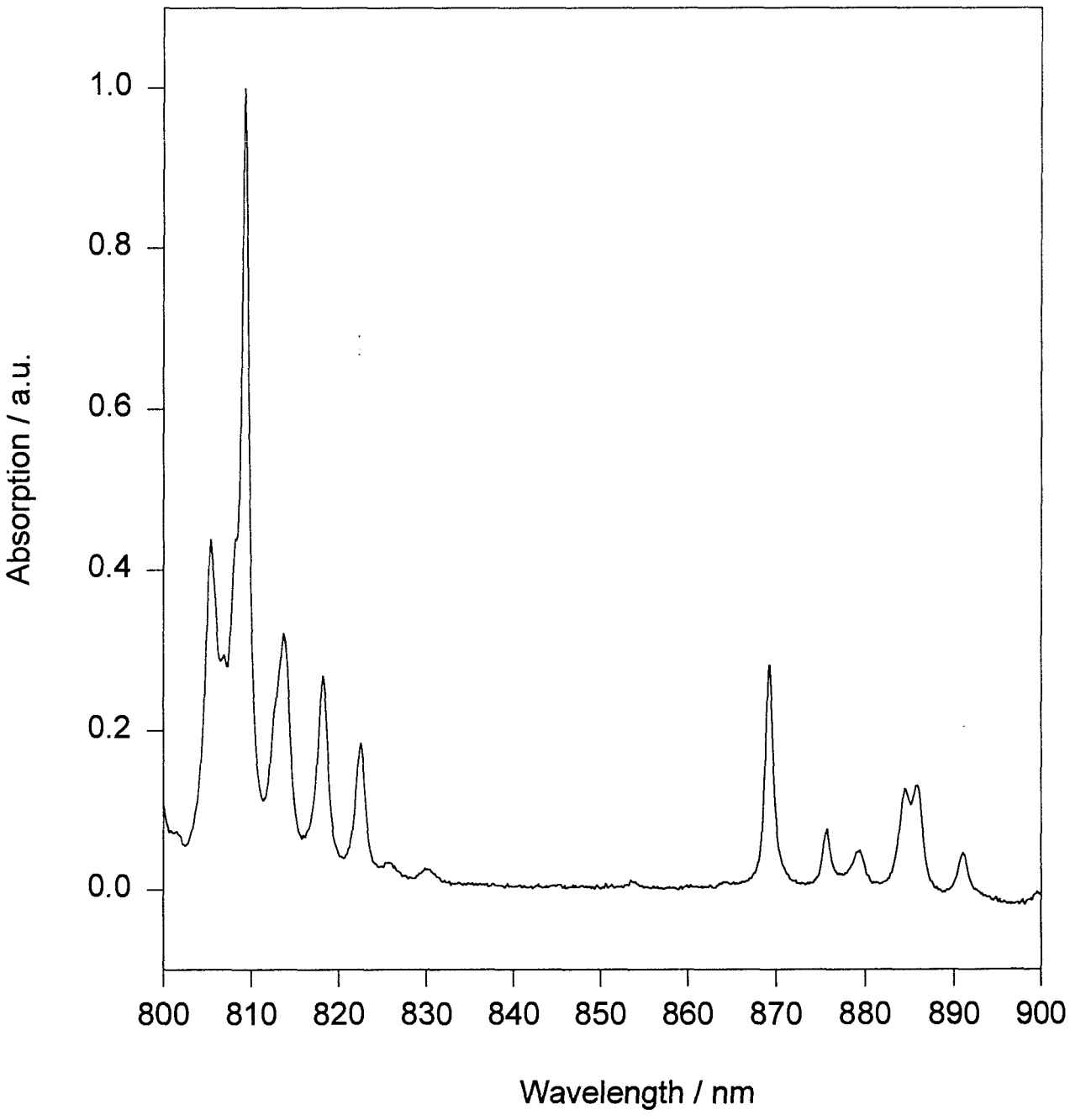

Figure 6.2 White light absorption spectrum of 1 at% Nd:YAG showing absorption peaks around 807nm and 869nm

6.3 shows the input / output characteristics for the optimised in-band pumped and 807nm pumped lasers at output levels up to 10W. At high output levels around 4W the effect of the increased reabsorption loss for the 869nm pumped case relative to the 807nm pumped case, which initially leads to lower output power due to a higher threshold, is compensated for by the increase in slope efficiency due to a lower quantum defect for the former case; this leads to similar pump level requirements for such an output power. At output powers above this level in-band pumping gives a higher output than the 807nm pumped laser. This fairly simple analysis neglects, however, any consideration of the lower thermal input, lower birefringence and hence less thermal lensing, or indeed pump saturation effects which would decrease the performance of the 807nm pumped laser relative to the in-band pumped laser.

Waveguide vs Bulk Laser

An important factor to consider when trying to optimise the output of an in-band pumped 946nm laser is whether it would be advantageous to use a planar waveguide or a bulk crystal as the gain medium. Nd:YAG waveguides grown by liquid-phase epitaxy, that were available in Southampton, had either 0% Ga doping and a 38μm depth, or 12% Ga doping and depths of ~ 4-20μm. Typical propagation losses in a bulk Nd:YAG rod are around 0.03dB / cm, in an epitaxial Nd:YAG waveguide the loss was estimated to be ~ 0.05dB / cm [17] whereas the loss in a 12% Ga doped Nd:YAG waveguide is ~ 0.15dB / cm [9]. A 12% Ga doping level also results in a reduction in the peak emission and absorption cross sections to a value of 0.58 of that in a bulk sample [9]; liquid-phase epitaxy itself has a very slight effect on the cross sections due to negligible broadening of the emission lines [9].

Figure 6.4 shows the modelled output of optimised bulk and planar waveguide in-band pumped 946nm Nd:YAG lasers. Both the bulk crystal and the waveguides are assumed to have a length equivalent to one absorption length and a 5% output coupler has been used. It is apparent that due to the reduction in cross section for the Ga doped waveguide a longer length is required than in the bulk crystal resulting in increased

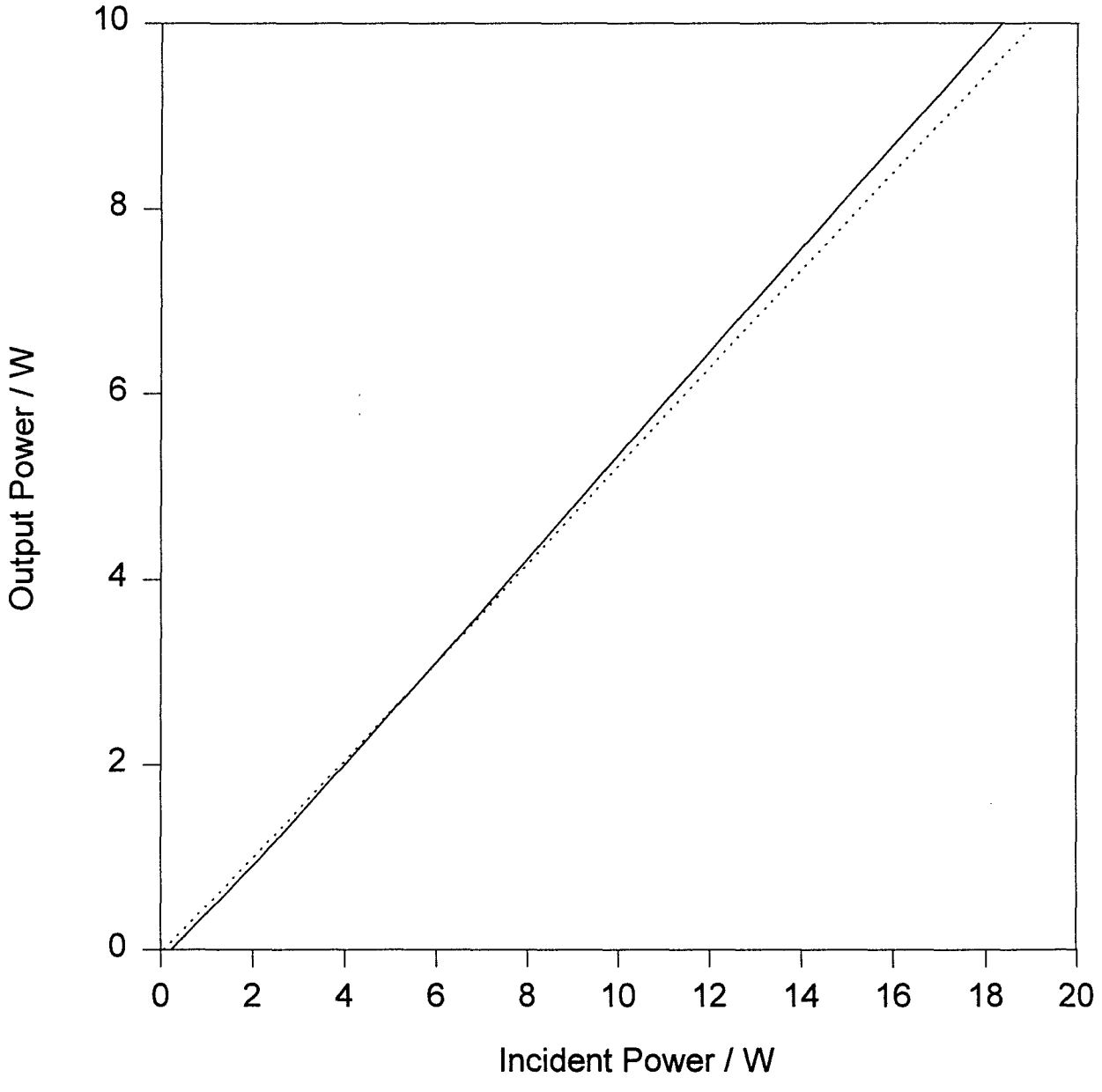

Figure 6.3 Theoretical 946nm output vs incident pump power for optimised in-band pumped and 807nm pumped lasers

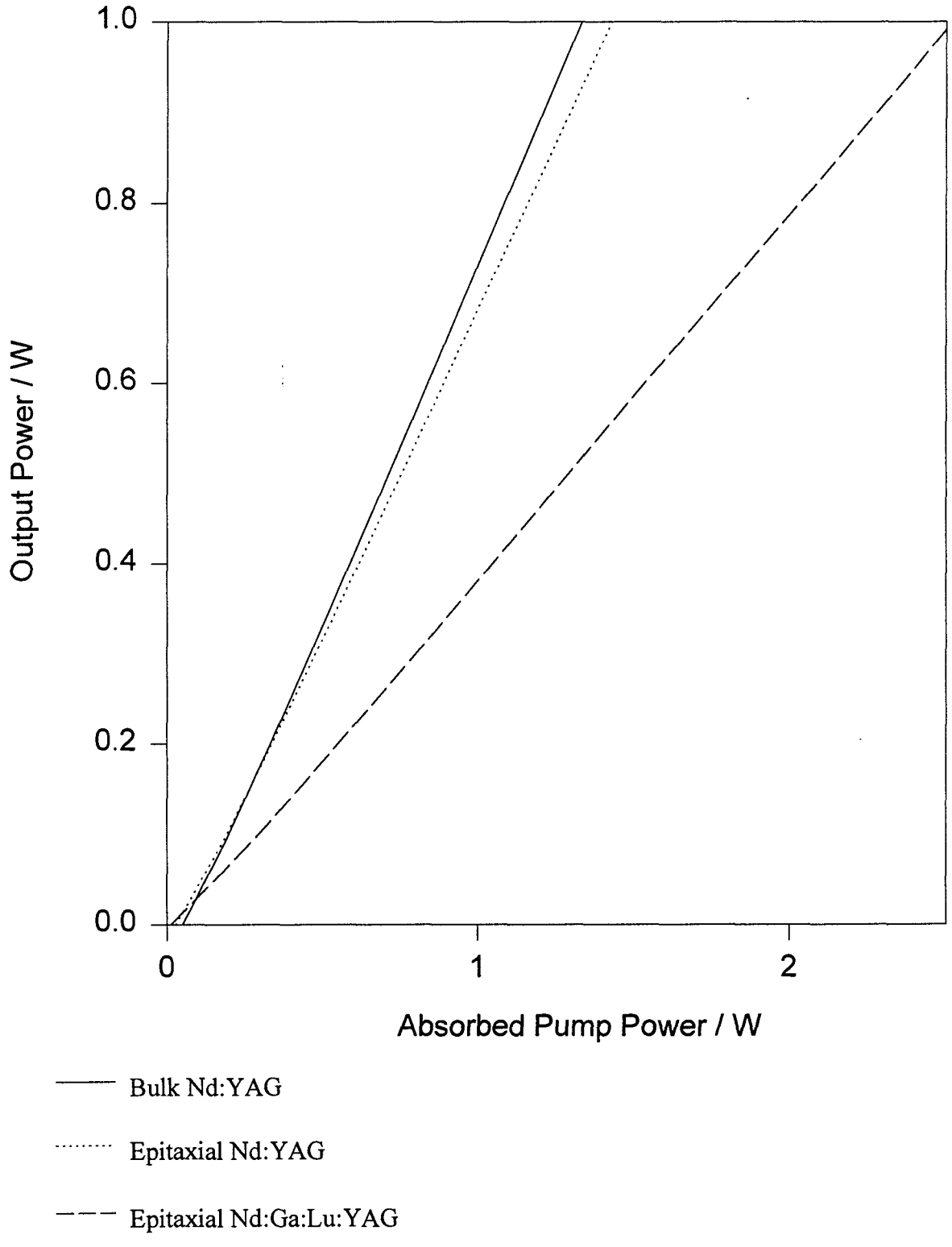

Figure 6.4 Theoretical output power vs absorbed pump power for bulk and waveguide in-band pumped 946nm Nd:YAG lasers

reabsorption loss over a cavity round trip. This results in a reduced laser slope efficiency relative to the other lasers. The 38μm Nd:YAG waveguide shows little advantage in pump and signal spot sizes to that which could be obtained in a bulk rod; the slightly increased propagation loss in the waveguide case accounts for the decrease in output performance. It can be deduced that due to the low absorption coefficient for an in-band pumped laser and the corresponding long lengths of gain material needed there is no advantage in a move to a planar geometry relative to a bulk device in this case. It should be noted, however, that it should be possible to grow planar waveguides of a 4μm depth with a lower Ga doping level than has been used here which would result in lower propagation losses and higher cross sections than have been used in this analysis; in such a case the additional confinement of the planar geometry may compensate for the additional losses and an advantage could be obtained over a bulk laser in terms of threshold and slope efficiency.

6.4 In-Band Pumped 946nm Nd:YAG Lasers

Laser operation was achieved in a Nd:YAG rod with ~ 1at% Nd doping, which had a diameter of 4mm and a 5mm length. Two lasers experiments were performed one in each of the arrangements described in section 3.10.

946nm Nd:YAG Laser with Brewster Angled Rod

For this experiment the Nd:YAG rod was positioned so as to be at Brewster's angle to the incident pump beam in order to minimise any reflections of the pump and signal which would cause a loss in the laser cavity. The pump beam, from a Ti:sapphire laser, was focused into the crystal using a 130mm focal length lens to a waist spot size of 26μm on the plane mirror.

With two highly reflecting mirrors forming the laser cavity the absorbed pump power laser threshold was measured to be 105mW when in-band pumped at 869nm, this compares with the theoretical value of 54mW. The discrepancy between this value and that experimentally observed was corroborated when the Ti:sapphire was tuned to the

strong absorption at 807nm. Possible reasons for the apparent cavity losses of ~ 4% could be a slight reflection due to the rod faces not being exactly at Brewster's angle to the pump (and therefore laser) beam. Such an effect could be expected to produce a loss of ~ 1.6% over a cavity round trip, this would be further increased were the 946nm laser not linearly polarised. Due to the necessity of positioning the rod at Brewster's angle it was not possible to place it in a heat sink which prevented efficient cooling. From [12,18] it is possible to calculate the temperature rise in the centre of the rod relative to the air due to the heat deposited during optical pumping, which for 807nm pumping is approximately 20K at the laser threshold, this in turn increases the reabsorption loss at the laser wavelength resulting in a cavity loss of ~ 1.5%. Including these additional losses into the expression for laser threshold gives an absorbed power threshold of 89mW which compares well with the experimentally obtained threshold of 92mW for 807nm pumping. It was therefore apparent that to improve the performance of this laser significantly in terms of threshold, and indeed slope efficiency it would be necessary to have the end faces of the rod antireflection coated. With coated end faces it would be possible to position the rod so as to be perpendicular to the direction of the pump beam, eliminating the reflection losses, furthermore with a highly reflecting coating on the end face it would be possible to house the rod in a metal heat sink and so remove the loss due to the heating effects.

946nm Nd:YAG Laser with Coated End Faces

One face of the Nd:YAG rod was coated with a broad band antireflection coating, with < 0.5% reflectivity between 800nm and 1μm. The other face was coated so as to be highly reflecting (~0.01% transmission) at 946nm and had a transmission of 87% at the pump wavelength, 869nm. The laser resonator consisted of a simple plano-convex cavity, as described in section 3.10, with the curved output couplers having 3% or 5% transmission at 946nm. The Ti:sapphire pump light was focused into the rod through the highly reflecting coated face to a waist spot size of ~ 30μm using a 130mm focal length lens; this is equivalent to confocal focusing over the length of the crystal, with the waist located at the highly reflecting mirror so as to give the best overlap with

the lasing mode which was measured to have a 26μm waist spot size. Both the coated faces had transmissions in excess of 95% at 1.064μm in order to suppress parasitic lasing on the high gain transition at this wavelength. The rod was mounted with an indium foil surround in a metal block which acted as a heat sink.

Using the 3% output coupler an absorbed power threshold of 49.4mW was obtained with a maximum output power of over 200mW for ~ 450mW (~800mW) of absorbed (incident) pump power. The slope efficiency for pump powers more than four times above threshold was 72%, equivalent to 42% with respect to incident power, as shown in figure 6.5. These values for threshold and slope efficiency are in good agreement with those obtained from the theory of Chapter 2 which yields values of 41mW for the threshold and 74% for the slope efficiency.

Replacing the 3% output coupler with a mirror with 5% transmission at 946nm results in a threshold of 70mW with respect to absorbed power (119mW with respect to incident power). The slope efficiency at output powers more than four times above threshold was 75% which is equivalent to 51% with respect to incident power, as shown in figure 6.6. The maximum output power was 470mW for 820mW of absorbed pump power. These results were again in fair agreement with the theoretical values of a 58mW threshold and a 76% slope efficiency. The output beam quality of the laser was very good with M^2 values <1.1, measured using a Coherent Modemaster. This is, to our knowledge, the highest efficiency yet reported for a laser on the 946nm transition in Nd:YAG.

There were some discrepancies between the initial theoretical and experimental slope efficiencies, with the experimental slope efficiencies at low pump powers being lower than those predicted. At pump power levels four times above threshold the two results were, however, in excellent agreement. Although the exact reason for such a discrepancy is not known it could be due to uncertainties in the values of absorption and emission cross sections or as a result of changes in the laser spot size with increasing

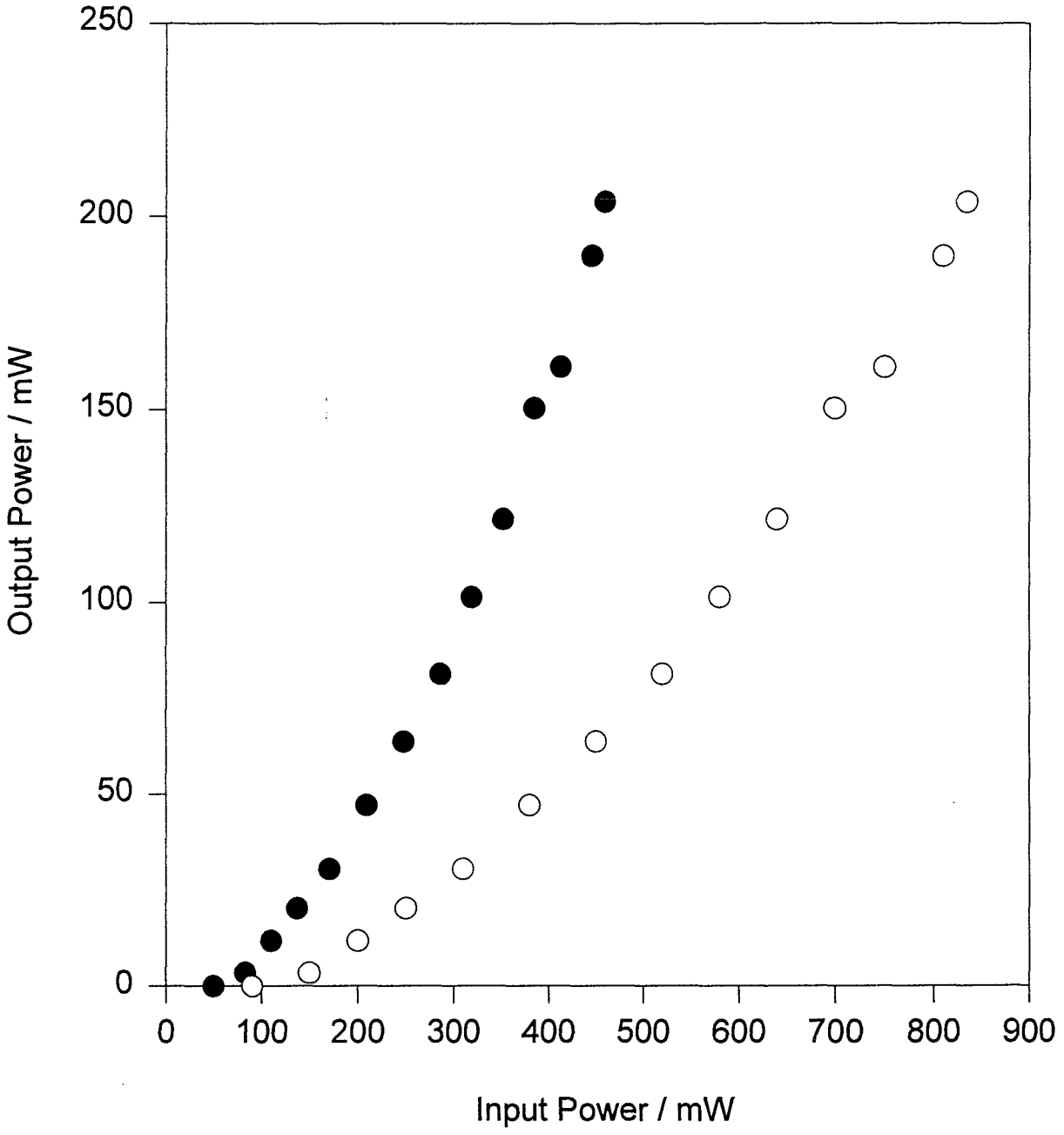

Figure 6.5 Laser output power and slope efficiency for an in-band pumped 946nm Nd:YAG laser with a 3% output coupler

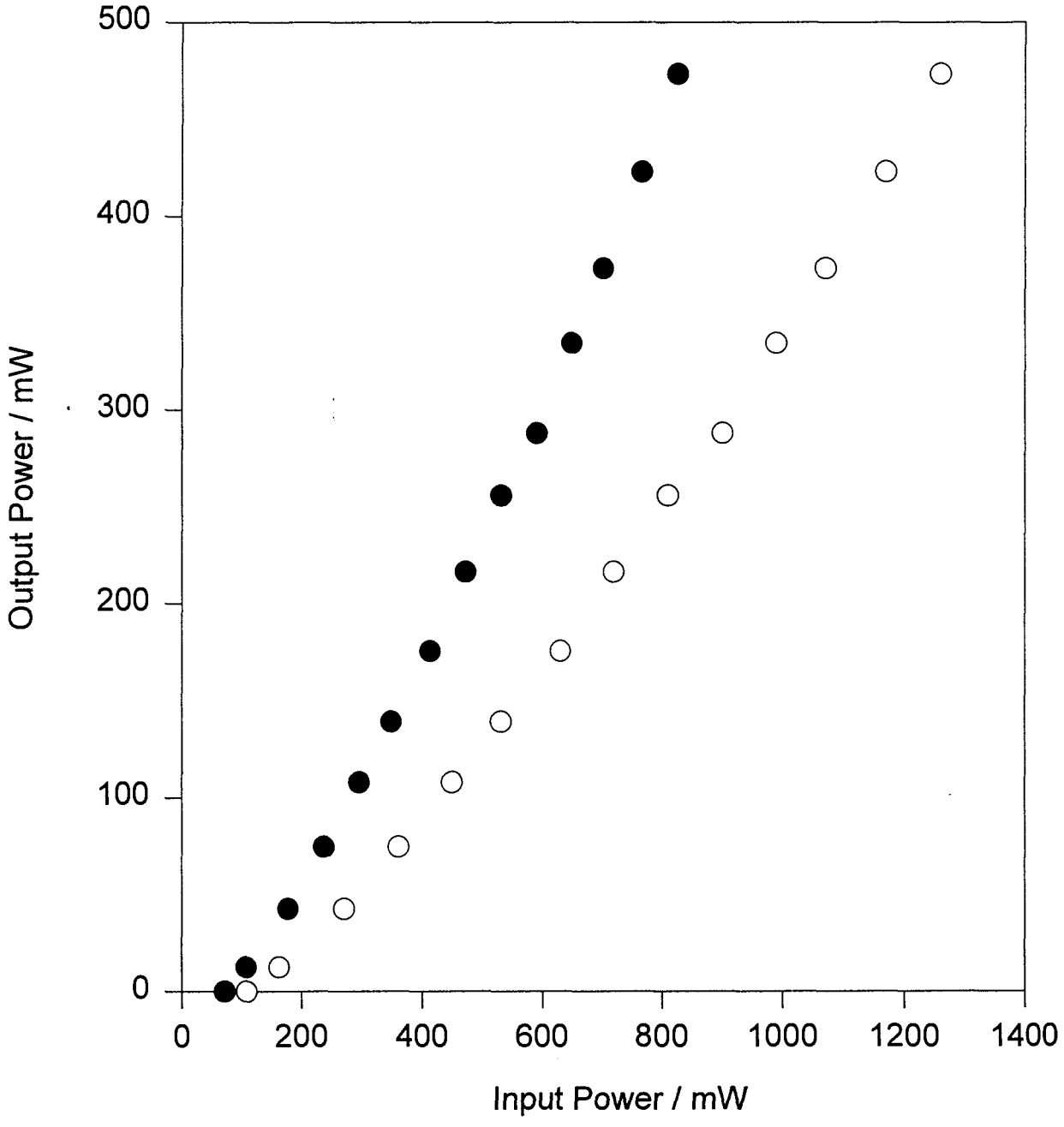

○ Incident power slope efficiency = 51%

● Absorbed power slope efficiency = 75%

Figure 6.6 Laser output power and slope efficiency for an in-band pumped 946nm Nd:YAG laser with a 5% output coupler

output power.

Discussion

There are several methods which should allow improved operation of a laser on the $^4F_{3/2}$ - $^4I_{9/2}$ transition in Nd:YAG. One simple improvement could be made by feeding back the unabsorbed pump light into the laser rod by using a suitably coated output mirror. This would enable a shorter length of rod to be used to absorb the same amount of incident power reducing the reabsorption loss and so decreasing the threshold and increasing the slope efficiency. An extreme case of the recycling of unabsorbed pump light would be to use a resonator enhanced pump absorption technique which has been used to produce a 48% output efficiency in a 946nm Nd:YAG laser [19].

At room temperature the lower laser level for the 946nm transition contains 0.7% of the total population of the ground state manifold resulting in a reabsorption loss of ~0.8% / mm for a 1 at% Nd doped rod. If the rod were to be cooled to a temperature of 100K the lower laser level would be effectively depopulated resulting in negligible reabsorption loss enabling more efficient laser operation.

Cooling of the laser rod may enable lasing on transitions which have an even lower pump defect than the in-band pumped 946nm laser. The transition at 891nm is such an example which terminates on the third Stark level of the ground state manifold and has been observed to operate even at room temperature [20]. An alternative would be the 884nm transition, also down to the third Stark level, which has an emission cross section comparable to that for the 946nm transition. Even at 100K, however, this transition has a lower level population of 5% and although the projected slope efficiency of such a laser would be around 90% when pumped sufficiently hard the threshold requirement may be excessively high to allow efficient diode pumped operation.

6.5 Summary

In summary, highly efficient room temperature operation of a 946nm Nd:YAG

laser has been demonstrated using an in-band pumping scheme at 869nm. Slope efficiencies as high as 75% with respect to absorbed power, or 51% with respect to incident power have been observed at output powers nearing the half a watt level. These results suggest that for high power diode laser pumped operation of Nd:YAG lasers at 946nm consideration should be given to the uses of in-band pumping due to the benefits of higher output efficiencies and lower thermal loading than in 807nm pumped lasers.

References

1. W.Koechner and D.K.Rice, IEEE Journal of Quantum Electronics **QE-6**, 557-566, 1970

2. A.K.Cousins, IEEE Journal of Quantum Electronics **28**, 1057-1069, 1991

3. W.Koechner, Applied Optics **9**, 11, 2548-2553, 1970

4. P.Lacovara, H.K.Choi, C.A.Wang, R.L.Aggarwal and T.Y.Fan, Optics Letters **16**, 14, 1089-1091, 1991

5. H.Bruesselbach and D.S.Sumida, Optics Letters **21**, 7, 480-482, 1996

6. D.Pelenc, B.Chambaz, I.Chartier, B.Ferrand, C.Wyon, D.P.Shepherd, D.C.Hanna, A.C.Large and A.C.Tropper, Optics Communications **115**, 491-497, 1995

7. M.Ross, Proceedings of the IEEE **56**, 196-197, 1968

8. T.Y.Fan and R.L.Byer, Optics Letters **12**, 10, 809-811, 1987

9. D.C.Hanna, A.C.Large, D.P.Shepherd, A.C.Tropper, I.Chartier, B.Ferrand and D.Pelenc, Applied Physics Letters **63**, 1, 7-9, 1993

10. W.A.Clarkson, R.Koch and D.C.Hanna, Optics Letters **21**, 10, 737-739, 1996

11. R.Koch, W.A.Clarkson, D.C.Hanna, S.Jiang, M.J.Myers, D.Rhonehouse, S.J.Hamlin, U.Griebner and H.Schonnagel, Optics Communications **134**, 1-6, 175-178, 1997

12. W.Koechner, Applied Optics **9**, 6, 1429-1434, 1970

13. S.Singh, R.G.Smith and L.G.Van Ultert, Physical Review B **10**, 2566-2572, 1970

14. D.S.Sumida and T.Y.Fan, Optics Letters **19**, 17, 1343-1345, 1994

15. B.F.Aull and H.P.Jensen, IEEE Journal of Quantum Electronics **QE-18**, 5, 925-930, 1982

16. W.P.Risk, Journal of the Optical Society of America B **5**, 7, 1412-1423, 1988

17. I.Chartier, B.Ferrand, D.Pelenc, S.J.Field, D.C.Hanna, A.C.Large, D.P.Shepherd and A.C.Tropper, Optics Letters **17**, 11, 810-812, 1992

18 J.P.Gordan, R.C.C.Leite, R.S.Moore, S.P.S.Porto, J.R.Whinney, Journal of Applied Physics **36**, 1, 3-8, 1965

19. W.J.Kozlovsky and W.P.Risk, IEEE Journal of Quantum Electronics **28**, 4, 1139-1141, 1992

20. M.Birnbaum, A.W.Tucker and P.J.Pomphrey Jr, IEEE Journal of Quantum Electronics **QE-8**, 6, 501, 1972

Chapter 7 - Conclusion

7.1 Results and Conclusions

The most significant advance resulting from work done in producing this thesis has been a further demonstration of the advantages that a planar waveguide geometry can offer over traditional systems for high gain amplifiers and low threshold lasers. This work can be divided into two sections; the first part was, to some extent, a continuation of the work previously done on waveguide lasers grown by liquid-phase epitaxy (LPE) and demonstrated a high efficiency Tm:YAG laser. The second part described the use, for the first time, of planar waveguides to make high gain amplifiers even when pumped with only modest powers. The final part of the work reported in this thesis was involved with a very high efficiency bulk Nd:YAG laser operating on the quasi-three-level 946nm transition.

Tm^{3+} doped crystals are of interest as lasers operating around 2μm due to the applications of laser radiation at this wavelength in the fields of lidar, medicine etc. The quasi-three-level nature of this transition, resulting in relatively high thresholds in bulk materials [1,2], suggests that such lasers could greatly benefit from being operated in optical waveguides. The reabsorption loss at the laser wavelength makes any waveguide propagation loss less significant than it is in four level systems and so the advantage of confining the pump and laser radiation can lead to lower threshold lasers than are obtainable in bulk devices. Rare earth doped YAG waveguides, grown by liquid-phase epitaxy, have previously been used to make low threshold lasers due to the low loss nature of guides grown using this technique. Tm:YAG waveguides grown by LPE have been operated as lasers at 2.012μm with lower thresholds and higher slope efficiencies than have been reported in bulk lasers.

Although liquid-phase epitaxy has been proved to grow low loss waveguides in YAG the technique had not previously been extended to the growth of other laser host crystals. Tm:YSO planar waveguides were grown by LPE at LETI which lased at

1.884μm with thresholds lower than reported in bulk Tm:YSO and with similar slope efficiencies. This is an important step for LPE growth and suggests that other crystal waveguides may be suitable for growth using this technique.

The planar geometry is a very attractive one for optical amplifiers for several reasons. The confinement of the pump and signal radiation can lead to higher gains for lower pump powers than in bulk amplifiers. The planar geometry is uniquely compatible with the elliptical output beam shape of broad stripe diode and diode bar lasers suggesting the use of simple pump focusing optics is possible. Finally the slab geometry should allow efficient cooling for high power device operation. A Nd:YAG waveguide grown by liquid-phase epitaxy, has been operated as a high gain amplifier at 1.064μm when pumped with both a Ti:sapphire laser and a broad stripe diode laser. Small-signal gains of 686 (>28dB) were obtained with ~550mW of absorbed pump power from a 1.2W broad stripe diode laser. This result is significantly better than any reported in a bulk amplifier with the same level of pump power.

A rare earth doped waveguide was fabricated, for the first time, using thermal bonding by Onyx Optics of California. Lasing experiments determined the propagation loss in the Nd:YAG waveguide to be ~2dB/cm, it has subsequently been shown that this loss may be as low as 0.7dB/cm. A Ti:sapphire pumped amplifier set up in this waveguide showed small-signal gains of 23.6dB with ~250mW of absorbed pump power. Waveguide propagation loss is not such an important factor for amplifiers as it is in lasers because even a loss of 2dB/cm is relatively insignificant when gains >20dB can be obtained. The discrepancy between theoretical and experimentally observed small-signal gains was investigated and was found, in the low gain, low pump power limit, to be due to a decreased overlap between the pump and signal beams than that employed in the original theory.

The final experimental part of this thesis described the use of in-band pumping at 869nm, directly into the upper laser manifold, to produce a high efficiency Nd:YAG

laser. The pump defect between the 869nm pump and 946nm laser is significantly smaller than that in conventionally pumped Nd:YAG lasers allowing higher slope efficiencies than would be possible using an 807nm pump source. The low thermal input of the in-band pumped laser will allow high power operation with low thermal lensing and birefringence which degrade the laser output performance. Using a Ti:sapphire pump source slope efficiencies as high as 75% with respect to absorbed power were obtained, which is equivalent to 51% with respect to incident power on the crystal face. This, to the best of our knowledge, is the highest efficiency reported for a 946nm Nd:YAG laser.

7.2 Future Work

The inevitable thrust of much of the future work will be towards high power operation of waveguide devices. With the wide availability of high power diode lasers as pump sources there is an opportunity to prove some of the proposed advantages that the planar geometry can offer. For both lasers and amplifiers there is the possibility of pumping in the longitudinal manner described in this thesis and to side pump the planar waveguide, which will enable easy scaling of the device to the very high powers possible using diode bars as the pump source. Using a side-pumped geometry it should be possible to fabricate a device which can amplify several signal sources at once. Due to the compatibility between the output beam shape from such diodes and the planar geometry direct butting of the diode laser to the waveguide is feasible; to achieve this waveguides with high numerical apertures will be required to collect the highly diverging laser output. Thermal bonding looks as though it may be a useful fabrication procedure which should enable waveguides with very high numerical apertures to be made. For high power lasers the face-pumped geometry is an extremely attractive one due to its simplicity which requires no focusing of the incident pump light, large depths of waveguide may be needed, however, to absorb a significant fraction of the diode output power.

The quasi-three-level nature of the 946nm transition suggests that a planar

waveguide laser using the in-band pumping scheme could result in a lower threshold than in the bulk device which could result in a higher output for a given pump power. It would be necessary to have a low loss waveguide of depth < ~10nm to achieve an improvement due to the long lengths needed to absorb the 869nm pump light. Waveguides of such depths could be grown by liquid-phase epitaxy with a lower level of gallium doping than has previously been employed, this would result in lower losses than in higher Ga doped waveguides[1] and with greater peak emission cross sections; such a waveguide could well further improve the performance of the in-band pumped 946nm Nd:YAG laser. This laser also needs to be operated at high power to demonstrate fully the advantages that the low pump defect can offer.

There are several other directions of future work which, I believe, should not be overlooked in the quest for power. To improve the performance of longitudinally pumped lasers the fabrication of low loss channel waveguides is a priority. Liquid-phase epitaxial growth has so far only produced planar waveguides, a channel waveguide offering guidance in two dimensions should lower the laser threshold by about an order of magnitude if the losses are no greater than those in a planar waveguide. Several methods of producing channel guides have been suggested such as etching the planar waveguide, mechanically cutting a rib in the waveguide or cladding layer, ion implanting low refractive index sidewalls into the planar guide or by growing a rib on top of the planar waveguide by pulsed laser deposition, for example. None of these methods have yet proved successful but a solution to this problem would be an important breakthrough.

Liquid-phase epitaxy has been seen to grow very good optical quality, very low loss planar waveguides in the YAG host crystal. Future work which needs to be addressed is the growth of other laser hosts using this technique, this has been started with the growth of YSO waveguides however an ultimate goal might be to grow low

---

[1] 0% Ga: loss ~ 0.05dB/cm [3]
12% Ga: loss ~ 0.15dB/cm [4]

phonon energy hosts such as fluorides which would open up the possibility of producing room temperature waveguide upconversion lasers, this would be particularly facilitated by the fabrication of channel waveguides by LPE. It might be the case that thermal bonding, for example, could be used to fabricate waveguides in fluoride crystals which have a lower loss than the YAG crystal so far investigated in which case this might be the way forward especially as channel waveguides can be made using this technique[2].

Another avenue which would be interesting to explore would be to find a method of tuning waveguide lasers; bulk Tm:YAG has been tuned over a range of ~ 260nm [1] and a broadly tunable low threshold waveguide laser would be a very attractive device. Tunability might be achieved by using an extended cavity, for example, with a tuning element placed in the laser cavity before the output mirror. There are other dopants such as chromium which can also operate as broadly tunable lasers [5,6] therefore the fabrication of low loss waveguides with such dopants is another future direction.

The undeniable potential advantages of the waveguide geometry over bulk systems is now starting to be realised and a bright future for waveguide devices is beckoning. The next few years may see the fabrication of a whole range of high power, tunable, or upconversion waveguide lasers and high power, high gain, diode pumped waveguide amplifiers.

---

[2] This is as yet unproven, although the manufacturers claim it can be done

References

1. R.C.Stoneman and L.Esterowitz, Optics Letters **15**, 9, 486-488, 1990

2. T.Yokozawa and H.Hara, Applied Optics **35**, 9, 1424-1426, 1996

3. I.Chartier, B.Ferrand, D.Pelenc, S.J.Field, D.C.Hanna, A.C.Large, D.P.Shepherd and A.C.Tropper, Optics Letters **17**,11, 810-812, 1992

4. D.C.Hanna, A.C.Large, D.P.Shepherd, A.C.Tropper, I.Chartier, B.Ferrand and D.Pelenc, Applied Physics Letters **63**, 1, 7-9, 1993

5. H.Eilers, W.M.Dennis, W.M.Yen, S.Kück, K.Peterman, G.Huber and W.Jia, IEEE Journal of Quantum Electronics **29**, 9, 2508-2512, 1993

6. P.M.W.French, N.H.Rizvi, J.R.Taylor and A.V.Shestakov, Optics Letters **18**, 1, 39-41, 1993

Appendix A - Pump and Signal Overlap for Waveguide Modes and Gaussian Beams

A.1 Introduction

The analysis of optical lasers and amplifiers presented in Chapter 2 assumes that the pump and signal have Gaussian beam profiles in both the guided and unguided planes of the waveguide. It was shown that in the guided direction the waveguide mode has, in fact, a cosine shaped mode. This appendix will present a derivation of the overlap integrals for two Gaussian modes and two waveguide modes in order to assess the accuracy of the assumption made, and to calculate any compensating factor needed in the theory to account for the waveguide mode profile. As the pump and signal have Gaussian profiles in the unguided plane we only need to consider the overlap in the guided, or x, direction. The effect of the pump and signal beams being at an angle to one another in the unguided direction will also be analysed. Finally an expression for the maximum possible launch efficiency of pump light into a waveguide will be derived.

A.2 Overlap Integrals in the Guided Direction

Gaussian Beam Overlap

A Gaussian beam can be written in the form

$$E_y(x) = e^{-x^2/w^2} \tag{A.1}$$

where w is the spot size in the x direction. The intensity distribution is given by $E_y(x)\cdot E_y^*(x)$ and should be normalised in such a way that

$$\int_{-\infty}^{\infty} |I_y(x)|^2 dx = 1 \tag{A.2}$$

The overlap integral between pump and signal Gaussian beams is defined in equation (A.3)

$$\eta = \int_{-\infty}^{\infty} \frac{I_s(x)}{\sqrt{N_s}} \cdot \frac{I_p(x)}{\sqrt{N_p}}\, dx \qquad \text{(A.3)}$$

N_s and N_p are normalising constants for the signal and pump respectively. From equations (A.2) and (A.3) we can write

$$\eta = \int_{-\infty}^{\infty} \left(\frac{2}{w_s\sqrt{\pi}}\right)^{1/2} \cdot \left(\frac{2}{w_p\sqrt{\pi}}\right)^{1/2} \cdot e^{-x^2(2/w_s^2+2/w_p^2)}\, dx \qquad \text{(A.4)}$$

Integration of the equation (A.4) with respect to x gives the overlap integral to be

$$\eta = \frac{2(w_s w_p)^{1/2}}{(2w_s^2+2w_p^2)^{1/2}} \qquad \text{(A.5)}$$

where w_s and w_p represent the signal and pump spot sizes respectively.

Waveguide Mode Overlap

I will consider the case of a symmetric slab waveguide as this not only simplifies somewhat the following analysis, but is the basis of many practical waveguide systems, such as the thermally bonded and liquid-phase epitaxially grown waveguides described in this thesis. The intensity distribution for such a waveguide, of depth d, can be written in the form of equation (A.6), overleaf

$$I_y(x) = \begin{cases} \cos^2(k_{2x}d/2)\ e^{-2\alpha_x(x-d/2)} & x>d/2 \\ \cos^2(k_{2x}x) & |x|\le d/2 \\ \cos^2(k_{2x}d/2)\ e^{+2\alpha_x(x+d/2)} & x<-d/2 \end{cases} \qquad \text{(A.6)}$$

where k_{2x} is the transverse wavenumber in the guided region and α_x is the transverse wavenumber in the substrate regions. This, again, is normalised such that

$$\int_{-\infty}^{\infty} |I_y(x)|^2 dx = 1 \qquad \text{(A.2)}$$

This can be evaluated to give normalising constants N_s and N_p of the form

$$N_{s/p} = \frac{3d}{8} + \frac{\sin(k_{s/p}d)}{2k_{s/p}} + \frac{\sin(2k_{s/p}d)}{16k_{s/p}} + \frac{\cos^4(k_{s/p}d/2)}{2\alpha_{s/p}} \qquad \text{(A.7)}$$

where $k_{s/p}$ is the transverse wavenumber in the guided region for the signal and pump respectively, likewise $\alpha_{s/p}$ is the transverse wavenumber in the substrate regions. The transverse wavenumbers may be written as

$$k_{s/p} = k_{2x} = \frac{2\pi}{\lambda_{s/p}} \left(n_2^2 - n_e^2 \right)^{1/2} \qquad \text{(A.8)}$$

$$\alpha_{s/p} = \alpha_x = \frac{2\pi}{\lambda_{s/p}} \left(n_e^2 - n_1^2 \right)^{1/2} \qquad \text{(A.9)}$$

where n_e is the effective refractive index. In the symmetric waveguides being considered the dopant ion is only present in the core region hence the overlap is only required to be evaluated in this region. The overlap integral can be written

$$\eta = \int_{-d/2}^{d/2} \frac{\cos^2(k_s x)}{\sqrt{N_s}} \cdot \frac{\cos^2(k_p x)}{\sqrt{N_p}}\, dx \qquad \text{(A.10)}$$

This equation can be solved numerically using a computer program to give a value for the overlap integral. Evaluation of equation (A.10) requires knowledge of the effective refractive indices for the pump and signal modes which can be found using a computer program which solves the guidance condition, equation (2.24), using a bisection technique to find the waveguide b parameter, giving n_e.

A.3 Overlap in the Plane of the Waveguide

In the unguided direction of a planar structure the pump and signal beams will have Gaussian profiles, the analysis for which would thus be analogous to that presented earlier for beams which are perfectly colinear. In a practical amplifier geometry, however, there may be some angular tilt between the pump and signal beams together with a possible spatial offset between the axes of the two. The following analysis will consider the effect of tilt and offset on the overlap between two Gaussian beams.

If we consider the signal to be offset from the pump by a distance Δ, and have an angular tilt, θ, to the pump we can write the electric field distribution as [1]

$$E(y) = e^{(y-\Delta)^2/w_s^2} \cdot e^{ik\theta(y-\Delta)} \qquad \text{(A.11)}$$

The intensity distribution, $I(y) = E(y) \cdot E(y)^*$, is therefore given by

$$I(y) = e^{-2(y-\Delta(z))^2/w_s^2} \tag{A.12}$$

where $\Delta(z)$ is given by $\Delta_0 + z\tan\theta$, Δ_0 being the initial offset between the axes of the pump and signal. The pump is normalised as in equation (A.4). The signal is normalised in a similar manner, such that

$$N_s = \int_{-\infty}^{\infty} e^{-\frac{4y^2}{w_s^2}+\frac{8\Delta(z)y}{w_s^2}-\frac{4\Delta(z)^2}{w_s^2}} dy \tag{A.13}$$

where N_s is the normalising constant for the signal, this can be evaluated using the relation below

$$\int_{-\infty}^{\infty} e^{-p^2y^2 \pm qy} dy = \frac{\sqrt{\pi}}{p} \cdot e^{\frac{q^2}{4p^2}} \tag{A.14}$$

using the substitutions $p^2 = 4/w_s^2$, and $q = 8\Delta(z)/w_s^2$, this yields

$$N_s = \frac{w_s\sqrt{\pi}}{2} \tag{A.15}$$

which is the same as for a Gaussian beam without tilt or offset, as one might expect. The resulting overlap integral is therefore given by

$$\eta(z) = \frac{1}{\sqrt{N_s N_p}} \int_{-\infty}^{\infty} e^{-y^2\left(\frac{2}{w_p^2}+\frac{2}{w_s^2}\right)+\frac{4\Delta(z)y}{w_s^2}-\frac{2\Delta(z)^2}{w_s^2}} dy \tag{A.16}$$

This can be evaluated using equation (A.14) to give the overlap integral at a position z in the guide

$$\eta(z) = \frac{2(w_s w_p)^{1/2}}{(2w_s^2+2w_p^2)^{1/2}} e^{-\Delta(z)^2\left(\frac{2}{w_s^2}-\frac{4}{w_s^4(2/w_s^2+2/w_p^2)}\right)} \qquad (A.17)$$

It is evident from equation (A.17) that when the offset, $\Delta(z)$, is equal to zero the overlap integral is identical to that in equation (A.5), as one would expect. To get the average overlap in the unguided plane of a waveguide, equation (A.17) should be evaluated and averaged over the length of the guide.

A.4 Maximum Launch Efficiency into a Planar Waveguide

An interesting extension of the techniques used above is to determine the maximum theoretical launch efficiency of light into a planar waveguide which can be deduced from the overlap of a waveguide mode with a Gaussian beam of the same spot size as the mode. This overlap gives the maximum efficiency with which light can be launched from a Gaussian laser beam into a planar waveguide.

The intensities of a normalised Gaussian beam and a waveguide mode are shown in equations (A.18,19), below

$$I_{gaussian} = \left(\frac{2}{w}\sqrt{\pi}\right)^{1/2} e^{-2x^2/w^2} \qquad (A.18)$$

$$I_{waveguide} = \frac{1}{\sqrt{N_{wg}}} \cos^2(k_{2x}x) \qquad (A.19)$$

where N_{wg} is equal to N_p in equation (A.7) and w is the waveguide mode spot size. The maximum launch efficiency is given by

$$L_{\max} = \int_{-d/2}^{d/2} I_{gaussian} \cdot I_{waveguide}\, dx \qquad \text{(A.20)}$$

This equation can be solved numerically to give a value for the maximum launch efficiency into a planar waveguide. For the thermally bonded waveguide used in experiments described in Chapter 5, this can be evaluated to give a value for the maximum launch to be 99.0%, the maximum launch efficiency into the epitaxially grown waveguide of chapter 5 is 99.5%.

Reference

1. Pentti Karioja and Dennis Howe, Applied Optics **35**, 3, 404-416, 1996

Appendix B - A Thermally Bonded 1.064μm Nd:YAG Planar Waveguide Laser

B.1 Introduction

In this appendix results will be reported of laser experiments at 1.064μm on the Nd:YAG planar waveguide fabricated by thermal bonding which was used in the amplifier experiment described in Chapter 5. The waveguide was fabricated by Onyx Optics, California. One important reason for performing laser experiments on this guide was to get a measure of the propagation loss which was an unknown quantity in this first Nd:YAG waveguide fabricated using the thermal bonding technique.

B.2 Nd:YAG Planar Waveguide Laser Results

The waveguide used in this experiment had a 1at% Nd doping level, was 20μm deep, 5mm long and polished to an optical finish by Onyx Optics. The pump source used for these experiments was a Ti:sapphire laser tuned to the strongest absorption around 807nm and launched into the waveguide with a ×5 microscope objective. The launch × absorption was measured to be 0.84. In the experimental configuration described in Chapter 3, using two highly reflecting mirrors to form the laser cavity, the power threshold was measured to be 35mW incident on the mirror, which was equivalent to an absorbed power threshold of 26mW. With a 14% transmission output coupler replacing one of the highly reflecting mirrors the threshold was 27mW with respect to absorbed power and the slope efficiency was 25%. With the Fresnel reflection from the end face / air interface (8% reflection) providing feedback from one face and with a highly reflecting mirror on the other end face, the absorbed power threshold was 172mW. Lasing was also observed with the feedback being provided by two Fresnel reflections off the end faces of the crystal (2 × 8% Fresnel reflections) with a threshold of 285mW and a slope efficiency of 28.5%. The input / output characteristics of these two lasers are shown in figure B.1. The laser mode spot sizes were measured to be 7μm × 64μm in the guided and unguided planes respectively.

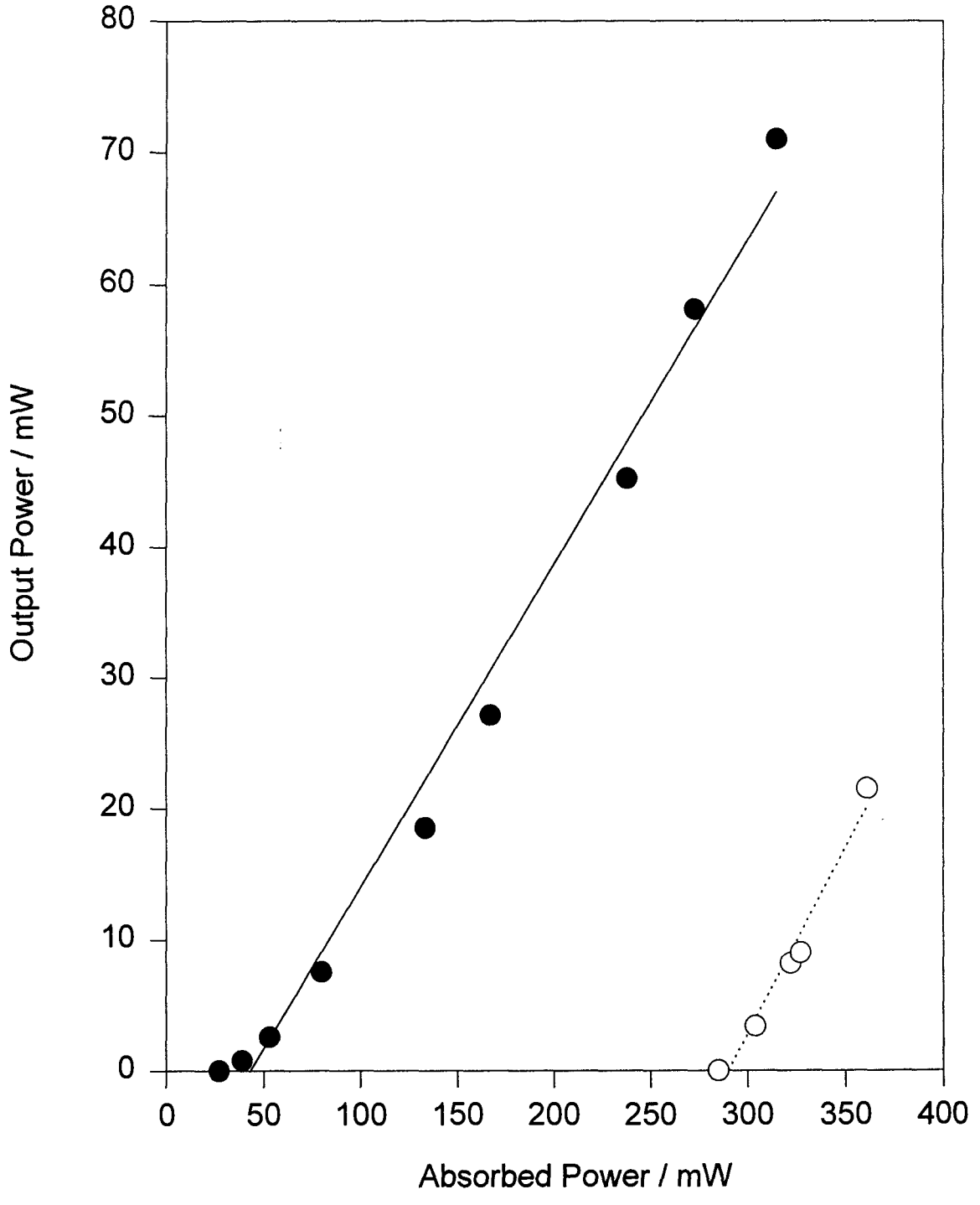

● HR / 14% output coupler : Threshold = 27mW, Slope efficiency = 25%

○ End faces : Threshold = 285mW, Slope efficiency = 28%

Figure B.1. Output power vs absorbed pump power for a 1.064μm Nd:YAG laser in a thermally bonded planar waveguide pumped by a 807nm Ti:sapphire laser

By plotting a graph of laser threshold against $\ln(R_1R_2)$ (where R_1 and R_2 are the reflectivities of the two cavity mirrors) it is possible to get a measurement of the round trip loss in the cavity, and hence the propagation loss in the waveguide. This can be explained by considering the equation for laser threshold for a four level laser (equation 2.33) which can be written in the form of equation (B.1)

$$P_{th} = C\times[2\alpha l - \ln(R_1R_2)] \qquad \text{(B.1)}$$

where C is a constant, l is the length of the crystal, α is the propagation loss term, and $-\ln(R_1R_2)$ gives the transmission of the cavity mirrors. A plot of P_{th} against $-\ln(R_1R_2)$ will be a straight line with the intercept on the x - axis ($P_{th} = 0$) giving the value of the round trip loss, this can be seen in figure B.2. The loss was calculated to be 2.1dB / cm for this thermally bonded waveguide although it should be noted that this apparent loss may be due, at least in part, to the waveguide end faces not being polished perfectly parallel to one another. [1]

The experimentally determined value for propagation loss could then be used to calculate theoretical thresholds, figure B.3, which shows good agreement between the theory and experiment. The experimental thresholds are slightly higher than those one would expect from the theory, especially at higher output coupling. This may be due, for example, to mirror coupling losses or as a result of imperfect polishing of the waveguide end faces.

---

[1]Experiments were performed subsequent to this work by C.T.A.Brown, at the Optoelectronics Research Centre, using the same method. In this case, however, the waveguide end faces had been polished parallel to one another. The results suggested that the waveguide propagation losses may be as low as 0.7dB / cm, indicating that a significant part of the loss measured beforehand was due to the inadequate polishing of the as-bought waveguide, as proposed above.

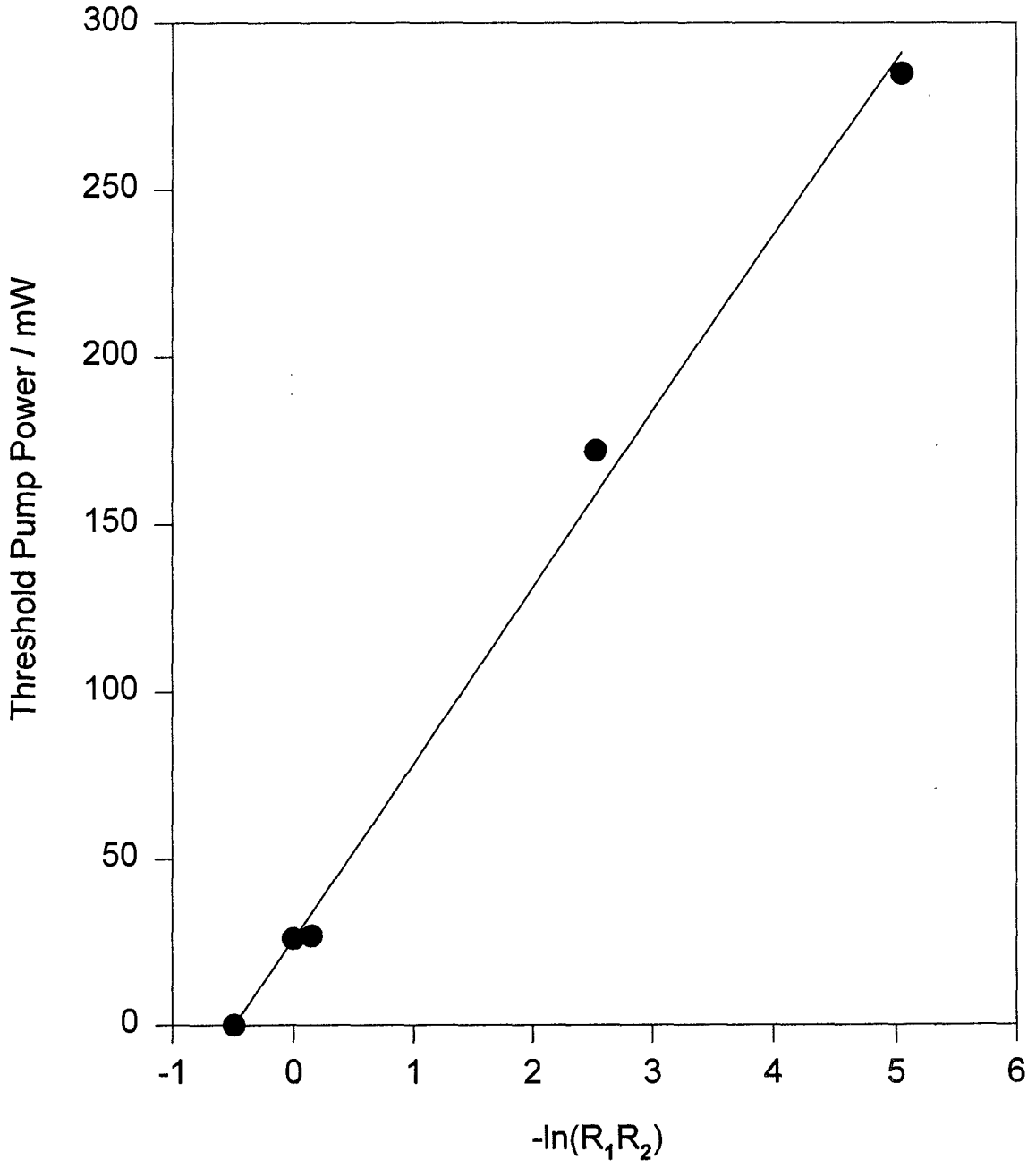

Propagation loss = 2.1 dB / cm

Figure B.2. Threshold vs Output coupling for a 1.064μm Nd:YAG laser in a thermally bonded planar waveguide to give an estimation of the waveguide propagation loss

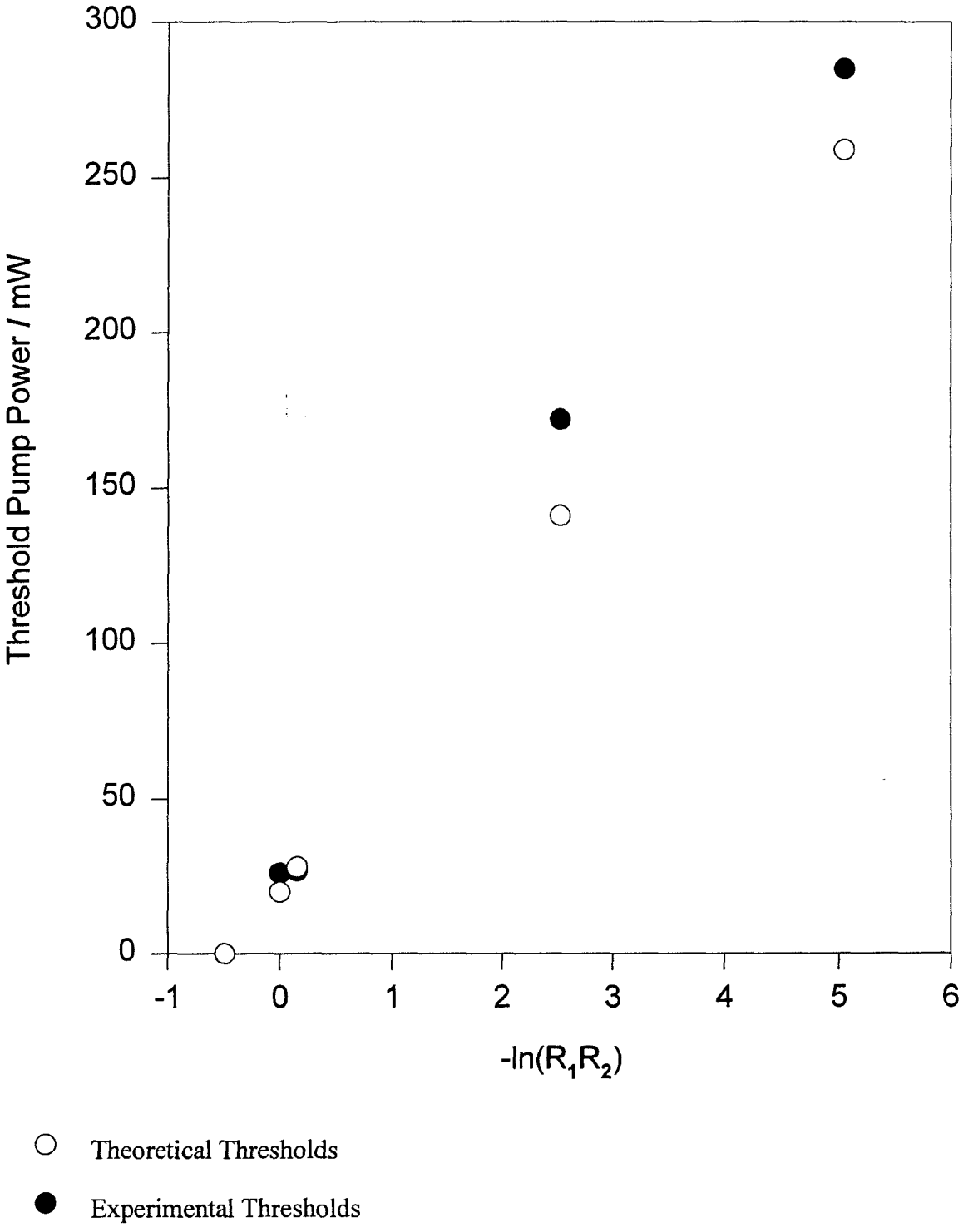

Figure B.3. Theoretical and experimental thresholds for a 1.064μm Nd:YAG laser in a thermally bonded planar waveguide

Appendix C - A Face Pumped Nd:YAG Waveguide Laser

C.1. Introduction

In a search for simple methods of converting the highly non-diffraction limited output of high power diode bars into diffraction limited, or nearly diffraction limited, laser sources various techniques have been suggested [1,2,3]. Most of these techniques, however, require focusing, or beamshaping and then focusing, of the diode output. One method of producing compact, simple high power lasers could be to face pump a planar waveguide; this is a technique which is already being used to provide high power outputs from Nd:YAG slabs [4].

In essence the technique involves butt-coupling a diode bar to the top face of the planar waveguide and lasing in the plane perpendicular to the pumping direction. It is evident that in order to get high power output from the planar laser a significant amount of the diode pump light should be absorbed, which will require a combination of high doping levels and large depths of guide.

Liquid-phase epitaxy (LPE) can be used to grow waveguides with higher doping levels than would be possible in bulk crystals, with neodymium levels as high as 15% having been doped into YAG at LETI. Waveguides can be grown by LPE with depths of around 100μm; with a doping level of 15%; the absorption length for diode bar pumping, however, is around 220μm so a multiple pump pass arrangement may be required to absorb the pump light efficiently. For a 5mm long diode bar the average spot size in the plane of the waveguide would be around 100μm for a thinly clad layer, the signal spot sizes therefore would be in the order of 50μm ×100μm orthogonal to the direction of propagation. A beam shaped 20W diode bar can have M^2 values of ~60×95 enabling focusing to spot sizes, in a 5mm longitudinally pumped bulk laser, of ~ 155μm ×170μm [5]. The lack of significant advantage in terms of spot sizes and (hence possibly performance) compared to a bulk laser may be seen to be compensated for by the significantly simpler design of a face pumped laser and the simple heat removal

capabilities of this near slab geometry, where cooling could be applied to the lower face of the guide.

C.2. A Face Pumped Laser in an Epitaxially Grown Nd:YAG Planar Waveguide

As a first test of some of the principles of face pumping waveguides an experiment was set up using a Ti:sapphire pump source and an epitaxially grown Nd:Lu:YAG waveguide. The waveguide was 54μm deep with a 26μm undoped YAG cladding layer, it was doped with 6 at.% Nd and 15 at.% Lu. The experimental arrangement is shown in Figure C.1.

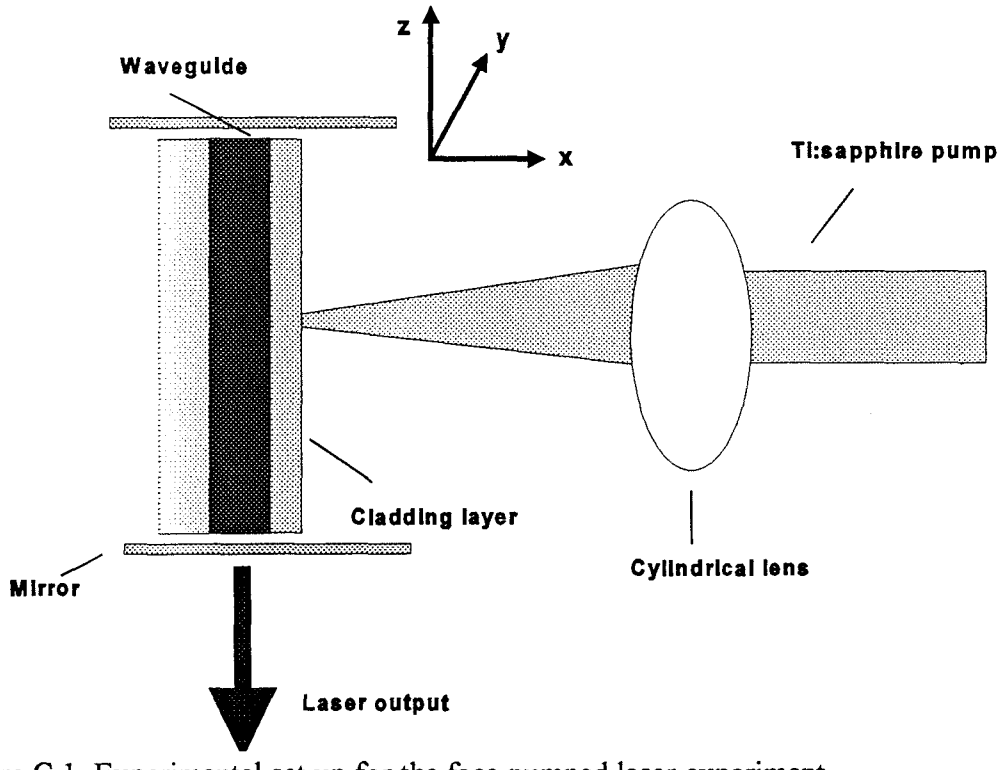

Figure C.1. Experimental set up for the face pumped laser experiment

The Ti:sapphire pump light was focused onto the top face of the waveguide to a spot size of ~ 5μm × 5mm using a 25mm focal length cylindrical lens, in an attempt to simulate the spot sizes obtainable if a 20W diode bar were to be used as the pump source. The two plane mirrors had a transmission at 1.064μm of 0.2% and were close

coupled to the end faces of the waveguide. The output laser signal was collected using a microscope objective and focused onto a silicon photodiode connected to an oscilloscope to observe the onset of lasing.

The absorption of the 807nm pump light through the depth of the guide was measured to be 13%. The lasing threshold was 214mW incident on the top face of the guide which correspond to an absorbed power threshold of only 25mW. The laser output was either single or double mode in the guided plane, depending on the exact alignment of the mirrors to the end face of the waveguide. When in single mode operation the spot sizes were measured to be 7.8μm ×98μm in the guided and unguided planes respectively. Output powers of < 1mW were obtained for absorbed pump powers of ~60mW; it should be noted, however, that the mirrors had a very low transmission at the laser wavelength preventing maximum output extraction.

This first demonstration of a face pumped laser in a planar waveguide shows the possibility of using diode face pumping of an epitaxially grown Nd:YAG waveguide as a high power laser source. With a deeper, more heavily Nd doped guide using mirrors with a higher transmission at 1.064μm an extremely simple face pumped laser should be possible which could operate at a multiwatt output level. This technique could also be extended to produce lasers using other rare earth dopants, for example ytterbium where very high doping levels are possible using liquid-phase epitaxy (up to 100% Yb substitution for Y, with negligible concentration quenching). The high doping level possible might enable a significant improvement in pump absorption even for much smaller waveguides.

References

1. H.Plaessman, S.A.Ré, J.J.Alonis, D.L.Vecht and W.M.Grossman, Optics Letters **18**, 17, 1420-1422, 1993

2. T.M.Baer, D.F.head, P.Gooding, G.J.Kintz and S.Hutchinson, IEEE Journal of Quantum Electronics **28**, 1131-1138, 1992

3. W.A.Clarkson and D.C.Hanna, Optics Letters **21**, 6, 375-377, 1996

4. A.Faulstich, H.J.Baker and D.R.Hall, Optics Letters **21**, 8, 594-596, 1996

5. W.A.Clarkson, R.Koch and D.C.Hanna, Optics Letters **21**, 10, 737-739, 1996

Appendix D - Publications and Conference Papers

Publications

1. D.P.Shepherd, D.C.Hanna, A.C.Large, A.C.Tropper, **T.J.Warburton**, C.Borel, B.Ferrand, D.Pelenc, P.Thony, F.Auzel and D.Meichenin, *A Low Threshold, Room Temperature 1.64μm Yb:Er:$Y_3Al_5O_{12}$ Waveguide Laser*, Journal of Applied Physics **76**, 11, 7651-7653, 1994

2. C.Borel, A.Rameix, P.Thony, B.Ferrand, D.P.Shepherd, A.C.Large, **T.J.Warburton**, A.C.Tropper and D.C.Hanna, *Growth by Liquid Phase Epitaxy and Low Threshold Laser Oscillation at 2.012μm of a Tm:YAG Laser*, in Proceedings of the SPIE, Vol. 2380, UV and Visible Lasers and Laser Crystal Growth, Richard Scheps and Milan R.Kokta eds., 1995, p.14-22,

3. C.Borel, A.Rameix, P.Thony, B.Ferrand, D.P.Shepherd, A.C.Large, **T.J.Warburton**, A.C.Tropper and D.C.Hanna, *Growth by Liquid Phase Epitaxy and Laser Performance at 2.012μm of a Tm:YAG Planar Waveguide*, in OSA Proceedings on Advanced Solid State Lasers, Optical Society of America, Washington, DC, 1995, Vol.11, p.149-151

4. D.S.Gill, A.A.Anderson, R.W.Eason, **T.J.Warburton** and D.P.Shepherd, *Laser Operation of an Nd:$Gd_3Ga_5O_{12}$ Thin-Film Optical Waveguide Fabricated by Pulsed Laser Deposition*, Applied Physics Letters **69**, 1, 10-12, 1996

5. D.P.Shepherd, C.T.A.Brown, **T.J.Warburton**, D.C.Hanna, A.C.Tropper, B.Ferrand, *A Diode-Pumped, High Gain, Planar Waveguide, Nd:$Y_3Al_2O_5$ Amplifier*, submitted to Applied Physics Letters 1997

6. A.Rameix, C.Borel, B.Chambaz, B.Ferrand, D.P.Shepherd, **T.J.Warburton**, D.C.Hanna and A.C.Tropper, *An Efficient, Diode-Pumped, 2μm Tm:YAG Waveguide Laser*, to be published Optics Communications, 1997

7. **T.J.Warburton**, D.P.Shepherd, D.C.Hanna and A.C.Tropper, *A High Efficiency, In-Band Pumped Nd:YAG Laser at 946nm*, to be submitted

8. C.T.A.Brown, C.L.Bonner, **T.J.Warburton**, D.P.Shepherd, A.C.Tropper, D.C.Hanna and H.E.Meissner, *Thermally Bonded Planar Waveguide Lasers*, to be submitted Applied Physics Letters, 1997

Conference Papers : I presented those in which my name is underlined

1. A.C.Large, D.C.Hanna, D.P.Shepherd, A.C.Tropper, **T.J.Warburton**, C.Borel, B.Ferrand, A.Rameix and P.Thony, *Low Threshold Operation of a Yb:Er:YAG Waveguide Laser*, Conference on Lasers and Electro-Optics / Europe, Amsterdam, 1994, paper CMF4

2. D.P.Shepherd, A.C.Large, **T.J.Warburton**, A.C.Tropper, D.C.Hanna, C.Borel, A.Rameix, P.Thony, B.Ferrand, S.Guy, B.Jaquier and M.F.Joubert, *Epitaxial Tm:YAG Waveguide Lasers at 2μm and Upconversion Fluorescence in the Blue and U.V. Regions*, Postdeadline Conference on Lasers and Electro-Optics / Europe, Amsterdam, 1994, paper CPD1.8

3. **T.J.Warburton**, D.C.Hanna, A.C.Large, D.P.Shepherd, A.C.Tropper, C.Borel, B.Ferrand, A.Rameix and P.Thony, *Low Threshold Planar Waveguide Lasers Fabricated by Liquid Phase Epitaxy*, Society of Glass Technology, UK GO Meeting, Chelmsford, 1994

4. C.Borel, A.Rameix, P.Thony, B.Ferrand, D.P.Shepherd, A.C.Large,

T.J.Warburton, A.C.Tropper and D.C.Hanna, *Growth by Liquid Phase Epitaxy and Laser Oscillation at 2.012μm of a Tm:YAG Waveguide Laser*, SPIE International Symposium on Photonics West '95, San Jose, 1995, paper 2380-03

5. C.Borel, A.Rameix, P.Thony, B.Ferrand, D.P.Shepherd, A.C.Large, **T.J.Warburton**, A.C.Tropper, D.C.Hanna, *Growth by Liquid Phase Epitaxy and Laser Performance at 2.012μm of a Tm:YAG Planar Waveguide*, Advanced Solid State Lasers, Memphis, 1995, paper TuB2

6. C.Borel, A.Rameix, P.Thony, B.Ferrand, D.P.Shepherd, A.C.Large, **T.J.Warburton**, A.C.Tropper and D.C.Hanna, *Comparative Optical Properties and Laser Performance at 2.012μm of Tm:YAG Bulk Crystals and Planar Waveguides*, The Twelth National Quantum Electronics Conference, Southampton, 1995, paper 5-3

7. D.P.Shepherd, **T.J.Warburton**, D.C.Hanna, A.C.Tropper, C.Borel, B.Ferrand and A.Rameix, *High Gain Amplification in a Liquid-Phase Epitaxial Nd:YAG Waveguide*, Conference on Lasers and Electro-Optics, Anaheim, California, 1996, paper CFJ4

8. **T.J.Warburton**, D.P.Shepherd, A.C.Tropper and D.C.Hanna, *A Thermally Bonded Nd:YAG Planar Waveguide Laser and Amplifier*, Conference on Lasers and Electro-Optics / Europe, Hamburg, 1996, paper CFH6

9. A.Rameix, C.Borel, B.Ferrand, C.Wyon, D.P.Shepherd, **T.J.Warburton**, A.C.Tropper and D.C.Hanna, *First Laser Operation of an Epitaxially Grown Tm:Y_2SiO_5 Waveguide*, Conference on Lasers and Electro-Optics / Europe, Hamburg, 1996, paper CFD1

10. C.T.A.Brown, **T.J.Warburton**, D.P.Shepherd, A.C.Tropper, D.C.Hanna and

B.Ferrand, *An Efficient, High-Gain Diode Pumped Nd:YAG Planar Waveguide Amplifier*, to be presented Conference on Lasers and Electro-Optics, Baltimore, Maryland, 1997, paper CWQ2